

© 2018

Yuanwang Pan

ALL RIGHTS RESERVED

MECHANICAL CONTROL OF TISSUE GROWTH THROUGH HIPPO SIGNALING

by

YUANWANG PAN

A dissertation submitted to the

School of Graduate Studies

Rutgers, The State University of New Jersey

In partial fulfillment of the requirements

For the degree of

Doctor of Philosophy

Graduate Program in Cell and Developmental Biology

Written under the direction of

Kenneth D. Irvine

And approved by

New Brunswick, New Jersey

May, 2018

ABSTRACT OF THE DISSERTATION

MECHANICAL CONTROL OF TISSUE GROWTH THROUGH HIPPO SIGNALING

By YUANWANG PAN

Dissertation Advisor: Kenneth D. Irvine

Tissue growth needs to be properly controlled for organs to reach their correct size and shape, but the mechanisms that control growth during normal development are not fully understood. Recently, mechanical forces have emerged as an important regulator of tissue growth: high cytoskeletal tension enhances tissue growth while low cytoskeletal tension decreases tissue growth. Our lab also discovered that cytoskeletal tension regulates tissue growth through a biomechanical Hippo signaling pathway. However, how mechanical forces are modulated and experienced by cells within developing tissues is not clear. Moreover, whether and how mechanical forces contribute to growth patterns in vivo was not known. To answer these questions, I focused my study on the mechanical feedback model of tissue growth and how mechanical forces contribute to growth control in vivo.

Mechanical feedback. How cells sense mechanical forces and coordinate their growth rates is not clear. One way cells could experience tension in a growing organ was provided by the mechanical feedback model: 1) differential growth rates could lead to

local tissue compression as faster-growing cells push against surrounding slower-growing cells, and 2) that this local tissue compression would then decrease growth, thereby restoring even growth rates and minimizing further compression.

I tested the mechanical feedback hypothesis by inducing differential growth in *Drosophila* wing disc epithelia through distinct approaches. I showed that differential growth triggers a mechanical response that lowers cytoskeletal tension along apical cell junctions within faster-growing cells. This reduced tension modulates a biomechanical Hippo pathway, decreasing recruitment of Ajuba LIM protein and the Hippo pathway kinase Warts to junctions, and reducing the activity of the growth-promoting transcription factor Yorkie. This provides the experimental support and a molecular mechanism for lowering growth rates within faster-growing cells by mechanical feedback. Collaborating with another lab, we also proposed a theoretical model to explain the observed reduction of tension within faster-growing clones, supported through simulations using a modified vertex model. Finally, I found that bypassing mechanical feedback induces tissue distortions and inhomogeneous growth. Thus my research further identifies the roles of mechanical feedback in maintaining tissue shape and controlling patterned growth rates during development.

Growth control in vivo. How tissue growth is modulated in vivo is an important but unsolved question in developmental biology. During *Drosophila* wing disc development, the cell proliferation rate gradually slows down. But what contributes to this growth reduction is not clear. Recent studies identified that mechanical stress and Hippo

signaling are required in organ size control. However, how they are regulated in vivo and their contributions to normal development are largely unknown.

I discovered that the activity of the Hippo signaling transcriptional activator Yorkie gradually decreases in the central region of the developing *Drosophila* wing disc. Spatial and temporal changes in Yorkie activity can be explained by changes in cytoskeletal tension and biomechanical regulators of Hippo signaling. These changes in cellular biomechanics correlate with changes in cell density, and experimental manipulations of cell density are sufficient to alter biomechanical Hippo signaling and Yorkie activity. I also related the pattern of Yorkie activity in older discs to patterns of cell proliferation. This study shows that spatial differences in Hippo signaling contribute to spatial patterns of growth in vivo, and provides evidence for a contribution of tissue mechanics to regulating patterns of Yorkie activity and growth during wing development.

Acknowledgement

I would like to thank my advisor, Ken, for his support, training and amazing mentorship over these years. He is an excellent scientist and a great mentor. Thanks for his patience in guiding me to identify and tackle important scientific questions. Thanks for helping me to resolve problems when I had questions in my projects. Thanks for giving me freedom to explore my interest. I learned a lot from him on how to approach research questions, how to be an excellent scientist and an effective person.

I would like to thank my committee members, Dr. Richard Padgett, Dr. Martha Soto and Dr. Sunita Kramer for their support and suggestions about my research and future career. I appreciate for the insightful comments and stimulating discussions on my project. Thanks for being so supportive for my career during my graduate study.

Working in Ken's lab is a really a wonderful experience. I am grateful to my current and former lab members. Thanks to Cordelia for training me with the confocal imaging, dissection, immunostaining, for the suggestions and motivations to my project, and for being a nice collaborator. Thanks for Abhijit for being so approachable and helpful when I joined the lab and for being a friend and encouraging me. Thanks to Shuguo and Gongping for guiding me through the graduate school and giving me suggestions for my career. Thanks to Consuelo and Herve for being such nice collaborators and teachers. Thanks to Mao, Ed, Elmira, Jenny, Jyoti for all the help and support during my graduate school. You bring a lot of joy and energy to the lab.

I also would like to thank our collaborators. Thanks to Dr. Idse Heemskerk and Dr. Boris Shramain for the nice help and collaboration. Thanks for the image analysis, modeling and insightful suggestions to my project.

Thanks to my friends in China, especially Yuchun and Wei. Thanks for being so supportive and help me to go through the difficult times during my graduate study. Thanks to my friends at Rutgers. Thanks to Chenchao and Xilong for helping a lot when I started my graduate school. Thanks to Qing, Chen, Shidi, Chengsheng, Zhichao, Na (I can't list them all) for encouraging me and going to gym together. Thanks to Ying for being like a caring sister and always cheered me up.

Above all, I would like to thank my parents, who always provide love, support, help, and encouragement and have faith in me and in what I am doing. I appreciate for your caring, trust and inspiration.

Table of Contents

Abstract.....	ii
Acknowledgement.....	v
Table of Contents.....	vii
List of Figures.....	xii
Chapter 1.....	1
General Introduction	
Organ size control	2
<i>Drosophila</i> wing imaginal disc	3
Mechanical stress and growth	5
Hippo signaling	7
Figures	10
Figure 1. Organ size control	10
Figure 2. Size-regulatory signaling pathways	11
Figure 3. <i>Drosophila</i> wing imaginal disc	12
Figure 4. The mechanical feedback hypothesis	14

Figure 5. The Hippo signaling network	16
---------------------------------------	----

Figure 6. The biomechanical Hippo signaling	17
---	----

Chapter 2.....18

Differential growth triggers mechanical feedback that elevates Hippo signaling

Summary	19
---------	----

Introduction	20
--------------	----

Results	23
---------	----

Discussion	34
------------	----

Materials and methods	38
-----------------------	----

Figures	47
---------	----

Fig. 1. Overview, and tissue distortion induced by ban-expressing clones	47
--	----

Fig. 2. Reduced tension within faster-growing clones	49
--	----

Fig. 3. Reduced junctional Jub and Wts within faster-growing clones	52
---	----

Fig. 4. Increasing myosin activity suppresses reductions of Jub in faster-growing clones	54
--	----

Fig. 5. Influence of ban-expressing clones on Yki activity	56
--	----

Fig. 6. Influence of wild-type clones in Minute heterozygotes on Yki activity	58
---	----

Fig. 7. Influence of mechanical feedback on cell proliferation	60
Supplemental Fig. S1 Clones lacking evidence of tissue distortion	62
Supplemental Fig. S2 Additional analysis of myosin and F-actin	64
Supplemental Fig. S3 Additional analysis of Jub and Wts	66
Supplemental Fig. S4 Duration of ban clone growth correlates with loss of Jub	69
Supplemental Fig. S5 Additional analysis of Yki activity related to ban-expressing clones	71
Supplemental Fig. S6 Additional analysis of Yki activity	74
Supplemental Fig. S7. Summary and model	76

Chapter 3.....78

The Dynamics of Hippo Signaling during *Drosophila* Wing Disc Development

Summary	79
Introduction	80
Results	82
Discussion	92
Materials and methods	95
Figures	100
Figure 1: Dynamics of Yki activity during wing disc development	100

Figure 2. Cytoskeletal tension declines during wing development	102
Figure 3: Dynamics of biomechanical Hippo signaling during wing disc development	104
Figure 4: Spatial and temporal differences in response to altered tension	106
Figure 5. Influence of cell density on cytoskeletal tension and Hippo signaling	108
Figure 6. Degrading basement membrane does not increase cytoskeletal tension	110
Figure 7: Patterns of cell proliferation during wing disc development	111
Supplement 1: Additional analysis of Yki activity during wing disc development	113
Supplement 2: Additional analysis of the biomechanical Hippo signaling during wing disc development	114
Supplement 3: Relationship of Ds-Fat signaling to patterns of Yki activity	116

Chapter 4.....117

The potential roles of peripodial membrane and hinge on tissue mechanics and wing growth

Summary	118
Introduction	119
Results and discussion	120

Materials and methods	122
Figures	124
Figure 1. <i>Drosophila</i> wing disc structure	124
Figure 2. The role of peripodial membrane on wing size control	126
Figure 3. The roles of hinge on wing pouch growth	128
Chapter 5.....	129
General discussion	
Figure 1. Patterns of Dpp activity and cell proliferation in the wing disc	138
Figure 2. The dynamics of Hippo signaling activity and growth in vivo	139
References.....	140

List of figures

Chapter 1

Figure 1. Organ size control	10
Figure 2. Size-regulatory signaling pathways	11
Figure 3. <i>Drosophila</i> wing imaginal disc	12
Figure 4. The mechanical feedback hypothesis	14
Figure 5. The Hippo signaling network	16
Figure 6. The biomechanical Hippo signaling	17

Chapter 2

Fig. 1. Overview, and tissue distortion induced by ban-expressing clones	47
Fig. 2. Reduced tension within faster-growing clones	49
Fig. 3. Reduced junctional Jub and Wts within faster-growing clones	52
Fig. 4. Increasing myosin activity suppresses reductions of Jub in faster-growing clones	54
Fig. 5. Influence of ban-expressing clones on Yki activity	56
Fig. 6. Influence of wild-type clones in Minute heterozygotes on Yki activity	58
Fig. 7. Influence of mechanical feedback on cell proliferation	60
Supplemental Fig. S1 Clones lacking evidence of tissue distortion	62
Supplemental Fig. S2 Additional analysis of myosin and F-actin	64

Supplemental Fig. S3 Additional analysis of Jub and Wts	66
Supplemental Fig. S4 Duration of ban clone growth correlates with loss of Jub	69
Supplemental Fig. S5 Additional analysis of Yki activity related to ban-expressing clones	71
Supplemental Fig. S6 Additional analysis of Yki activity	74
Supplemental Fig. S7. Summary and model	76

Chapter 3

Figure 1: Dynamics of Yki activity during wing disc development	100
Figure 2. Cytoskeletal tension declines during wing development	102
Figure 3: Dynamics of biomechanical Hippo signaling during wing disc development	104
Figure 4: Spatial and temporal differences in response to altered tension	106
Figure 5. Influence of cell density on cytoskeletal tension and Hippo signaling	108
Figure 6. Degrading basement membrane does not increase cytoskeletal tension	110
Figure 7: Patterns of cell proliferation during wing disc development	111
Supplement 1: Additional analysis of Yki activity during wing disc development	113
Supplement 2: Additional analysis of the biomechanical Hippo signaling during wing disc development	114
Supplement 3: Relationship of Ds-Fat signaling to patterns of Yki activity	116

Chapter 4

Figure 1. <i>Drosophila</i> wing disc structure	124
Figure 2. The role of peripodial membrane on wing size control	126
Figure 3. The roles of hinge on wing pouch growth	128

Chapter 5

Figure 1. Patterns of Dpp activity and cell proliferation in the wing disc	138
Figure 2. The dynamics of Hippo signaling activity and growth in vivo	139

Chapter 1

General Introduction

Organ size control

How organs reach their correct size and shape constitutes one of the key questions in developmental biology, but the mechanism is still a mystery (Hafen and Stocker, 2003; Vogel, 2013). During development, organs need to grow to the appropriate size, and many organs of adult organisms also display homeostatic size-control mechanisms. Decades of experimentation have identified multiple regulators of organ size: both organ-extrinsic and intrinsic factors could regulate the size of organs (Irvine and Harvey, 2015). Organ-extrinsic regulators provide systemic information about the organism status, like nutrition and developmental stage (Boulant et al., 2015). For example, in *Drosophila*, starvation or mutations of components affecting nutrition pathways can lead to small, but well-proportioned flies (Stocker and Hafen, 2000). On the other hand, organ-intrinsic regulators act in a local manner to modulate the size and shape of individual organs (Vollmer et al., 2017). In 1931, zoologists Victor C. Twitty and Joseph L. Schwind transplanted limbs between different species of salamander (Twitty and Schwind, 1931). Despite the early stage of transplantation during development, the limb still grows to the size of their own species, not the host body (Figure 1). In *Drosophila*, when immature wing discs were transplanted into the abdomen of adult females, they still grew to their appropriate size, despite the extended growth period in new locations (Bryant and Levinson, 1985). Therefore, organs must have intrinsic mechanisms for them to know when to stop growing.

In the last decades, numerous signaling pathways that respond to the intrinsic or extrinsic factors have been identified (Gokhale and Shingleton, 2015) (Figure 2). For example, the Insulin/Insulin-like growth factor (IGF) signaling pathway regulates growth in response

to IGFs in a nutrition dependent manner. The TOR signaling pathway also regulates growth with respect to nutrition, cellular energy, and oxygen. Organ patterning signaling like Wnt and TGF- β control both cell positional information and growth. And Hippo signaling, which will be discussed in detail later, links cell-cell contact and mechanical stress to growth. In addition to the biochemical signals, cells in a developing organ also experience a mechanical environment in which they are subject to forces through their contact with neighboring cells and the extracellular matrix (Eder et al., 2017; Irvine and Shraiman, 2017; LeGoff and Lecuit, 2016). Emerging evidence suggests that tissue mechanics affects growth. Reversely, the mechanical state of a tissue is also modulated by the patterns of growth. Tissue growth and tissue mechanics need to be coordinated for the organs to reach their appropriate size (LeGoff and Lecuit, 2016).

***Drosophila* wing imaginal disc**

The *Drosophila* wing imaginal disc has been extensively used to study growth regulation in vivo (Hariharan, 2015). It is a cluster of undifferentiated epithelial cells that will give rise to the wing and notum of the fly. During larval stages, wing disc grows from 30-50 cells to 30,000-50,000 cells (Milan et al., 1996; Worley et al., 2013). In wing disc, the region that will give rise to the adult wing is called wing pouch, while the regions that will become hinge and body wall in adult are called hinge and notum, respectively. The disc comprises a columnar cell monolayer covered by a squamous epithelium known as the peripodial membrane (Figure 3A). Wing disc can be subdivided into distinct lineage-restricted compartments: the anterior compartment and posterior compartment as well as the dorsal compartment and ventral compartment (Figure 3B). Signaling between cells in

different compartments establishes specialized cells along the compartment boundaries that organize further wing patterning and growth (Lawrence and Struhl, 1996).

Both extrinsic and intrinsic factors regulate the wing size. For example, systematic signals like nutrition and hormones regulate wing growth (Stocker and Hafen, 2000). Wing growth also depends on local growth factors. One of the most important local factors is Decapentaplegic (Dpp; a bone morphogenetic protein family member), which is secreted by a stripe of cells near anterior-posterior compartment boundary of the developing wing disc, and then spreads out to more lateral cells and forms a gradient (Irvine and Harvey, 2015; Restrepo et al., 2014) (Figure 3C). Thus Dpp is considered as a morphogen that distributes in a concentration gradient across a tissue and specifies distinct fates as a function of its concentration (Tabata, 2001). Dpp is required for wing growth and overexpression of Dpp leads to increased growth (Spencer et al., 1982; Zecca et al., 1995). Interestingly, despite the gradient of Dpp activity, the growth is uniformly distributed for most stages of wing development (Milan et al., 1996) (Figure 3D and E). Models involving Dpp gradient slope (Rogulja and Irvine, 2005), the dynamic Dpp increases (Wartlick et al., 2011) and different responses to Dpp in different regions (Restrepo et al., 2014) have been proposed to explain this dilemma. In addition, mechanical stress models have also been suggested to explain the uniform growth pattern: the mechanical compression in the center of wing disc could counterbalance the growth promoting effects of Dpp, thus this results in uniform growth (Aegerter-Wilmsen et al., 2007; Aegerter-Wilmsen et al., 2012; Hufnagel et al., 2007; Shraiman, 2005). Growth rate is also decreased from early larval development to later larval development (Martin et al., 2009; Wartlick et al., 2011) (Figure 3D and E). Mechanisms that modulate this

reduction of growth are not well understood. And both the dynamics of morphogens and the changes in mechanical stress during wing disc development have been proposed to explain this growth rate reduction (Buchmann et al., 2014; Irvine and Harvey, 2015; Shraiman, 2005). However, whether and how mechanical stress contributes to the uniform growth and reduction in growth rate has not been experimentally tested.

Mechanical stress and growth

Mechanical stress has been increasingly appreciated as an important regulator of tissue growth. In vitro, mechanical stress can influence proliferation of cultured cells (Curtis and Seehar, 1978; Huang and Ingber, 1999). For many cell types, stretching stimulates cell proliferation, whereas compression inhibits it (Brunette, 1984; Codelia et al., 2014; Eder et al., 2017; Helmlinger et al., 1997). In addition, patterns of cell proliferation were correlated with patterns of mechanical stress by culturing cells on micropatterned substrates with distinct geometries. Contact inhibition is a phenomenon when cultured cells stop proliferating when they grow at high cell densities (Holley and Kiernan, 1968). Contact inhibition depends not only on cell contact but also on crowding (Streichan et al., 2014). Mechanical stress has been proposed to contribute to contact inhibition (Aragona et al., 2013; McClatchey and Yap, 2012).

Due to the inaccessibility of developing organs and lack of experiment tools to measure and manipulate tension, how mechanical force modulates growth in vivo remains less clear. Theoretically, how cells in a growing tissue sense mechanical stress and coordinate

their growth rates have been suggested by the mechanical feedback model (Shraiman, 2005) (Figure 4). In this model, Dr. Shraiman suggested that differential growth could lead to local tissue compression as faster-growing cells push against surrounding slower-growing cells; this tissue compression could feedback into those cells to slow down growth, thereby restoring even growth rates and reducing further compression. Mechanical feedback is thus a negative feedback mechanism that limits the extent to which a population of cells can overgrow, potentially providing a homeostatic mechanism that ensures cells proliferate at similar rates to minimize tissue distortion. In this context, the mechanical feedback hypothesis has been proposed to explain the homogeneous growth rates despite the uneven distribution of growth factors like Dpp. Moreover, as cells becoming increasingly crowded in the later stages of development, has also been suggested as an explanation for why organs stop growing when they reach their final size (Hufnagel et al., 2007) (Figure 4D and E). Indeed, several models involving mechanical feedback or mechanical stress on *Drosophila* wing size control have been proposed (Aegerter-Wilmsen et al., 2007; Aegerter-Wilmsen et al., 2012; Hufnagel et al., 2007).

The past decade has witnessed exciting progress on understanding the molecular mechanisms that mediate mechanical stress to growth. Among them, Hippo signaling is essential for transducing the mechanical input of cells to gene transcription that affects growth. I will talk about Hippo signaling in detail in the next section. Taking advantage of the molecular understanding of mechanical transduction pathways, I tested the mechanical feedback hypothesis and evaluated if mechanical stress contributes to normal growth *in vivo*.

Hippo signaling

Hippo signaling has emerged as an essential growth control pathway from arthropods to vertebrates (Pan, 2010; Yu et al., 2015) (Figure 5). It is a conserved signal transduction network and was first discovered in *Drosophila* through the overgrowth phenotypes associated with mutations in pathway components (Pan, 2010; Reddy and Irvine, 2008). Hippo signaling has been shown to be involved in many physiological and pathological conditions, such as organ size control, tissue homeostasis, and cancer (Yu et al., 2015). The central core of this pathway comprises of a kinase cascade including the NDR family kinase Warts (Wts in *Drosophila*, and LATS1 and LATS2 in mammals), Hippo (Hpo), and the adaptor proteins Salvador (Sav) and Mob as tumor suppressor (Mats). Most upstream components of Hippo signaling converge on modulation of Wts (Meng et al., 2016). The primary target of this kinase cassette is the transcriptional co-activator Yorkie (Yki in *Drosophila*, YAP and TAZ in mammals) (Huang et al., 2005). Wts phosphorylates and inhibits Yki by promoting its cytoplasmic localization (Oh and Irvine, 2008, 2010). When entering the nucleus, Yki transcribes the target genes with several DNA-binding transcription factors like Scalloped (Sd), Homothorax, and Mad, driving a transcriptional program that specifies cell growth and proliferation, as well as a number of cell fate decisions (Irvine and Harvey, 2015; Meng et al., 2016; Yu and Guan, 2013).

One remarkable feature of Hippo signaling is that it serves as an integrator of growth control signals involving both biochemical and biomechanical inputs (Irvine, 2012; Meng et al., 2016; Sun and Irvine, 2016). Diverse signals from positional information,

organismal nutrition, developmental stage, cell contacts and mechanical stress regulate or have cross talk with Hippo signaling. Hippo signaling appears to be predominantly regulated by a network of proteins that affect cell adhesion, polarity, and the actin cytoskeleton. Many of the upstream regulators of the pathway, such as Expanded, Merlin and angiomotins, localize to cell-cell junctions, and they assemble into protein complexes that promote Hippo signaling activation (Sun and Irvine, 2016). In addition, growth factors like EGF and G-protein coupled receptor (GPCR) signaling could regulate the Hippo pathway (Fan et al., 2013; Yu et al., 2012). Nutrient-sensing and metabolic pathways could also modulate Yki activity (Santinon et al., 2016). And the cross-talk between tissue patterning signaling (like Dpp) and Hippo signaling has been identified (Irvine and Harvey, 2015).

Importantly, mechanical stress and the cytoskeleton have emerged to be the essential upstream regulators of Hippo signaling and Yki activity (Schroeder and Halder, 2012; Sun and Irvine, 2016). Recent studies suggested that flow-induced shear stress, tension sensed at focal adhesion and tension sensed at adherens junctions could modulate Yki activity (Dupont, 2016; Low et al., 2014; Sun and Irvine, 2016). For example, Yki activity is affected by the attachment to the ECM (extracellular matrix) (Dupont, 2016; Dupont et al., 2011; Kim and Gumbiner, 2015; Zhao et al., 2012). F-actin levels, which are sensitive to the mechanical environment, could modulate Yki/Yap1 activity (Aragona et al., 2013; Fernandez et al., 2011; Sansores-Garcia et al., 2011). The spectrin cytoskeleton has also been shown to regulate Hippo signaling, but the mechanisms remain unclear (Deng et al., 2015; Fletcher et al., 2015; Wong et al., 2015).

Moreover, epithelial cells are also mechanically coupled to each other at adherens junctions, which are attached to the actin cytoskeleton. Thus the adherens junctions are well-suited for mechanotransduction (Lecuit and Yap, 2015). Indeed, alterations in adherens junction components influence Yki activity (Kim et al., 2011; Schlegelmilch et al., 2011; Yang et al., 2015). And tension at adherens junctions can also promote Yki activity (Benham-Pyle et al., 2015; Rauskolb et al., 2014). Recently, cytoskeletal tension was identified to regulate Hippo signaling through an Ajuba-Warts complex (Rauskolb et al., 2014) (Figure 6). The Wts inhibitor LIM domain protein Ajuba (Jub) can be recruited to the adherens junctions with Wts in a tension-dependent manner. The recruitment of Jub to adherens junctions is mediated through α -catenin, which can act as a mechanotransducer (Yonemura et al., 2010). When the cytoskeletal tension is high, Jub and Wts are recruited to the adherens junctions, Yki is not inhibited and thus enters the nucleus to promote transcription and growth. When the cytoskeletal tension is low, Jub and Wts move away from the junctions, Yki is phosphorylated and excluded from the nucleus. Therefore the growth is low (Rauskolb et al., 2014).

Despite these encouraging progress in the past years, most of previous studies on Hippo signaling regulation were based on genetic manipulations or drug treatment in cell cultures or in vivo. Therefore, how Hippo signaling activity is regulated during normal development is largely unknown. Moreover, how mechanical stress and Hippo signaling contribute to normal growth in vivo and size control is not clear.

Figure 1. Organ size control

Victor C. Twitty and Joseph L. Schwind removed embryonic tissue that would become a leg in the large salamander species, *Ambystoma tigrinum*, and transplanted it into the embryo of a smaller species, *Ambystoma punctatum*. Despite the early stage of the transplant—before limb buds even appear in the subsequent larvae—the legs grew to the size that they would have on their original body; small salamanders ended up with a longer-than-normal leg, and large salamanders with a short leg. Image from (Twitty and Schwind, 1931).

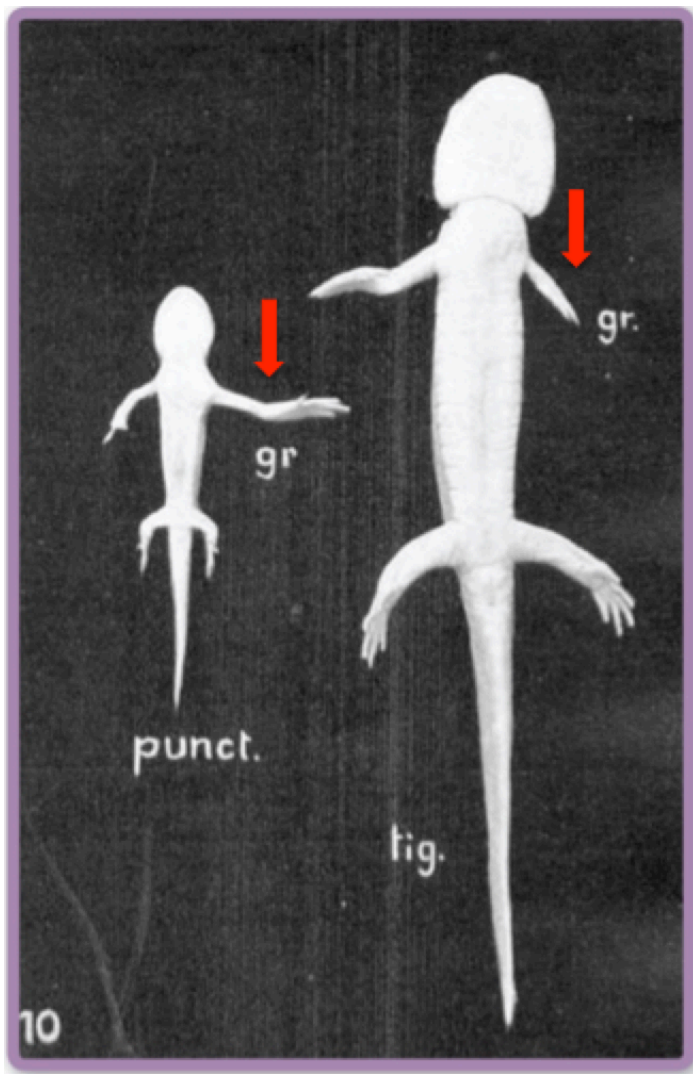


Figure 2. Size-regulatory signaling pathways

(a) The insulin/IGF1-signaling (IIS) pathway. (b) The RAS/RAF/MAPK-signaling pathway. (c) The TOR-signaling pathway. (d) The Hippo-signaling pathway. (e) The JNK-signaling pathway. Image from (Gokhale and Shingleton, 2015).

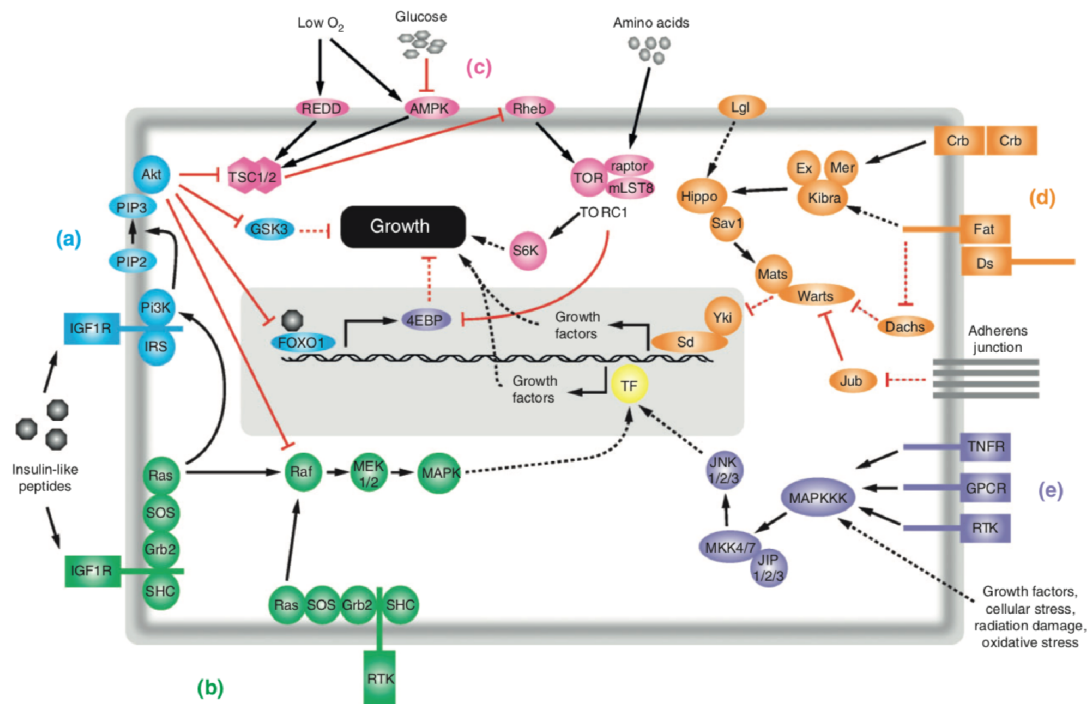


Figure 3. *Drosophila* wing imaginal disc

(A) Top and lateral view of the wing imaginal disc at third instar. The wing pouch will develop into the wing blade of the adult fly. The wing pouch is surrounded by the hinge tissues and the region becomes body wall in adult is called notum. Disc comprises a columnar cell monolayer covered by a squamous epithelium known as the peripodial membrane. Pictures modified from (Eder et al., 2017) (B) Wing disc can be subdivided into distinct lineage-restricted compartments: the anterior compartment and posterior compartment as well as the dorsal compartment and ventral compartment. (C) The morphogen Dpp is secreted by a stripe of cells near the anterior-posterior compartment boundary of the developing wing disc, and then spreads out to more lateral cells and forms a gradient. (D and E) Wing disc proliferation pattern. For most stages of development, proliferation is relatively uniform across the disc. The proliferation rate decreases from early (D) to late (E) stage. (B-E) Pictures adapted from (Irvine and Harvey, 2015).

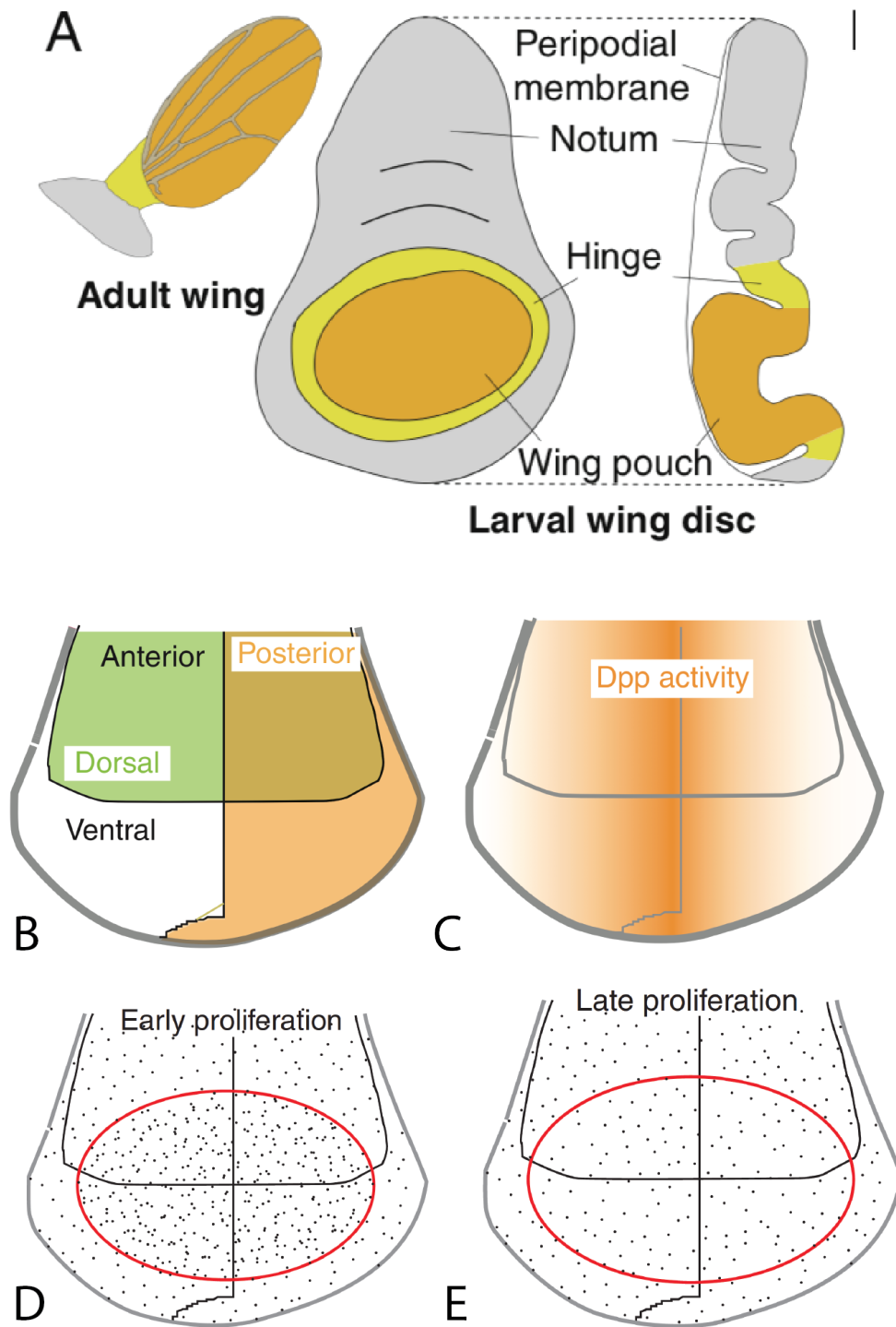
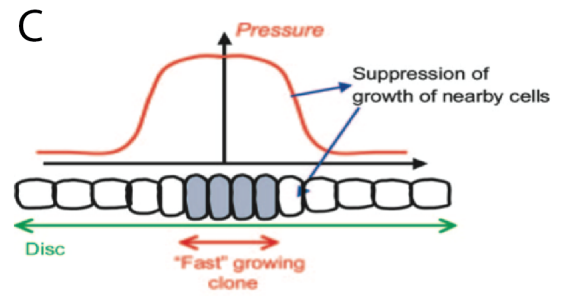
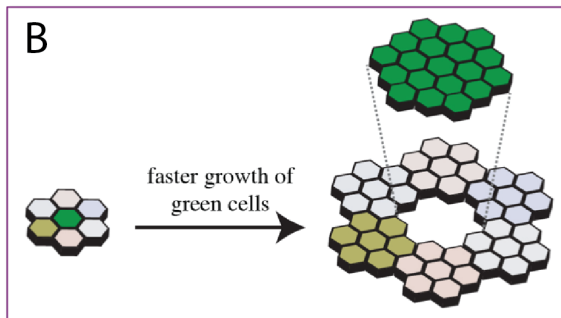
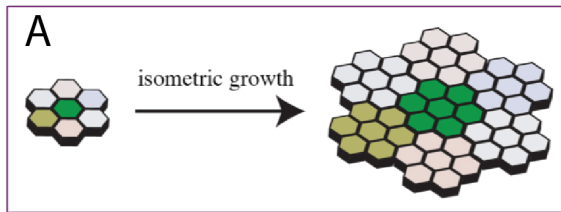
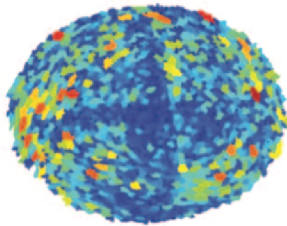


Figure 4. The mechanical feedback hypothesis

(A) A clone of cells grows at the same rate as neighboring cells. The tissue could expand nicely. (B and C) A clone of cells grows at faster rate than the neighboring cells. The mechanical feedback hypothesis suggests that these faster-growing cells are under compression; this compression could feedback in to the cells to slow down the growth rate. (C) is modified from (Shraiman, 2005) (D and E) Cell apical area map of wing disc from early (D, 84h after egg laying) and late (E, 120h after egg laying) stage. Red means the cell is large while blue means the cell is small. Cell apical areas become smaller in older disc, especially the central region. Pictures adapted from (Mao et al., 2013). The mechanical feedback hypothesis suggests that the mechanical compression in the central wing disc would counterbalance the growth factors, which have higher concentration in the center. Therefore the growth is homogenous across the wing disc. The mechanical feedback hypothesis also proposes that the increasing crowding from early to late stage could slow down cell growth rates, thus help to determine the organ size.



D 84 h



E 120 h

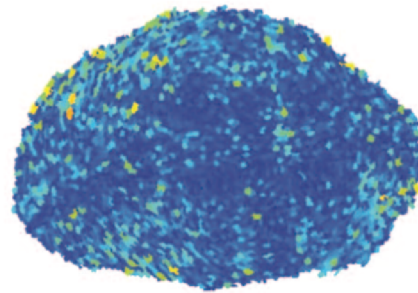


Figure 5. The Hippo signaling network

(A) Hippo signaling in *Drosophila*. The *Drosophila* Hippo pathway is regulated by cell-adhesion molecules (Ed), determinants of cell polarity (Crb, Fat/Ds, Scrib complex), mechanical cues and others. (B) Hippo signaling in mammals. The mammalian Hippo pathway can be regulated by (1) determinants of cell polarity and cell-cell junctions, (2) mechanical cues, (3) soluble factors and metabolic status. (A and B) modified from (Yu et al., 2015) (C) A normal (left) and a Yki-overexpressing (right) *Drosophila* wing imaginal disc. (D) A normal (left) and a YAP-overexpressing (right) mouse liver. (C and D) pictures modified from (Pan, 2010).

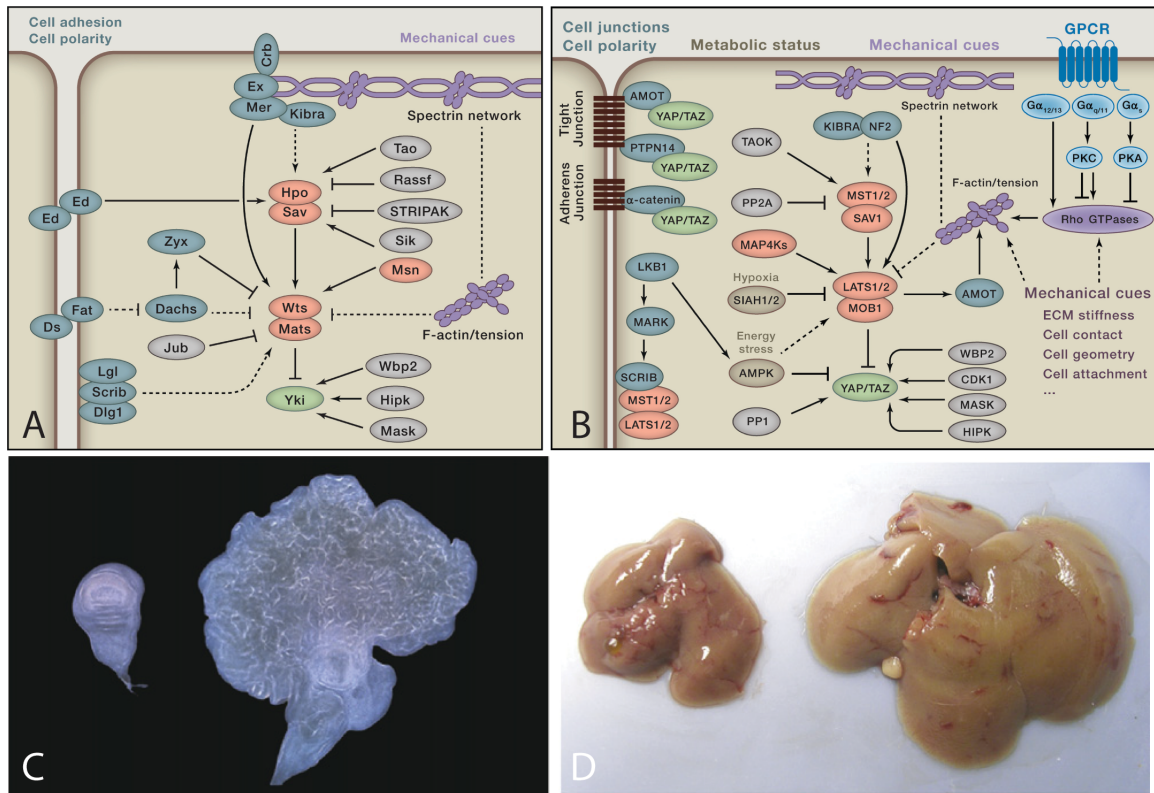
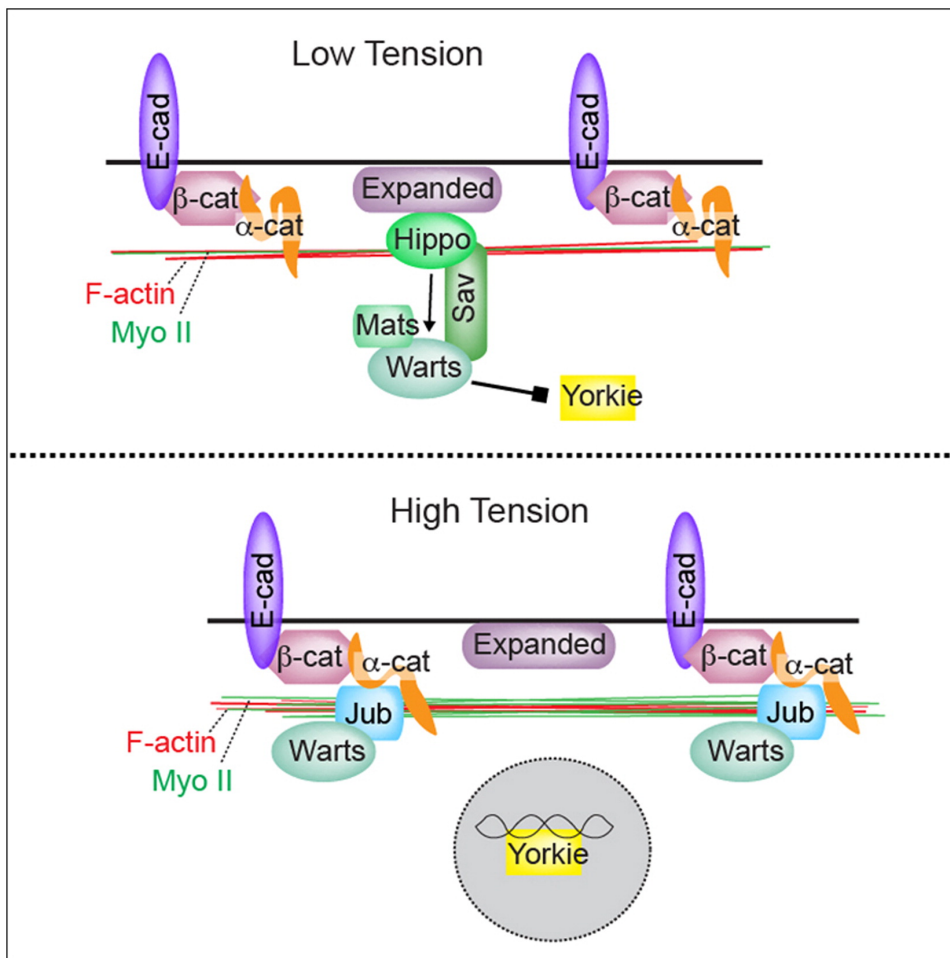


Figure 6. The biomechanical Hippo signaling

Cytoskeletal tension induces recruitment of Ajuba LIM protein (Jub) to α -catenin, and thence recruitment of Wts to Jub. Jub is an inhibitor of Wts, and this tension-dependent corecruitment of Jub and Wts to adherens junctions is associated with reduced Wts activity, and hence increased Yki activity. Conversely, under conditions of lower cytoskeletal tension, recruitment of Wts and Jub to adherens junctions is decreased, Wts activity is increased, and consequently Yki activity is decreased (Rauskolb et al., 2014).



Chapter 2

Differential growth triggers mechanical feedback that elevates Hippo signaling

Results described in this chapter were published in:

Pan Y, Heemskerk I, Ibar C, Shraiman BI, Irvine KD. Differential growth triggers mechanical feedback that elevates Hippo signaling. Proc Natl Acad Sci U S A. 2016 Oct 26. pii: 201615012.

Author contributions:

Yuanwang Pan, Boris Shraiman and Kenneth Irvine designed research. Yuanwang Pan, Idse Heemskerk, Consuelo Ibar, and Boris Shraiman performed research. Yuanwang Pan, Idse Heemskerk, Consuelo Ibar, and Kenneth Irvine analyzed data. Yuanwang Pan, Idse Heemskerk, Boris Shraiman and Kenneth Irvine wrote the paper. Cordelia Rauskolb performed the EdU labeling experiments. Consuelo Ibar performed the experiments on Ras^{V12} clones. Idse Heemskerk analyzed the anisotropy of clones and performed the simulations. All other experiments were performed by Yuanwang Pan.

Summary

Mechanical stress can influence cell proliferation in vitro, but whether it makes a significant contribution to growth control in vivo, and how it is modulated and experienced by cells within developing tissues, has remained unclear. Here I report that differential growth reduces cytoskeletal tension along cell junctions within faster-growing cells. Together with my collaborators, we propose a theoretical model to explain the observed reduction of tension within faster-growing clones, supporting it by computer simulations based on a generalized vertex model. This reduced tension modulates a biomechanical Hippo pathway, decreasing recruitment of Ajuba LIM protein and the Hippo pathway kinase Warts, and decreasing the activity of the growth-promoting transcription factor Yorkie. These observations provide a specific mechanism for a mechanical feedback that contributes to evenly distributed growth, and I show that genetically suppressing mechanical feedback alters patterns of cell proliferation in the developing *Drosophila* wing. By providing experimental support for the induction of mechanical stress by differential growth, and a molecular mechanism linking this stress to the regulation of growth in developing organs, my results confirm and extend the mechanical feedback hypothesis.

Introduction

Growth regulation is needed to form organs of correct size and proportion, but the mechanisms that define organ and organism size remain poorly understood (Hafen and Stocker, 2003). Cells in a developing organ are exposed to multiple growth factors, at concentrations that can vary depending upon cellular location, developmental stage, and nutrition. Signaling pathways that conduct these biochemical signals have been extensively studied, and in many cases their contributions to growth control are well characterized. However, in addition to the biochemical environment, cells in a developing organ also experience a mechanical environment in which they are subject to forces through their contact with neighboring cells and the extracellular matrix. The mechanical environment has also been proposed to modulate organ growth, yet how this occurs and what it contributes to in vivo growth regulation remains unclear.

The Hippo signaling pathway plays an essential role in regulating organ growth from arthropods through vertebrates (Meng et al., 2016; Yu and Guan, 2013). One remarkable feature of Hippo signaling is its role as an integrator of growth control signals (Fig. 1A). Indeed Hippo signaling is influenced by or cross-talks with multiple biochemical pathways that can act as general growth regulators, or promote growth linked to positional information, nutritional status, or developmental stage. Hippo signaling is also affected by contacts with neighboring cells and the extracellular matrix, and by mechanical stress (Sun and Irvine, 2016). However, most prior studies of Hippo pathway regulation by mechanical cues have examined it in the context of in vitro models, or employed non-physiological manipulations such as drugs or mutations that disrupt the cytoskeleton, leaving unanswered the question of how Hippo signaling might

modulate growth in response to mechanical stresses that cells experience during developmental or physiological processes.

Hippo signaling regulates growth by controlling a transcriptional co-activator protein, Yorkie (Yki) (Huang et al., 2005; Oh and Irvine, 2010) (Fig. 1A). Yki activity is down-regulated through phosphorylation by the Warts (Wts) kinase, which promotes cytoplasmic localization of Yki. Wts is regulated in several ways, including phosphorylation by Hippo (Wu et al., 2003), regulation of Wts abundance (Cho et al., 2006), regulation of Wts localization (Sun et al., 2015; Yin et al., 2013), and regulation of Wts interaction with co-factors and inhibitors (Das Thakur et al., 2010; Lai et al., 2005; Rauskolb et al., 2011; Rauskolb et al., 2014; Vrabioiu and Struhl, 2015). We recently defined a mechanism for biomechanical regulation of Hippo signaling in which cytoskeletal tension induces recruitment of Ajuba LIM protein (Jub) to α -catenin, and thence recruitment of Wts to Jub (Rauskolb et al., 2014). Jub is an inhibitor of Wts (Das Thakur et al., 2010; Rauskolb et al., 2011), and this tension-dependent co-recruitment of Jub and Wts to adherens junctions is associated with reduced Wts activity, and hence increased Yki activity (Rauskolb et al., 2014), at least in part because it prevents Wts from moving to sites where Wts gets activated (Sun et al., 2015). Conversely, under conditions of lower cytoskeletal tension, recruitment of Wts and Jub to adherens junctions is decreased, Wts activity is increased, and consequently Yki activity is decreased.

A consideration of the mechanical stresses cells might experience in a growing organ and their influence on growth was provided by the mechanical feedback model (Shraiman, 2005). This model argued that differential growth could lead to local tissue

compression as faster-growing cells push against surrounding slower-growing cells, and proposed that this compression might then decrease growth, thereby restoring even growth rates and reducing further compression. Mechanical feedback is thus a negative feedback that limits the extent to which a population of cells can overgrow, potentially providing a homeostatic mechanism that ensures cells proliferate at similar rates to minimize tissue distortion. In this context, it has been suggested that it might explain how cell proliferation in organs like the *Drosophila* wing can be homogeneous despite inhomogeneous distributions of growth factors. The hypothesis that growth-induced compression inhibits further growth, along with the observation that cells are more tightly packed at later stages of development, has also been suggested as an explanation for why organs stop growing when they reach their final size (Aegerter-Wilmsen et al., 2007; Aegerter-Wilmsen et al., 2012; Hufnagel et al., 2007; Shraiman, 2005). While mechanical feedback provides an attractive hypothesis for contributions of mechanics to organ size control, it has lacked direct experimental support or a molecular mechanism. Here, I use the wing imaginal discs of *Drosophila* (Fig. 1B) to perform the first experimental tests of mechanical feedback. Wing disc cells form a pseudostratified epithelial monolayer, connected to each other at apical adherens junctions, which are attached to an actin-myosin network that is under tension (Farhadifar et al., 2007). My analysis takes advantage of recent progress in characterizing Jub-mediated biomechanical Hippo signaling to define three critical stages of mechanical feedback (Fig. 1C). I first test the prediction that differential growth can lead to mechanical stress, and observe that accumulation of stress is most pronounced under conditions where mechanical feedback has been bypassed. I then show that mechanical stress induced by differential growth is

associated with reduced cytoskeletal tension within faster-growing cells, and explain this using a theoretical model of epithelial mechanics that incorporates adaptive tension. I next show that the Jub biomechanical Hippo pathway is influenced by differential growth through these associated reductions in cytoskeletal tension. Finally, I use this new understanding of mechanical feedback to demonstrate its role in modulating cell proliferation during wing development. These studies confirm the mechanical feedback hypothesis, provide a mechanistic basis for mechanical feedback, and argue that mechanical feedback contributes to growth regulation in vivo.

Results

Reduced cytoskeletal tension within faster-growing clones

One prediction of mechanical feedback is that a coherent population of cells growing at a faster rate than surrounding cells will become compressed (Shraiman, 2005). We tested this by using UAS-Gal4 driven expression to create clones of faster-growing cells. The microRNA gene *bantam* (*ban*) promotes growth in *Drosophila* (Brennecke et al., 2003) (Fig. S1A). Moreover, *ban* is a key downstream target of Yki, and *ban* can promote growth even in the absence of Yki (Nolo et al., 2006; Thompson and Cohen, 2006). Thus, if mechanical feedback acts through Yki, forced expression of *ban* under UAS-Gal4 control could bypass mechanical feedback, enabling growth to continue and tissue compression to accumulate. Indeed, *ban*-expressing clones in the wing disc deform surrounding cells, visible as anisotropic distortions with elongation aligned parallel to the edges of *ban*-expressing clones (Fig. 1D,G). Radial compression and azimuthal elongation of cells is exactly the pattern of deformation expected outside of over-growing

regions, as follows from continuum elasticity considerations elaborated in the Supplementary Text. Tissue distortion is also evident through a widening of clones between the apical and basal surfaces, and invagination of the apical and basal surfaces (Fig. 1E,F). All of these distortions are most evident near the center of the disc, where cells are already more compressed (LeGoff et al., 2013; Mao et al., 2013). Similar distortions have been reported for clones of cells expressing activated-Yki, or mutant for *wtls* (Heemskerk et al., 2014; LeGoff et al., 2013; Mao et al., 2013), which should also bypass any mechanical feedback that depends upon regulation of Yki activity.

Over-expression of *ban*, or expression of an activated form of Ras (Ras^{V12}) that promotes growth (Karim and Rubin, 1998), also result in a consistent reduction in apical accumulation of Non-Muscle Myosin II (myosin, visualized using GFP fusions to myosin regulatory light chain, Sqh, or to myosin heavy chain, Zip) (Figs 2A,F,G, S2B). Reduced myosin activity can also lead to reduced F-actin accumulation in wing discs (Rauskolb et al., 2014), and consistent with this, we observed modest reductions in F-actin levels within faster-growing clones (Fig. S2B,E,F). As myosin both creates and responds to tension (Kasza and Zallen, 2011), the reduction in its levels implies that cytoskeletal tension is lower within these fast-growing clones.

Expression of *ban* or Ras^{V12} in clones results in fast-growing cells surrounded by wild-type cells. Differential growth can also be introduced by creating a mosaic between wild-type cells and slow-growing cells. This can be done in *Drosophila* using *Minute* mutations, which are mutations in genes required for ribosome function that cause a dominant slow-growth phenotype (Marygold et al., 2007). Moreover, since *Minute* mutations simply reduce the capacity for protein synthesis, they are not expected to

directly increase myosin levels. Nonetheless, wild-type cells surrounded by cells heterozygous for *Minute* mutations exhibit lower apical and junctional myosin accumulation than their *Minute*/+ neighbors (Fig. 2B,G S2B). Thus, cells growing at a faster rate than their neighbors consistently have reduced levels of myosin. Wild-type clones within *Minute*/+ discs are not, however, associated with anisotropy of neighboring cells or invaginations of the disc epithelium (Fig. S1B,C), which might reflect a sensitivity to mechanical feedback that reduces growth rates to prevent extreme tissue compression.

To confirm that the reduced myosin accumulation observed within faster-growing clones is associated with decreased junctional tension, we used a junction cutting assay in which a laser is used to sever cell-cell junctions (Farhadifar et al., 2007). The retraction velocities of vertices neighboring the cut were lower within *ban*-expressing clones than in comparable regions of the wing disc without clones, and lower within *wild-type* clones than in comparable regions with *Minute*/+ cells (Fig. 2E, Supplemental videos 1, 2). Thus, differences in growth rates between neighboring cell populations can lead to decreased tension along cell junctions within the faster-growing cells.

To further confirm that altered myosin levels occur as a consequence of differential growth, we suppressed the overgrowth of *ban*-expressing clones by using RNAi to decrease the expression of either of two different genes that are required for normal clone growth: *E2f1* and *Myc* (Johnston et al., 1999; Neufeld et al., 1998). In both cases, the reduction of myosin in *ban*-expressing clones was suppressed (Fig. 2C,D,G, S2B), as was distortion of the disc epithelium (Fig. S1D). Conversely, RNAi of *E2f1* or *Myc* in otherwise wild-type cells did not significantly affect myosin (Fig S2B-D). Thus,

reduced levels of myosin in ban-expressing clones can be attributed to their elevated growth rates.

A model of epithelial mechanics that produces decreased tension in compressed cells

Our observations raised the question of whether compression of faster-growing cells could reduce their cytoskeletal tension. For an isolated cell, cell shape reflects a balance between (myosin-generated) cortical tension and intracellular pressure (reflecting compression of cellular components) (Fig. 2H). Within an epithelium, cells also experience external forces arising from interaction with neighboring cells in the tissue. If these external forces are compressive, then one would expect cell areas to become smaller than their intrinsic size (as defined by the balance between cortical tension and intracellular pressure in the absence of external forces). However, live tissue does not behave as a simple elastic medium as cells also adapt their mechanical properties to external forces. For example, when an external force pulls on cells, they increase actin-myosin contractility (Kasza and Zallen, 2011). Conversely, when subject to compressive forces, as is the case for faster-growing clones constrained by surrounding slower-growing cells, then we expect that the same cellular response would cause cells to reduce their cytoskeletal tension. In both cases, the compensating response reduces cell deformation; we demonstrate this explicitly by formulating and analyzing a physical model of cell area with adaptive response to external mechanical stress (see Supplemental Text).

To illustrate the sufficiency of this model to explain the reduced tension within faster-growing clones, we developed a simulation of a two-dimensional epithelial sheet

containing a clone growing more rapidly than the surrounding cells. The simulation is based on a vertex model representing epithelial tissue as a polygonal array of cells, with cell geometry determined by minimization of mechanical energy (representing intracellular pressure, cortical tension and mechanical interaction between adjacent cells). Cell growth and proliferation is represented by continuously increasing the intrinsic area of each cell followed, stochastically, by cell division. In contrast with earlier vertex models (Farhadifar et al., 2007), we allow for an adaptive cytoskeletal response, decreasing cortical tension proportionally with increasing pressure acting on a cell. The model of adaptive cytoskeletal response used here is consistent with the recently proposed “Active Tension Network” theory (Noll et al., 2017), which postulated that the rate of myosin recruitment (or release) into the actin-myosin cortex and concomitant changes in cortical tension is modulated by changes in mechanical stress. Model simulations considering cell growth and resulting heterogeneity of pressure confirm that differential clone growth leads to higher cellular pressure, and lower cortical tension, within faster-growing cells (Fig. 2I, Supplemental videos). This theoretical description of epithelial mechanics thus reproduces the lower tension observed within faster-growing clones.

In the model simulations, tension along clone boundaries is intermediate between the lower tension in the interior of clones and higher tension outside of clones, and it is also influenced by clone and cell shapes (Fig. 2I). This relatively higher tension at clone edges as compared with the clone interior is consistent with experimental observations that the area of reduced myosin sometimes (9/30 clones scored) appears smaller than the area of the clone (Fig. 2A).

Faster-growing cells reduce Wts and Jub localization to adherens junctions

Changes in cytoskeletal tension induced by genetic manipulations can modulate Hippo signaling through the tension-dependent recruitment of Jub to adherens junctions (Rauskolb et al., 2014). To determine whether the reduced tension observed within faster-growing clones is sufficient to alter Jub-recruitment, we assayed Jub localization using a genomic Jub:GFP line (Sabino et al., 2011). Indeed, Jub levels at adherens junctions were lower within clones of faster-growing cells as compared to their neighbors. Reduction in Jub was most obvious within *ban*-expressing clones (Fig 3A,J, S3J), but was also visible within *Ras*^{v12}-expressing clones and wild-type clones surrounded by *Minute*/+ cells (Fig. 3B,C,J, S3J). Thus, differences in growth rates between neighboring populations of disc cells are sufficient to reduce cytoskeletal tension within faster-growing clones in a manner and to a degree that decreases the recruitment of Jub to adherens junctions. As with the reduction in myosin, the area of lower Jub levels sometimes (7/28 clones scored) appeared slightly smaller than the clone (Fig. 3A). This is generally consistent with our modeling of tension in response changes in pressure, which results in intermediate levels of tension along clone borders (Fig. 2I).

We confirmed that this influence of *ban*-expressing clones on Jub is largely due to their elevated growth rates by suppressing their overgrowth through knockdown of *Myc* or *E2f1*. This largely reversed the lower levels of junctional Jub (Fig. 3D,E,J, S3J), whereas knockdown of *Myc* or *E2f1* on their own did not visibly influence Jub (Fig. S3E,F,J). Similarly, suppressing the growth differential between wild-type clones and *Minute*/+ neighbors by replacing wild-type clones with *ban*^{ΔI} mutant (slow-growing)

clones (Brennecke et al., 2003) suppressed the decrease in Jub levels associated with non-*Minute* clones in *Minute/+* discs (Fig. 3F,J, S3J), whereas *ban* ^{ΔI} mutant clones in a wild-type background did not visibly affect Jub levels (Fig. S3D,J). These observations confirm that elevated growth rates in clones are sufficient to lower Jub recruitment to adherens junctions within the faster-growing cells.

To confirm that the reductions in junctional levels of Jub within faster-growing cells were also associated with a reduction in co-recruitment of Wts, we monitored Wts localization using a genomic Wts:GFP line (Rauskolb et al., 2014). Wts levels at adherens junctions were lower within *ban*-expressing clones, Ras^{V12}-expressing clones, and wild-type clones surrounded by *Minute/+* cells (Fig 3G-I,K, S3J). Thus, a variety of manipulations that alter growth rates through distinct biochemical mechanisms all trigger a similar biomechanical response, which includes reduced junctional accumulation of both Jub and Wts.

To confirm that this decreased Jub and Wts accumulation within faster-growing clones is due to the decreased cytoskeletal tension that we detected, as opposed to other potential effects of these genotypes, we increased cytoskeletal tension within faster-growing clones by expressing an activated form of the myosin regulatory light chain (Sqh.EE) (Winter et al., 2001). Indeed, co-expression of Sqh.EE suppressed the reduction of junctional Jub within *ban*- or Ras^{V12}-expressing clones, as well as within *wild-type* clones in *Minute/+* discs (Fig. 4A-D,E). For *wild-type* clones in *Minute/+* discs, we also confirmed that the reduction of junctional Wts is suppressed by expression of Sqh.EE (Fig. S3H-J).

Spatial and temporal pattern of Jub regulation

The tension-dependent recruitment of Jub and its inhibition of Wts position Jub as a key link connecting cytoskeletal tension to Hippo signaling (Rauskolb et al., 2014). Thus we focused on Jub localization as a marker for evaluation of how faster-growing clones, exemplified by *ban*-expressing clones, influence cytoskeletal tension relevant to Hippo signaling. *ban*-expressing clones tend to have a stronger reduction of Jub in more distal regions of the wing disc (ie, nearer the center of the disc, Fig 1B) than in more proximal regions (Fig S3B). Cells nearer the center of the wing disc are more compressed, and have lower junctional tension than cells in more proximal regions (LeGoff et al., 2013; Mao et al., 2013; Nienhaus et al., 2009). These observations suggest that mechanical feedback is more evident where surrounding cells are already more compressed. The influence of *ban*-expressing clones also increased with the duration of clone growth, being barely detectable after 1 day, clearly visible after 2 days, and pronounced after 3 days (Figs 4G, S4). For comparison, a GFP-*ban* sensor that is a direct target of *ban* (Brennecke et al., 2003) was affected similarly between distal and proximal regions of the wing, and at two or three days after clone induction (Fig S4). These observations are consistent with the inference that the reductions in Jub localization at junctions associated with faster-growing clones result from growth-induced compression, as compression is expected to continually increase within *ban*-expressing clones.

Faster-growing cells reduce Yki activity

Decreased recruitment of Wts and Jub to adherens junctions induced by genetic inhibition of myosin activity is associated with increased Wts activity, and consequently

decreased Yki activity (Rauskolb et al., 2014). To confirm that Yki activity is lower within faster-growing clones, we examined both Yki localization, and the expression of Yki target genes. We were unable to examine the influence of mechanical feedback on Yki within Ras^{V12}-expressing clones because Ras^{V12} acts upstream of Yki, and promotes growth at least in part through Yki activation (Fan et al., 2013; Hong et al., 2014; Reddy and Irvine, 2013).

Nuclear localization of Yki was clearly lower within *ban*-expressing clones (Fig. 5A,G, S6E). Consistent with this, two different reporters of Yki's transcriptional activity, *ban-lacZ* and *Diap1*, were also decreased within *ban*-expressing clones in the developing wing (Fig. 5C,E,H,I). We note that *ban* was previously reported not to influence Yki activity (Nolo et al., 2006; Thompson and Cohen, 2006), based mostly on analysis of a distinct reporter, *ex-lacZ*. In our hands the influence of *ban*-expressing clones on *ex-lacZ* was complex, as *ex-lacZ* was increased in proximal regions of the wing, but not in distal regions (Fig. S5K). The observation that the influence of *ban* on *ex-lacZ* does not match its influence on Yki localization suggests that *ex* is also regulated by specific targets of the *ban* microRNA, and based on the consistent reductions in nuclear Yki, and in two out of three downstream target genes examined, we infer that Yki activity is lower within *ban*-expressing clones, consistent with the changes in Jub and Wts localization.

We also observed a reduction in Yki activity within wild-type clones in *Minute/+* mosaic discs, visible both through decreased nuclear Yki, and decreased expression of Yki target genes, including both *ban-lacZ* and *ex-lacZ* (Fig. 6A-C,E-G, S6E). Thus, two very different means of creating differential growth rates, *ban*-expressing clones in a wild-type disc, and wild-type clones in a *Minute/+* disc, both reduce Yki activity within

the faster-growing cells. Together with the observations described above, this implies that faster-growing clones trigger a mechanical feedback that down-regulates Yki activity. Consistent with this conclusion, co-expression of Sqh.EE suppressed the decrease in Yki activity both within *ban*-expressing clones, and within wild-type clones in *Minute/+* discs (Figs 5J,K, S6A-C,E).

To further confirm this relationship between differential growth and regulation of Yki, we suppressed the overgrowth of *ban*-expressing clones as compared to their *wild-type* neighbors, or the growth of *wild-type* clones as compared to their *Minute/+* neighbors. Within *ban*-expressing clones, RNAi of *E2f1* or *Myc* suppressed the influence of *ban*-expressing clones on Yki activity (Fig. 5B,D,F,G-I, S6E), whereas RNAi of these genes in otherwise wild-type cells does not significantly influence Yki activity (Fig. S5). Similarly, reduction of the growth differential between *Minute/+* cells and non-*Minute* cells using a *ban* mutation suppressed the reduced Yki activity within non-*Minute* cells (Fig. 6D,G, S6E), whereas *ban* mutant clones in a wild-type background don't increase Yki activity (Fig. S6D,E) (Nolo et al., 2006; Thompson and Cohen, 2006). These observations indicate that down-regulation of Yki activity is occurring within faster-growing clones as a consequence of their elevated growth rates.

Blocking mechanical feedback alters patterns of cell proliferation

The results described above establish that mechanical feedback can be induced in vivo by creating clones of cells that grow at different rates. We next considered the question of how mechanical feedback might contribute to growth control during normal development, by genetically preventing mechanical feedback (Fig. 7A). As mechanical

feedback acts on Yki, and *ban* promotes growth despite the absence of Yki (Nolo et al., 2006; Thompson and Cohen, 2006), forced expression of *ban* under UAS-Gal4 control effectively bypasses mechanical feedback. Since mechanical feedback acts through Jub-mediated regulation of Wts, knock-down of Wts should also block mechanical feedback. Forced activation of myosin could also suppress mechanical feedback, since it suppresses the down-regulation of myosin activity that would otherwise be introduced by tissue compression. Indeed, genetic activation of myosin suppressed the down-regulation of Jub and Yki that would otherwise occur within *ban*-expressing clones (Figs 4,5).

Thus, to assess the consequences of suppressing mechanical feedback we expressed *ban*, a transgene directing RNAi against *wts*, or *Sqh.EE*. They were expressed under *nub-Gal4* control, which drives expression throughout the developing wing (Fig 7B). Normally, cell proliferation is relatively evenly distributed in wing discs, as can be visualized by EdU labeling (Fig. 7C,D). In contrast, when mechanical feedback was blocked, cell proliferation at later larval stages was relatively higher in the medial region of the developing wing (Fig 7F,H,J). Increasing growth induced through an alternate method not expected to block mechanical feedback, knockdown of the tumor-suppressor *Pten*, did not result in the same spatial bias in disc cell proliferation (Fig 7L). These observations imply that the mechanical feedback mechanism that we identified modulates patterns of cell proliferation during normal wing development. The pattern that emerged is relevant to a long-standing question in the field: How is it that cells near the center of the disc experience higher levels of the key growth factor Decapentaplegic (Dpp), yet proliferate at similar rates as cells far from the Dpp source (Affolter and Basler, 2007)? A variety of models have been proposed to explain this, including one class of models that

essentially invoke the mechanical feedback hypothesis (Aegerter-Wilmsen et al., 2007; Aegerter-Wilmsen et al., 2012; Hufnagel et al., 2007; Shraiman, 2005). According to these models, uniform growth rates arise because higher mitogenic signaling in the center of the disc is counterbalanced by higher compression as cell numbers increase. Our observation that three distinct manipulations that suppress mechanical feedback lead to higher cell proliferation in the medial region of the wing disc, where Dpp signaling is higher, is consistent with this class of models.

Discussion

The hypothesis that organ growth is modulated by tissue mechanics *in vivo* has been popular, but untested. A key obstacle precluding attempts to investigate the role of mechanics in growth control has been the difficulty of distinguishing mechanical effects from influences on genetic or biochemical regulatory pathways. We have overcome this by identifying and characterizing biomechanical pathways that regulate growth, by analyzing combinations of genotypes whose only common feature is their influence on growth rates, and by characterizing influences of differential growth rates on tissue mechanics.

To establish that mechanical stresses within the range of what cells normally experience *in vivo* can influence growth, we took advantage of the insight, predicted by the mechanical feedback hypothesis, that local differences in growth rates should lead to mechanical strain. Indeed we found that this mechanical strain is particularly evident under conditions where mechanical feedback is blocked, as, for example, when *ban* is over-expressed. Moreover, we observed reduced myosin accumulation, and consequent

effects on Hippo signaling components, within wild-type cells, simply because surrounding cells have a reduced ribosome function, and hence reduced growth. This cannot be attributed to any direct, genetic regulation of myosin within clones. We assayed overgrowth clones induced using two independent genotypes (ban-expressing and Ras^{V12}-expressing), each of which has a distinct relationship to Hippo signaling, yet found they share this same reduction in myosin, Jub, and Wts accumulation. It was recently reported that Ras^{V12}-expressing clones did not autonomously reduce Myosin levels in the pupal notum under conditions where Ras^{V12}-expression was induced after clone growth was essentially completed (Bosveld et al., 2016); this observation further supports our conclusion that the reduction in Myosin we observed is not due to Ras^{V12}-expression per se, but rather the promotion of clone growth. Moreover, we observed that the influence of ban-expressing clones (or wild-type clones in a slow-growth disc) could be suppressed by knocking down the expression of single genes that reduce growth, but do not themselves directly regulate myosin. Together, these observations (Fig. S7A) indicate that Hippo signaling is activated within faster growing clones as a consequence of cellular compression, rather than through biochemical pathways dependent upon the various genotypes analyzed.

Quite generally, mechanical feedback regulation of growth is a homeostatic mechanism: by suppressing local over-growth, it reduces tissue distortion. Indeed, genotypes that we now know could block mechanical feedback (expression of ban or activated Yki, or knock-down of Wts) produce an evident strain within the disc epithelium, presumably because they allow growth-induced compression to accumulate. Conversely, wild-type clones within *Minute*/+ discs, which are presumably susceptible to

mechanical feedback, are not associated with equivalent distortions of the epithelium, and also have weaker effects on myosin, Jub, Wts, and Yki than *ban*-expressing clones. Additional processes could also contribute to minimizing distortions of epithelial tissues in response to differential growth. For example, differential growth is sometimes associated with a process of cell competition, in which slower-growing “loser” cells become eliminated by apoptosis. This removal of neighboring cells effectively creates space for faster-growing cells to occupy, and thus presumably reduces the compression, and ultimately mechanical feedback, that would otherwise be exerted on the faster-growing clones. The adaptive, mechanical stress-dependent recruitment of myosin into the cortical cytoskeleton that we invoke to explain reduced myosin within compressed cells serves as another, cell-level, homeostatic mechanism that reduces deformation in response to stress.

In addition to confirming the existence of mechanical feedback, our observations have identified a mechanism by which it occurs. This mechanism is initiated by a reduction in cytoskeletal tension within faster-growing clones, which we suggest stems from the responsiveness of myosin recruitment to stress exerted on actin-myosin networks (Kasza and Zallen, 2011). The decreased tension that results from cellular compression then triggers a biomechanical response that includes decreased recruitment of Jub and Wts to adherens junctions, and consequently decreased activity of Yki. Given the crucial role of Yki in promoting organ growth, this down regulation of Yki should be sufficient to reduce growth rates, and thus altogether our observations establish a mechanism for compression-induced growth inhibition. The Jub-dependent biomechanical pathway that is modulated by mechanical feedback was discovered in the

context of direct manipulations of myosin activity using transgenes or drugs (Rauskolb et al., 2014). The present study extends our understanding of the regulation of this pathway by establishing that stress experienced by cells *in vivo* as a simple consequence of differential growth is both qualitatively and quantitatively sufficient to modulate the Jub biomechanical pathway (Fig. S7B).

Mechanical feedback is a homeostatic mechanism, and to the extent that the growth of clones expressing an oncogene like Ras^{V12} is suppressed, mechanical feedback could provide a tumor suppressor function. However, mechanical feedback is not limited to situations where cells have genetically determined differences in growth rates. It could also occur under any conditions of growth-induced compression, and is an attractive mechanism to compensate for naturally occurring variation in growth rates. Indeed, by blocking mechanical feedback, we identified an influence on the normal patterning of cell proliferation within the developing wing. The elevated cell proliferation observed in the center of the wing disc, near the anterior-posterior compartment boundary, is consistent with the hypothesis that higher mitogenic signaling in the center of the disc is normally balanced by higher mechanical compression, which triggers mechanical feedback. Thus, when compression-induced growth suppression is bypassed by genetic manipulations that suppress mechanical feedback, higher cell proliferation is observed in the center of the wing disc. Thus, our observations also implicate mechanical feedback in the normal patterning of growth within developing organs.

Materials and Methods

Drosophila Culture

Unless otherwise indicated, crosses were performed at 25°C. For clone induction, larvae were grown on standard medium at 25°C. In most cases, larvae at 108±6h AEL (after egg laying) were fixed and used in the study. Heat shocks were performed at 37 °C 5-10 min two to three days before dissection. For *ban* overexpressing clones grown for 1, 2 or 3 days, larvae at 108±6h AEL were dissected and heat shocked at 37°C 5-10 min. For wild-type, *Sqh.EE*-expressing, or *ban*^{Δ1} clones in *Minute/+* backgrounds, larvae of 120h±6h AEL were used because of their developmental delay; and heat shocks were performed for 37°C 10 min 2.5 days before dissection.

To induce ectopic expression clones, *act>y+>Gal4* with *UAS-2xBFP* (described below) or *UAS-mCD8:RFP* (gift of G. Morata), or *act>Cd2>Gal4 UAS-nRFP* (Bloomington 30558) were crossed to the following UAS-transgenes with *hs-Flp*: *UAS-bantam* (Brennecke et al., 2003), *Gs-Bantam* (Reddy and Irvine, 2011), *UAS-Myc* (Johnston et al., 1999), *UAS-p35 [3-W]* (gift of B. Hay), *UAS-Yki:V5* (Oh and Irvine, 2009), *UAS-Ras^{v12}* (Karim and Rubin, 1998), *UAS-sqh.E20E21* (Winter et al., 2001), *UAS-Myc-RNAi* (VDRC 2948), *UAS-E2F1-RNAi* (VDRC 15886) and *UAS-Dcr2*. The *UAS-2xBFP* transgene was made by inserting two inframe copies of tagBFP into pUAST.

Protein or gene localization and expression was monitored using previously characterized transgenes: *ex-lacZ*, *ban-lacZ*, *Jub:GFP* (Sabino et al., 2011), *Wts:GFP* (Rauskolb et al., 2014), *zip:GFP*, *sqh:GFP* (Royou et al., 2004) and *Ubi-Ecad:GFP* (Oda and Tsukita, 2001).

For inducing wild-type clones in *Minute/+* backgrounds, FLP-FRT-mediated recombination was performed using: *y w hs-Flp; FRT80B*, *y w hs-Flp; FRT40A*, *y w hs-Flp; FRT80B Wts:GFP*, *y w hs-Flp; FRT80B Jub:GFP*, *y w hs-Flp; tub-Gal4 UAS-mCD8:RFP*; *Rps17⁴ tub-Gal80 FRT80B/TM6B*, *w; Rps17⁴ arm-lacZ FRT80B/TM6B* (Bloomington 6358), *hs-Flp tub-Gal4 UAS-GFP y w; Rps17⁴ tub-Gal80 FRT80B/TM6B* (Bloomington 42732), *M(2)25A Ubi-GFP FRT40A/CyO*, *w hs-FLP; arm-lacZ M(2)z FRT40A/CyO* (FBst1001673). For making *ban* mutant clones, *ban^{Δ1} FRT80B/TM6B* (Hipfner et al., 2002) was crossed to either *hs-Flp; Rps17⁴ arm-lacZ FRT80B/TM6B* or *y w hs-Flp; arm-lacZ FRT80B* (Bloomington 6341). To increase myosin activity within wild-type clones surrounded by *Minute/+* neighbors, MARCM clones were made using *y w hs-Flp; tub-Gal4 UAS-mCD8:RFP; Rps17⁴ tub-Gal80 FRT80B/TM6B*, *hs-Flp tub-Gal4 UAS-GFP y w; Rps17⁴ tub-Gal80 FRT80B/TM6B* and *UAS-Sqh.EE; FRT80B*.

For making bantam over-expressing and wild-type clones in the same disc, a TIE-DYE stock (Worley et al., 2013) was crossed to *hs-Flp; UAS-bantam* flies.

For the EdU labeling experiments, *nub-Gal4 UAS-dcr2* was crossed to *UAS-ban*, *UAS-wts-RNAi[vdrc101475]*, *UAS-sqh.EE*, or *UAS-Pten-RNAi[vdrc9928]*.

Histology and Imaging

For most experiments discs were fixed in 4% paraformaldehyde for 15 min. at room temperature. *Wts:GFP* discs were fixed for 8 min., and *Sqh:GFP* or *Zip:GFP* discs were fixed for 12 min. Primary antibodies used were rabbit anti-Yki (1:400) (Oh and Irvine, 2008), mouse anti-β-galactosidase (1:200, DSHB), mouse anti-Wg (DSHB), mouse anti-Diap1 (1: 200, B. Hay), rat anti- E-cad (1:400 DCAD2; DSHB), mouse anti-

Armadillo (1:200, DSHB), rabbit anti-cleaved Caspase (1:400 Dcp-1; Cell Signaling Technology). Secondary antibodies were purchased from Jackson ImmunoResearch Laboratories and Invitrogen. F-actin was stained using Alexa Fluor 488-phalloidin (Life Technologies), and DNA was stained using Hoechst (Invitrogen) or TO-PRO-3 (Life Technologies). Confocal images were captured on a Leica SP5 or a PerkinElmer Ultraview.

For EdU labeling, larvae were dissected in Ringers and anterior halves were immediately placed in 250uL WM1 (Zartman et al., 2013). An equal volume of 20uM EdU (Click-iT EdU Alexa Fluor 594 Imaging Kit, Life Technologies) in WM1 was added for a final concentration of 10uM EdU and samples incubated for 10 minutes. Tissue was then fixed for 20 minutes with 4% paraformaldehyde in PBS. Subsequent standard antibody staining protocol using mouse anti-WG (DSHB) was then followed by 30 minutes EdU detection using 0.6uL Alexa Fluor azide 594 per 500uL Click-iT reaction cocktail. Afterwards tissues were treated with Hoechst. Wing discs were removed and mounted on a slide in Vectashield.

Live Imaging and Laser Cutting of Cell Junctions

Live imaging and laser ablation experiments were performed as previously described (Rauskolb et al., 2014). To make discs with ban overexpressing clones, *act>y+>Gal4 UAS-mCD8:RFP* flies were crossed with *y w hs-Flp; Ubi-Ecad:GFP; Gs-Bantam* flies. Heat shocks were performed for 37°C 7 min to induce clones, and 2.5 days later wing discs were dissected at 108h \pm 4h AEL. For making wild-type clones in *Minute/+* background, *y w hs-Flp; tub-Gal4 UAS-mCD8:RFP; Rps17⁴ tub-Gal80*

FRT80B/TM6B flies were crossed to *y w-Flp; Ubi-Ecad:GFP; FRT80B* flies. Similarly, heat shock was done for 10min at 37°C; 2.5d days later wing discs were dissected at 120h \pm 4h AEL. In both cases, wing discs were cultured in WM1 media in a 4-well chambered coverglass (Nunc Lab-Tek II) coated with poly-lysine. Discs were imaged every 0.2 s on a Perkin Elmer Ultraview spinning disc confocal microscope, and ablation of junctions was achieved using a Micropoint pulsed laser (Andor) tuned to 365 nm. Paired cutting of junctions, one in the clone and another in a non-clone region at a similar location, were performed and compared in the wing discs. The displacement of vertices for the 1st second after ablation was used to calculate the velocities.

Image Processing and Quantitative Image Analysis

To compensate for aberrations due to the curvature of wing disc, clone induced distortions, and signals from the peripodial epithelium, we used the Matlab toolbox ImSAnE (Heemskerk and Streichan, 2015) to detect and isolate a slice of the disc epithelium surrounding the adherens junctions, using E-cadherin or Armadillo as a reference. ImSAnE projects a curved surface onto a flat surface. Projections of 5-7 ImSAnE generated surfaces (0.8-1.2 μ m in total) surrounding the center of E-cad or Arm were then used to identify the signal at this cell layer and create images showing for Sqh:GFP, Zip:GFP, Jub:GFP, F-actin and Wts:GFP localization.

Quantitation of junctional Jub:GFP, E-cad, Arm, F-actin, and Wts:GFP was performed as previously described (Rauskolb et al., 2014), using Volocity (Perkin Elmer) software. In brief, E-cadherin or Armadillo was used as a junctional reference to define the volumes to be quantified. To compare Jub:GFP, F-actin and Wts:GFP between clone

and the non-clone regions, we selected 10-20 cell regions of interest in the clone and defined mean fluorescence intensities over-lapping adherens junctions; and identically sized objects were assayed in a non-clone region at an equivalent location in another compartment of the same disc. Quantitation of Yki, ban-lacZ, and ex-lacZ was performed similarly, except we quantified and compared their nuclear intensities, using DNA staining to define nuclei.

Since both junctional and apical myosins are affected by differential growth, and myosin is not completely enclosed within E-cad or Arm staining, we used a different method to quantify Sqh:GFP or Zip:GFP. Confocal stacks were first processed using ImSAnE to detect the apical surface. The processed 2D images were then quantified using ImageJ. An area containing 10-20 cells was selected in the clone to quantify the mean fluorescence intensities; and an identically sized region was selected in a non-clone region at an equivalent location in another compartment of the same disc.

Variability in mean ratios is presented using 95% confidence intervals, determined using GraphPad Prism6 software. Statistical comparisons between these mean ratios was performed by One-way Anova with Tukey's correction, on the log of the ratios, using GraphPad Prism6 software.

To analyze cell anisotropy in and outside of clones (Fig 1D), confocal stacks were first processed by ImSAnE to make 2D surface images. The processed images were then segmented using ilastik software, and the segmented pictures were used to perform anisotropy analysis with a custom Matlab script. For quantification (Fig 1G), a standard measure of orientational order is the magnitude of the nematic order parameter (see e.g.

Chaikin & Lubensky, Principles of condensed matter physics). In two dimensions, it is given by

$$S = \langle 2 \cos^2 \phi - 1 \rangle$$

where ϕ is the angle between the local orientation and the mean orientation and $\langle \dots \rangle$ denotes an average. Here we modify this to measure cell orientation relative to the clone boundary, and define

$$S_d \equiv \frac{\langle a_c^2 (2 \sin^2 \phi_c - 1) \rangle_d}{\langle a_c^2 \rangle_d}.$$

The angle ϕ_c is between the normal to the clone boundary and the major axis of the cell, which is 90 degrees when the cells are stretched tangentially to the clone boundary. We take the distance function d to be signed, with positive sign outside and negative inside. The normal to the clone boundary is extended across the disk by taking the gradient of the distance function

$$\mathbf{n} = \nabla d$$

Cells are labeled by c the average is over cells in a bin centered around distance d from the clone boundary, and a_c is the cell anisotropy defined as

$$a = \frac{l_{\text{maj}} - l_{\text{min}}}{l_{\text{maj}} + l_{\text{min}}},$$

where l_{maj} and l_{min} are the major and minor axis lengths of the cell.

The graph in Fig 9G shows d versus S_d for a single clone. The scatter plot shows S_0 vs. S_{15} for a large number of clones, where S_0 and S_{15} are averages at the boundary and 15 microns outside, both over 2 micron wide bins.

Simulations

We are simulating a vertex model with the energy

$$E = \sum_c \left[T_c l_c + \frac{a_c}{A_c} \right],$$

where c labels the cells, T_c is the perimeter tension, l_c the perimeter length, a_c a parameter controlling the preferred cell size, and A_c the cell area.

The simulation runs the following in a loop:

1. Relax to mechanical equilibrium
2. Update tension and preferred cell size parameters
3. Divide

1. Relax to mechanical equilibrium

The energy is minimized with the GNU Scientific Library Multidimensional Minimizer, using Polak-Ribiere conjugate gradient algorithm. The pressure in each cell is then obtained from the work done by the cell under a dilation relative to the cell centroid:

$$p_c dA_c = - \sum_{i \in c} \frac{\partial E_c}{\partial \vec{r}_i} \cdot \delta \vec{r}_i, \quad \delta \vec{r}_i = \lambda (\vec{r}_i - \vec{r}_c)$$

$$\Rightarrow p_c = - \frac{1}{A_c} \sum_{i \in c} \frac{\partial E_c}{\partial \vec{r}_i} \cdot (\vec{r}_i - \vec{r}_c)$$

2. Parameter update

The parameters of each cell are updated according to the rules:

- $a_c(t+1) = a_c(t) + \gamma_c dt$
with γ_c the growth rate
- $T_c(t+1) = T_c(t) - k(p_c(t+1) - p_c(t))$
with k the strength of tension adaptation

3. Division

The probability to divide per unit time depends on the cell area $p(A)$.

The total probability in some time step dt is then $P = 1 - (1-p)^{dt}$.

For each cell, at each timestep, a coin is flipped with probability P , and if heads, the cell is divided. One choice for the function $p(A)$ that seems to work well is

$$p(A) = \Theta(N - 4)\Theta(A - A_0)\frac{A^n}{A_0^n + A^n}$$

Where $Q(x)$ is one for $x > 0$ and zero for $x \leq 0$. Therefore there is no division below some minimal area or when the number of neighbors is less than five and the probability saturates to one at large areas.

When a cell is divided the direction of division is randomly picked and an edge is inserted orthogonal to it. The relation between mother (m) and daughter (d) parameters is

- $T_d = T_m$, tension is kept the same from mother to daughter
- $a_d = a_m / 2^{3/2}$, to keep the total equilibrium area fixed. This rule is based on the fact that the equilibrium area of a cell is

$$A = \alpha l^2 = \alpha^{1/3} \left(\frac{2a}{T} \right)^{2/3}$$

where c is a factor encoding the perimeter squared to area ratio for a regular polygon of a given number of sides, e.g. $3^{1/2}/24$ for a hexagon. Holding T fixed, preserving the equilibrium area requires

$$A_m = A_{d1} + A_{d2}$$

$$\sqrt{\alpha_m} a_m = \sqrt{2\alpha_{d1}} a_d + \sqrt{2\alpha_{d2}} a_d,$$

and approximating that $\alpha_m = \alpha_{d1} = \alpha_{d2}$ we have the above rule.

Parameters used

The parameters that were used for the simulation shown in Figure 2 are

- $g=1$ inside the clone, $g=0.1$ outside the clone

- $k=0.05$
- $dt=0.05$
- $A_0=1.3, n=6$

With the initial conditions

- $T_c=1/2$
- $a_c=1$
- hexagonal initial lattice, which with these parameters has $A = 4^{2/3}\sqrt{3}/24 \approx 1$

Matlab scripts for analysis and simulations have been deposited at Github
(<https://github.com/idse/mechanicalFeedback>)

Fig. 1. Overview, and tissue distortion induced by ban-expressing clones

A) Simplified schematic of the Hippo pathway. B) Schematic of the wing imaginal disc. C) Schematic illustrating the mechanical feedback loop identified here, by showing that 1) growth can compress cells, 2) compression of cells can decrease cytoskeletal tension, and 3) the decreased cytoskeletal tension induced by cellular compression is sufficient to trigger changes in the localization of Jub and Wts, and in Yki activity. D) Cell anisotropy analysis of ban-expressing clones, green lines indicate long axis, which just outside the clone tends to align parallel to the clone boundary. E) Vertical section through a wing disc with ban-expressing clones, marked by BFP (blue). These clones typically induce distortions of the epithelium that include apical invaginations and lateral bulging. F) Vertical section through a wing disc with control clones (BFP-expressing). G) Influence of ban-expressing clones on cell orientation. Panels show example of segmentation (left, color scale shows anisotropy), average cell orientation radial to the center of the clone at different distances from the clone boundary (center, N=29). Far right panel summarizes analysis of clones, plotting average cell orientation at the clone edge versus 15 μm away for each clone. Color indicates relative clone area (as a heat map, red is bigger, blue is smaller), blue circles identify clones closer to the center of the wing pouch, open squares identify clones farther from the center of the wing pouch. The analysis shows cells tend to align parallel to the clone boundary at the clone edge but not 15 μm away, and this effect is more pronounced for clones closer to the center of the wing.

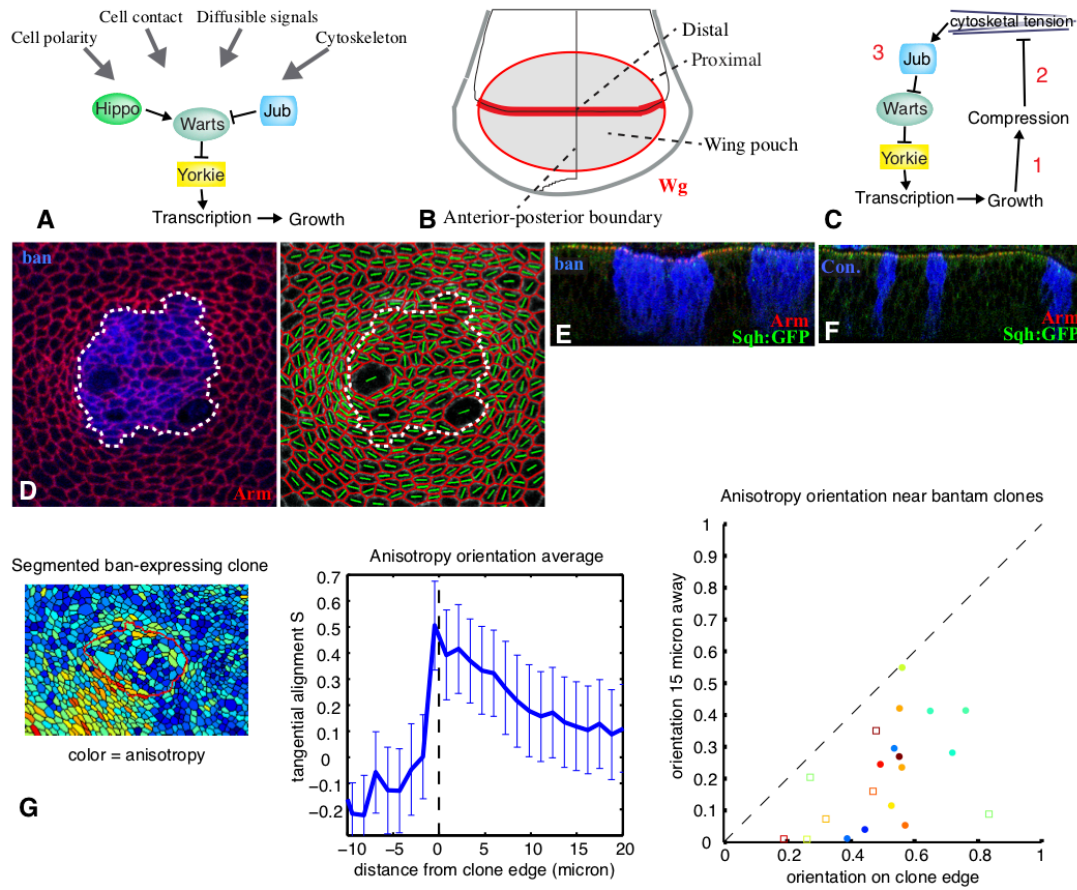


Fig. 2. Reduced tension within faster-growing clones

A) Wing disc with clones of *ban*-expressing cells grown for 2.5 days, labeled by co-expression of 2xBFP, with cell junctions labeled by Arm (red) and Myosin labeled by Sqh:GFP (green/white), showing reduced junctional myosin within clones. Panels to the right show higher magnification of the boxed regions. B) *Minute* heterozygous (*Rps17⁴*) wing disc with clones of wild-type cells grown for 2.5 days, labeled by absence of β -gal marker (blue), with cell junctions labeled by E-cad (red) and Myosin labeled by Zip:GFP (green/white). C,D) Wing discs with clones co-expressing *ban* and RNAi-E2f1 (C) or RNAi-Myc (D) grown for 2.5 days, labeled by co-expression of 2xBFP, with cell junctions labeled by Arm (red) and Myosin labeled by Sqh:GFP (green/white); reduction in junctional myosin is suppressed. E) Assessment of junctional tension by laser cutting. Junctions were cut within live discs with clones labeled by mCD8:RFP and junctions labeled by E-cad:GFP, examples of regions of discs inside and outside of *ban*-expressing clones 0.2s before and 0.8s after cutting are shown, histogram shows mean retraction velocities measured from 46 (left pair, UAS-*ban* clones in wild-type) or 42 (right pair, wild-type clones in *Minute/+*) pairs of cuts, error bars indicate 95% confidence interval. F) Wing disc with clones of Ras^{v12}-expressing cells grown for 2 days, labeled by co-expression of 2xBFP, with cell junctions labeled by Arm (red) and Myosin labeled by Sqh:GFP (green/white). G) Histogram showing relative levels of Myo:GFP in cells within clones of the indicated genotypes, as compared to cells outside of the clones at similar proximal-distal locations within the same wing disc. Values and numbers of clones analyzed are tabulated in Fig S2B. Comparisons of the significance (by One-way

Anova) of differences between some of these mean ratios is indicated by the gray lines, **** indicates $P < 0.0001$, *** indicates $P < 0.001$. H) Cartoon illustrating balancing forces that maintain cell shape. Internal cell pressure reflecting compression of nuclei and other cytoplasmic components generates an expanding force (blue arrows) that is balanced by myosin-generated cortical tension (red arrows). External forces provided by interaction with neighboring cells could compress (green arrows) cells, altering cell shapes, pressures, and tensions. I) Snapshots of simulations (videos are in supplemental material) showing altered cellular pressures and tensions that result from differences in growth rates, based on a modified vertex model. In this simulation (see Supplement for details), intrinsic cell area is larger for a clone of faster growing cells (identified by black line above, and gray shading below), pressure is increased as cells are constrained within an area smaller than their intrinsic size. Relative pressures and tensions are indicated by color scale (red=high, blue=low).

Fig. 3. Reduced junctional Jub and Wts within faster-growing clones

A) Wing disc with clones of *ban*-expressing cells grown for 2.5 days, labeled by co-expression of 2xBFP, with cell junctions labeled by Arm (red) and Jub labeled by Jub:GFP (green/white). Panels to the right show higher magnification of the boxed regions. B) *Minute* heterozygous (*Rps17⁴*) wing disc with clones of wild-type cells grown for 2.5 days, labeled by absence of β -gal marker (blue), with cell junctions labeled by E-cad (red) and Jub labeled by Jub:GFP (green/white). C) Wing disc with clones of Ras^{V12}-expressing cells grown for 2 days, labeled by co-expression of 2xBFP, with cell junctions labeled by E-cad (red) and Jub labeled by Jub:GFP (green/white). D,E) Wing disc with clones co-expressing *ban* and RNAi-Myc (D) or RNAi-E2f1 (E) grown for 2.5 days, labeled by co-expression of 2xBFP, with cell junctions labeled by Arm (red) and Jub labeled by Jub:GFP (green/white). F) *Minute* heterozygous (*Rps17⁴*) wing disc with clones of *ban^{Δ1}* mutant cells grown for 2.5 days, labeled by absence of β -gal marker (blue), with cell junctions labeled by E-cad (red) and Jub labeled by Jub:GFP (green/white). G) Wing disc with clones of *ban*-expressing cells grown for 2.5 days, labeled by co-expression of 2xBFP, with cell junctions labeled by Arm (red) and Wts labeled by Wts:GFP (green/white). H) *Minute* heterozygous (*Rps17⁴*) wing disc with clones of wild-type cells grown for 2.5 days, labeled by absence of β -gal marker (blue), with cell junctions labeled by E-cad (red) and Wts labeled by Wts:GFP (green/white). I) Wing disc with clones of Ras^{V12}-expressing cells grown for 2 days, labeled by co-expression of 2xBFP, with cell junctions labeled by E-cad (red) and Wts labeled by GFP:Wts (green/white). J-K) Histograms showing relative levels of Jub:GFP (J) and GFP:Wts (K) in cells within clones of the indicated genotypes, as compared to cells

outside of the clones at similar proximal-distal locations within the same wing disc. Values and numbers of clones analyzed are tabulated in Fig S3J. Comparisons of the significance (by One-way Anova) of differences between some of these mean ratios is indicated by the gray lines, **** indicates $P < 0.0001$.

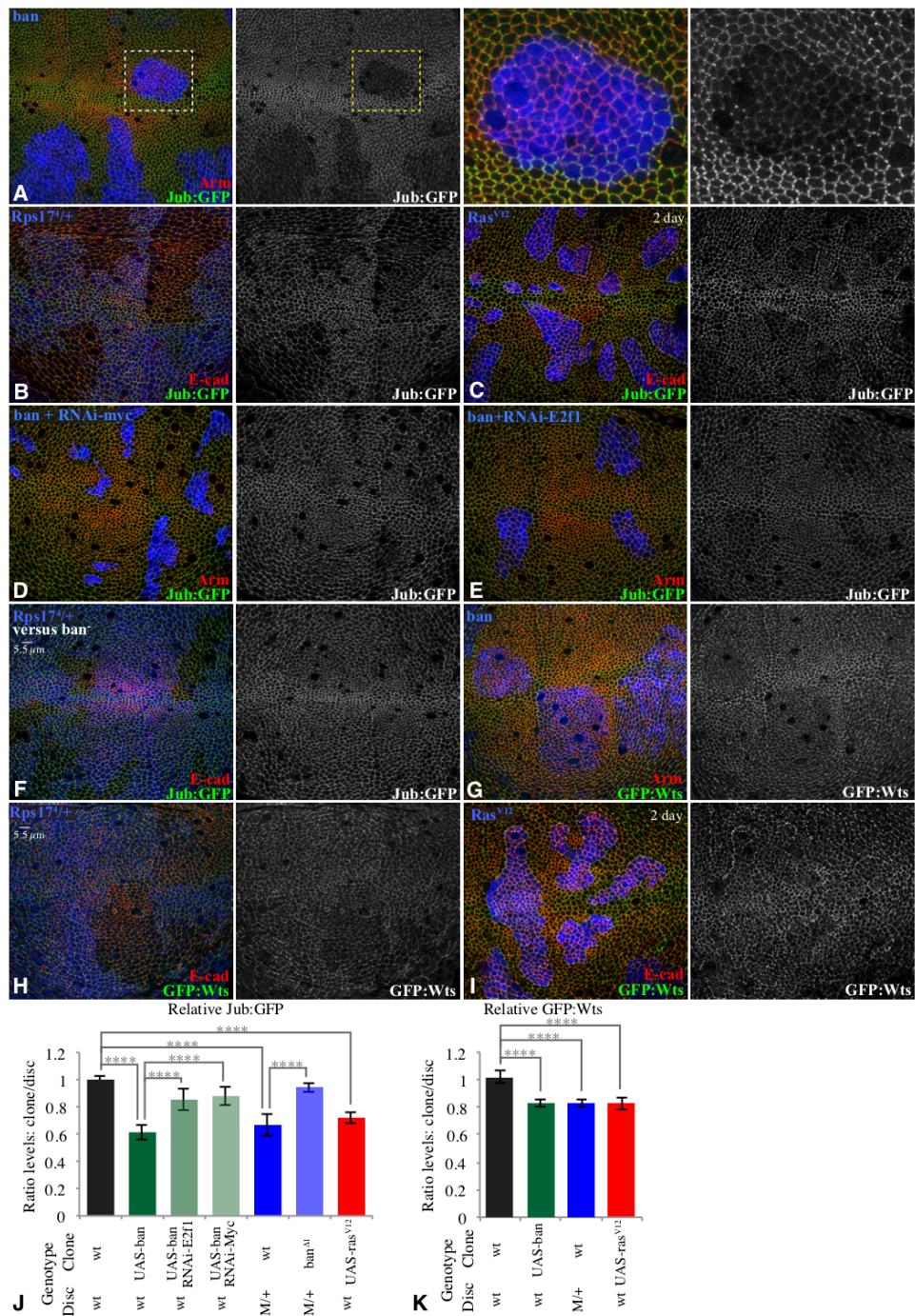


Fig. 4. Increasing myosin activity suppresses reductions of Jub in faster-growing clones

A) Wing disc with clones co-expressing *ban* and *Sqh.EE* grown for 2.5 days, labeled by co-expression of 2xBFP, with cell junctions labeled by Arm (red) and Jub labeled by Jub:GFP (green/white). B) Wing disc with clones co-expressing *Ras^{V12}* and *Sqh.EE* grown for 2 days, labeled by co-expression of 2xBFP, with cell junctions labeled by E-cad (red) and Jub labeled by Jub:GFP (green/white). C) *Minute* heterozygous (*Rps17⁴*) wing disc with clones of wild-type cells grown for 2.5 days, labeled by presence of BFP marker (blue) using MARCM, with cell junctions labeled by E-cad (red) and Jub labeled by Jub:GFP (green/white). D) *Minute* heterozygous (*Rps17⁴*) wing disc with clones of cells expressing *Sqh.EE* grown for 2.5 days, labeled by presence of BFP marker (blue) using MARCM, with cell junctions labeled by E-cad (red) and Jub labeled by Jub:GFP (green/white). E,F) Histograms showing relative levels of Jub:GFP (E) and GFP:Wts (F) in cells within clones of the indicated genotypes, as compared to cells outside of the clones at similar proximal-distal locations within the same wing disc. Values and numbers of clones analyzed are tabulated in Fig S3J. Comparisons of the significance (by One-way Anova) of differences between some of these mean ratios is indicated by the gray lines, **** indicates $P < 0.0001$. G) Quantitation of relative Jub levels over time (see Fig S3), based on paired measurements inside and outside of *ban*-expressing clones, 1 (N=14), 2 (N=13), or 3 (N=13) days after clone induction, error bars indicate c.i.

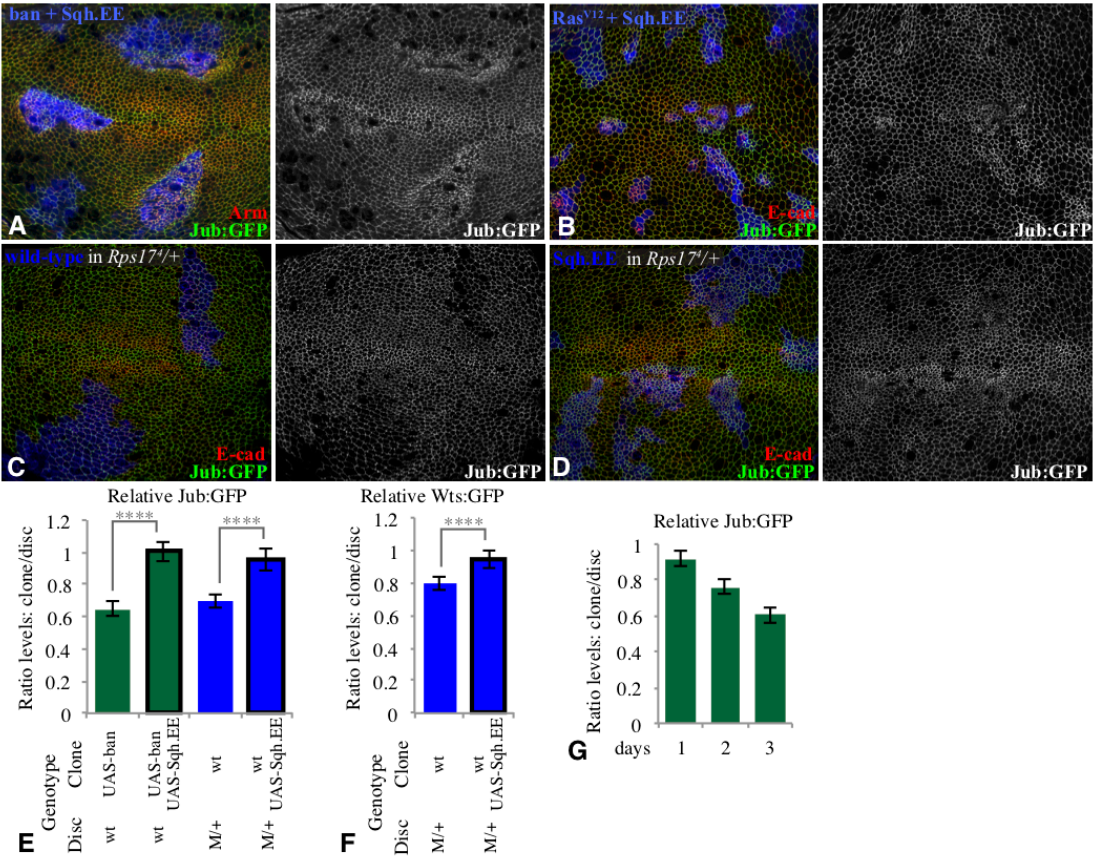


Fig. 5. Influence of ban-expressing clones on Yki activity

A) Wing disc with clones of ban-expressing cells grown for 2.5 days, labeled by co-expression of UAS-mRFP (blue), and stained for DNA (Hoechst, red) and Yki (green/white), showing reduced nuclear Yki in clones. Thin panels above show vertical sections. B) Wing disc with clones of cells co-expressing ban and a UAS-RNAi construct targeting E2f1, grown for 2.5 days, labeled by co-expression of 2xBFP (blue), stained for DNA (red) and Yki (green/white). Thin panels above show vertical sections. C) Wing disc with clones of ban-expressing cells grown for 2.5 days, labeled by co-expression of 2xBFP (blue), stained for DNA (red) and ban-lacZ (green). D) Wing disc with clones of cells co-expressing ban and a UAS-RNAi construct targeting Myc, grown for 2.5 days, labeled by co-expression of 2xBFP (blue), stained for DNA (red) and ban-lacZ (green). E) Wing disc with clones of ban-expressing cells grown for 2.5 days, labeled by co-expression of 2xBFP, and stained for expression of Diap1 (green). F) Wing disc with clones of cells co-expressing ban and a UAS-RNAi construct targeting E2f1, grown for 2.5 days, labeled by co-expression of 2xBFP (blue), stained for DNA (red) and Diap1 (green). G-J) Histograms showing relative levels of nuclear Yki (G), ban-lacZ (H,J), and Diap1 (I) in cells within clones of the indicated genotypes, as compared to wild-type cells outside of the clones at similar proximal-distal locations within the same wing disc. Values and numbers of clones analyzed are tabulated in Fig S6E. Comparisons of the significance (by One-way Anova) of differences between some of these mean ratios is indicated by the gray lines, **** indicates $P < 0.0001$. K) Wing disc with clones co-expressing ban and Sqh.EE grown for 2.5 days, labeled by co-expression of 2xBFP

Fig. 6. Influence of wild-type clones in *Minute* heterozygotes on Yki activity

A) *Minute* heterozygous (*Rps17⁴*) wing disc with clones of wild-type cells grown for 2.5 days, labeled by absence of β -gal marker (blue), and stained for DNA (Hoechst, red) and Yki (green/white), showing reduced nuclear Yki. Thin panels above show vertical sections. B) *Minute* heterozygous (*M(2)25A*) wing disc with clones of wild-type cells grown for 2.5 days, labeled by absence of GFP marker (blue), and stained for DNA (red) and *ban-lacZ* (green). C) *Minute* heterozygous (*Rps17⁴*) wing disc with clones of wild-type cells grown for 2.5 days, labeled by presence of GFP marker (blue) using MARCM, and stained for DNA (green) and *ex-lacZ* (red). D) *Minute* heterozygous (*Rps17⁴*) wing disc with clones of *ban^{ΔI}* mutant cells grown for 2.5 days, labeled by presence of GFP marker (blue) using MARCM, and stained for DNA (green) and *ex-lacZ* (red). E-G) Histograms showing relative levels of nuclear Yki (E), *ban-lacZ* (F), and *ex-lacZ* (G) in cells within clones of the indicated genotypes, as compared to wild-type cells outside of the clones at similar proximal-distal locations within the same wing disc. Values and numbers of clones analyzed are tabulated in Fig S6E. Comparisons of the significance (by One-way Anova) of differences between some of these mean ratios is indicated by the gray lines, **** indicates $P < 0.0001$.

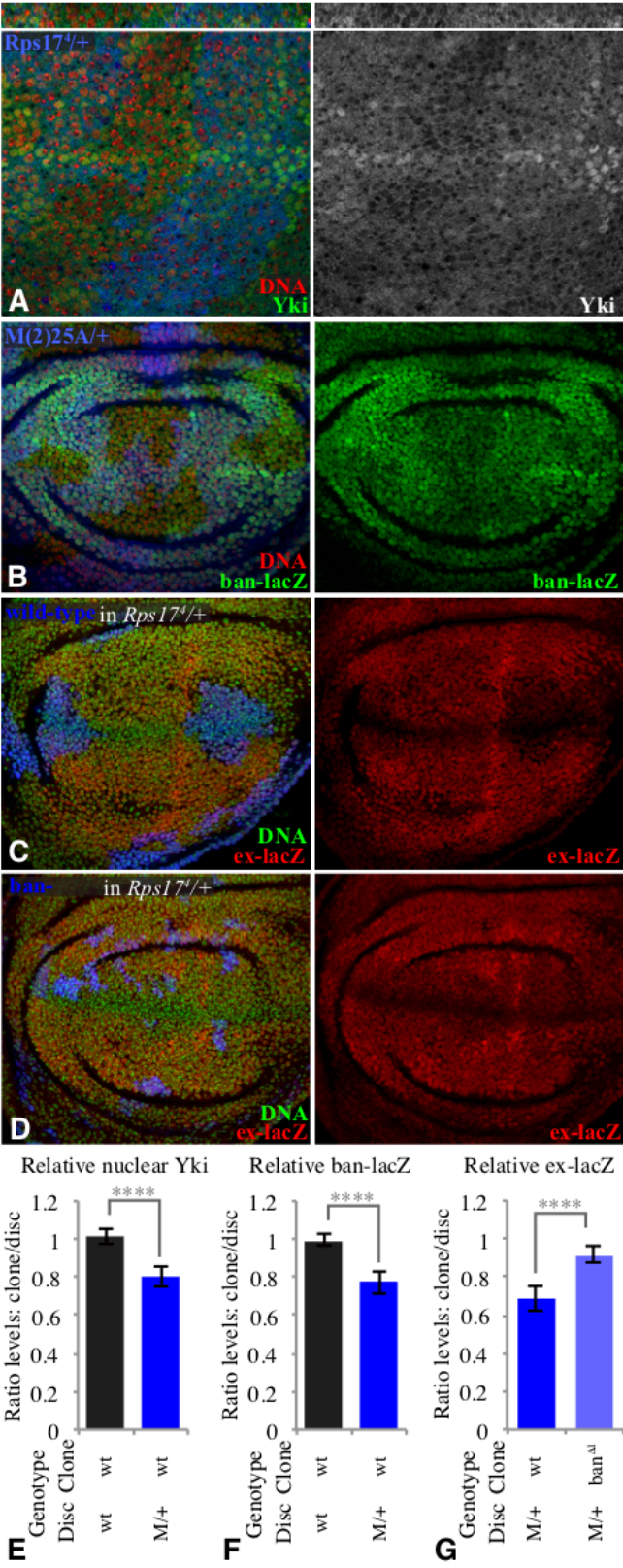
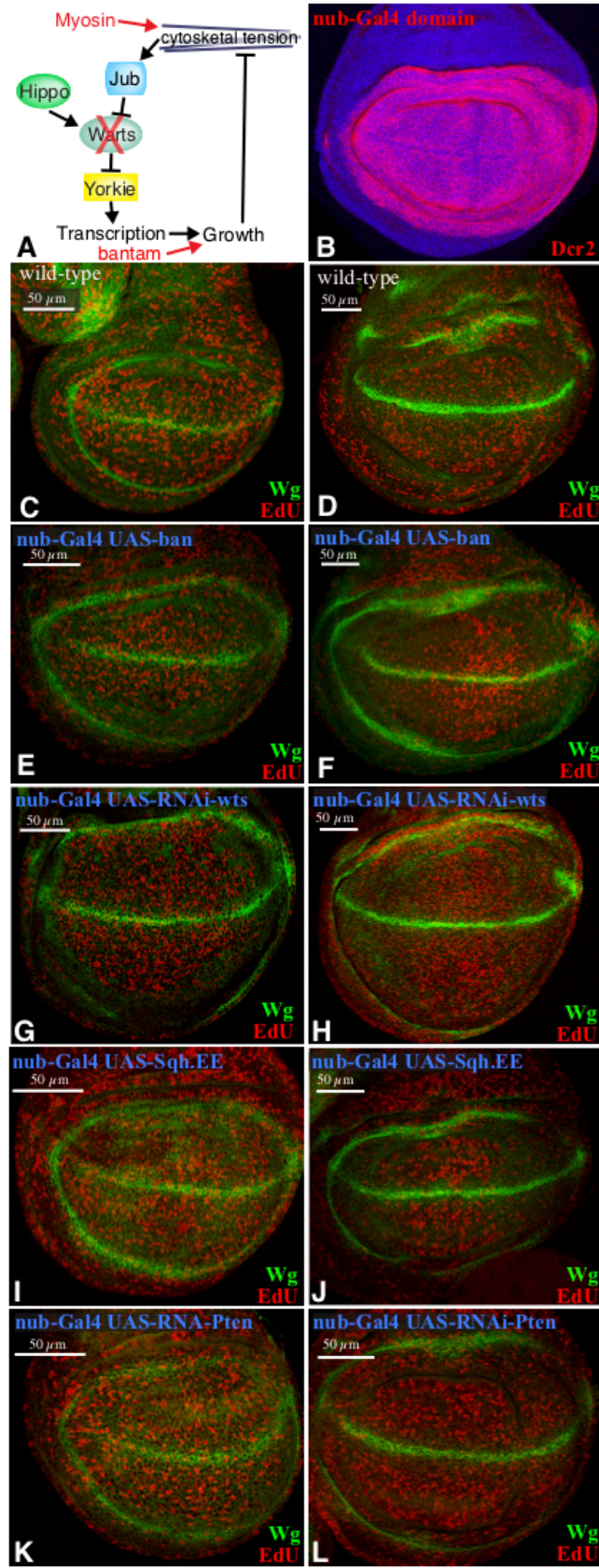


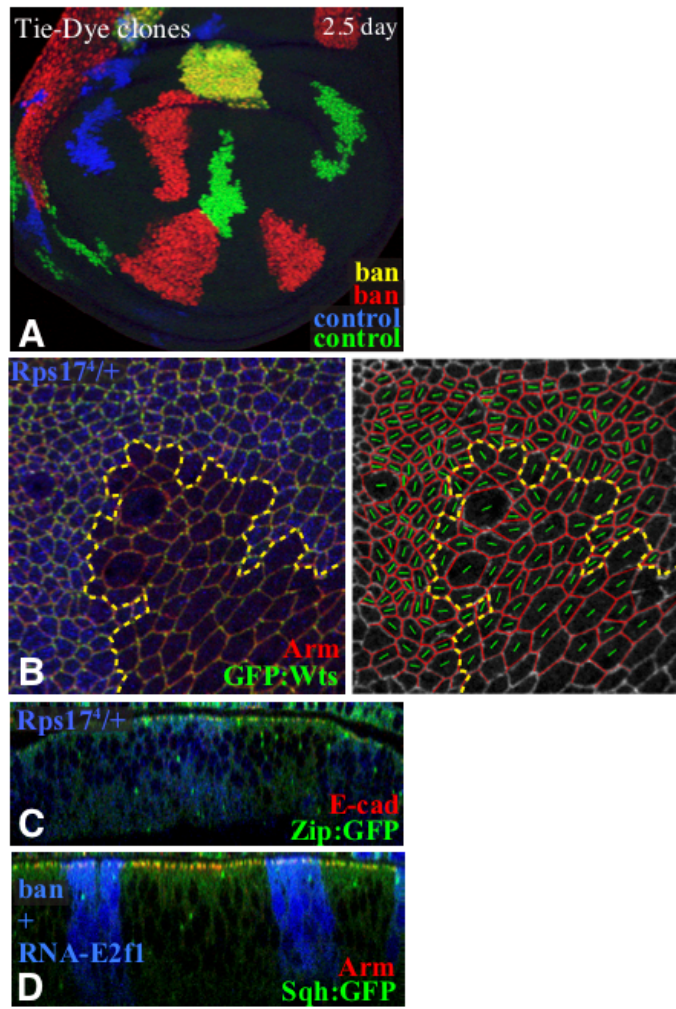
Fig. 7. Influence of mechanical feedback on cell proliferation

A) Schematic illustration of mechanical feedback loop, with points of experimental blockage or bypass in red. B) Wing disc expressing *UAS-Dcr2* under *nub-Gal4* control, stained for Dcr2 (red), to illustrate the nub-Gal4 expression domain. C-L) Wing discs subject to EdU labeling (red) for proliferating cells, and stained for Wingless (Wg, green), which is expressed along the D-V boundary and also encircles the developing wing. Wild-type (C,D), *nub-Gal4 UAS-ban* (E,F), *nub-Gal4 UAS-RNAi-wts* (G,H), *nub-Gal4 UAS-Sqh.EE* (I,J) and *nub-Gal4 UAS-Pten RNAi* (K,L) are shown, left panels (C,E,G,I,K) show discs from mid-third instar larvae, right panels (D,F,H,J,L) show discs from late third instar larvae. Cell proliferation is normally evenly distributed at these stages, but is relatively higher in the middle of the developing wing when mechanical feedback is bypassed (F,H,J).



Supplemental Fig. S1 Clones lacking evidence of tissue distortion

A) Wing disc with clones of cells labeled by the Tie-Dye technique (Worley et al., 2013) to illustrate faster growth induced by ban-expression. Neutral clones are labeled blue or green, ban-expressing clones are labeled red (and yellow due to overlap of red and green). B) Cell anisotropy analysis of wild-type clones in *Rps17⁴/+* background. Green lines indicate long axis of cell. In contrast to ban-expressing clones (Fig. 1D), no bias in cell anisotropy is observed along clone borders. C) Vertical section through a wing disc with wild-type clones in *Rps17⁴/+* background (marked by absence of β -gal marker, blue). D) Vertical section through a wing disc with clones co-expressing ban and RNAi-E2f1, marked by BFP (blue). The invaginations associated with ban-expressing clones (Fig. 1E) are not observed.



Supplemental Fig. S2 Additional analysis of myosin and F-actin

A) Wing disc with control clones grown for 2.5 days, labeled by expression of 2xBFP, with cell junctions labeled by Arm (red) and Myosin labeled by Sqh:GFP (green/white).

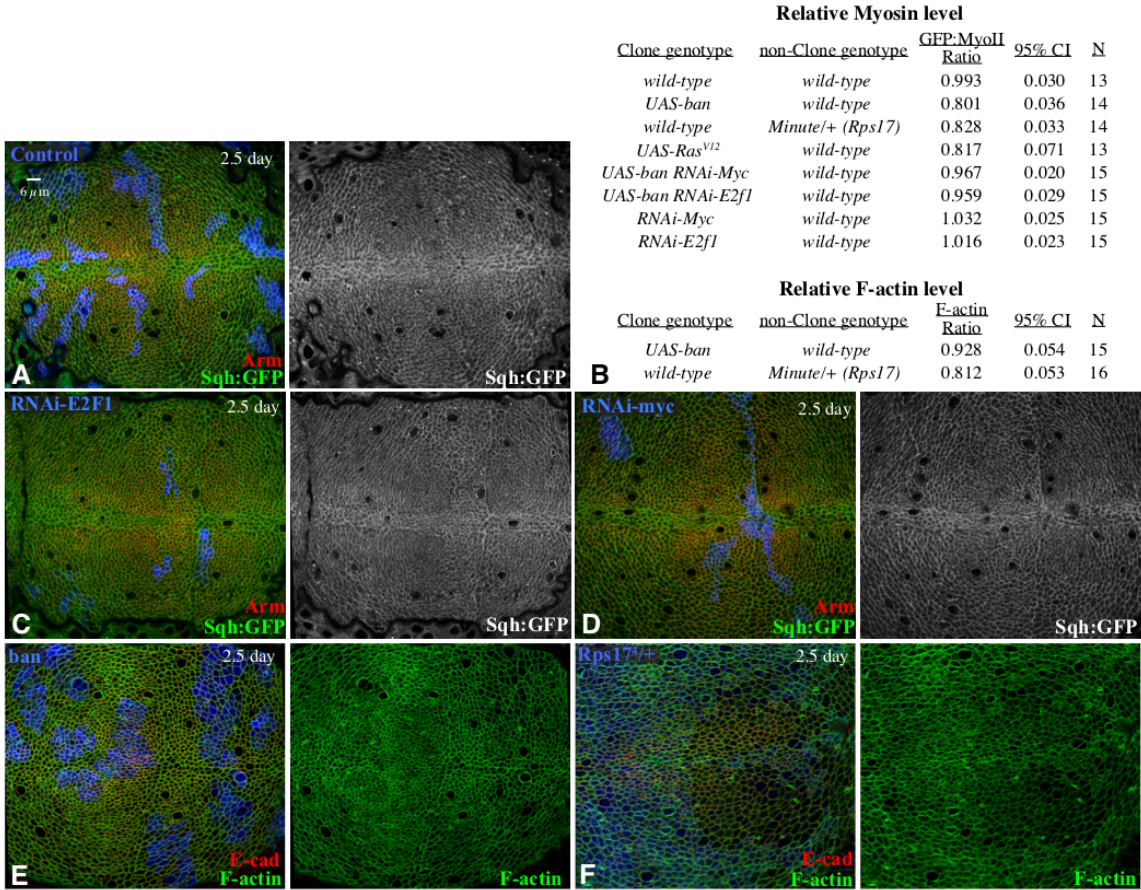
B) Tabulation of relative levels of Myosin or F-actin, based on paired measurements inside of clones of cells of the indicated genotypes, compared to equivalent non-clone regions of the same discs, with variation indicated by the 95% confidence interval (CI); N indicates number of clones measured.

C) Wing disc with clones expressing RNAi-E2f1 grown for 2.5 days, labeled by co-expression of 2xBFP, with cell junctions labeled by Arm (red) and Myosin labeled by Sqh:GFP (green/white).

D) Wing disc with clones expressing RNAi-Myc grown for 2.5 days, labeled by co-expression of 2xBFP, with cell junctions labeled by Arm (red) and Myosin labeled by Sqh:GFP (green/white).

E) Wing disc with clones of ban-expressing cells grown for 2.5 days, labeled by co-expression of 2xBFP, with cell junctions labeled by E-cad (red) and F-actin labeled by phalloidin (green).

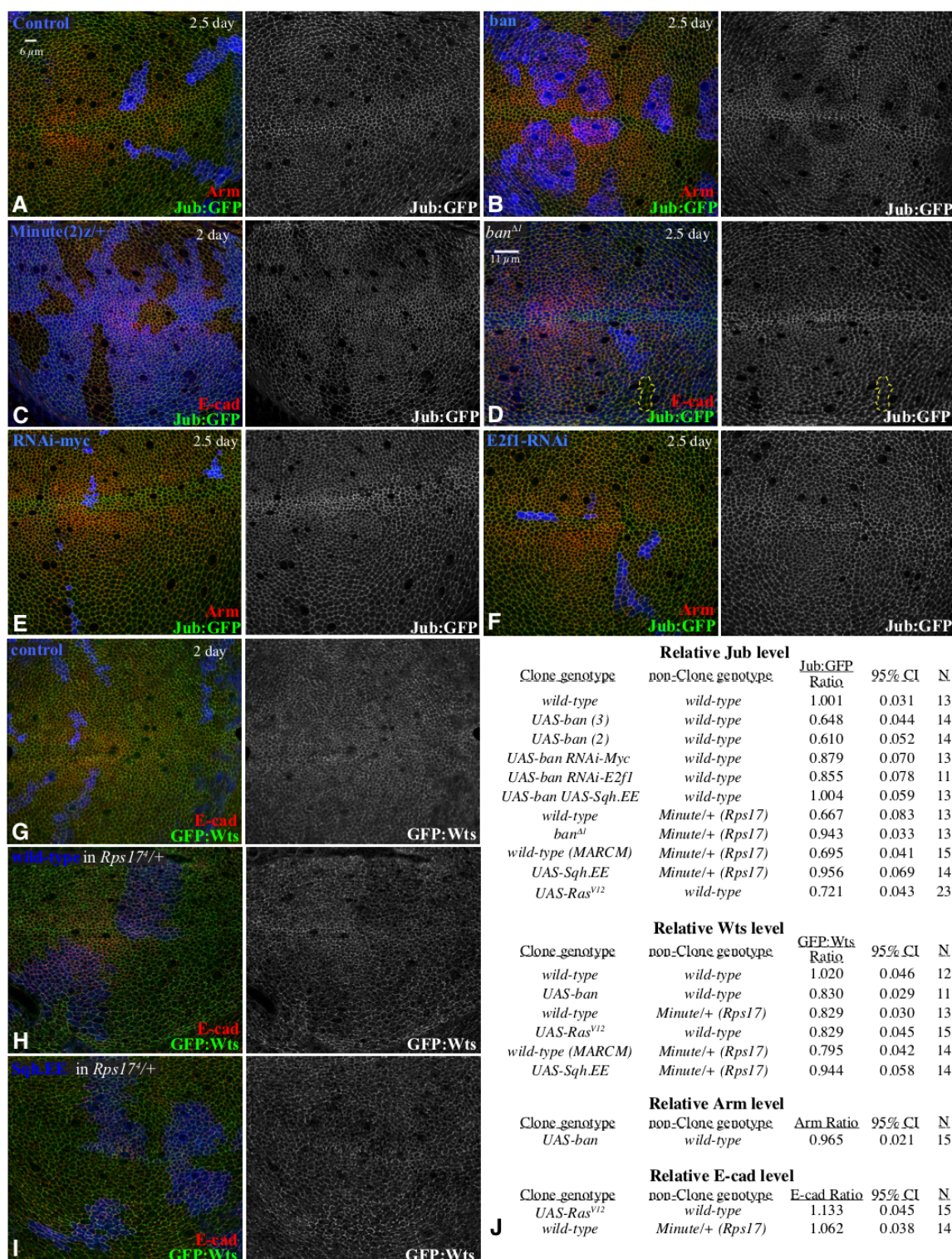
F) *Minute* heterozygous (*Rps17^d*) wing disc with clones of wild-type cells grown for 2.5 days, labeled by absence of β -gal marker (blue), with cell junctions labeled by E-cad (red) and F-actin labeled by phalloidin (green).



Supplemental Fig. S3 Additional analysis of Jub and Wts

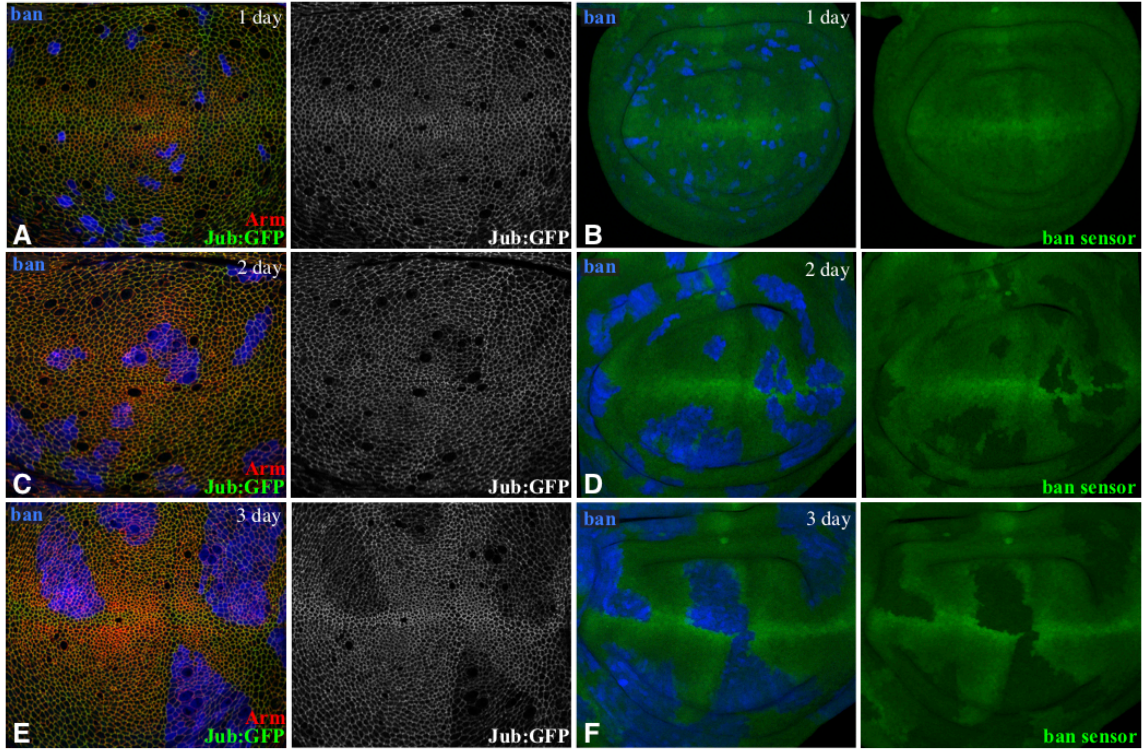
A) Wing disc with control clones grown for 2.5 days, labeled by expression of 2xBFP, with cell junctions labeled by Arm (red) and Jub labeled by Jub:GFP (green/white). B) Wing disc with clones of *ban*-expressing cells grown for 2.5 days, labeled by co-expression of 2xBFP, with cell junctions labeled by Arm (red) and Jub labeled by Jub:GFP (green/white); Jub levels at junctions are decreased within clones. C) *Minute* heterozygous (*Minute(2)z*) wing disc with clones of wild-type cells grown for 2 days, labeled by absence of β -gal marker (blue), with cell junctions labeled by E-cad (red) and Jub labeled by Jub:GFP (green/white); Jub levels at junctions are decreased within clones. D) Wing disc with clones of *ban* ^{Δ} mutant cells grown for 2.5 days, labeled by absence of β -gal marker (blue), with cell junctions labeled by E-cad (red) and Jub labeled by Jub:GFP (green/white). Mutant clone is outlined by dashed yellow line; Jub levels are unaffected. E) Wing disc with clones of RNAi-Myc-expressing cells grown for 2.5 days, labeled by co-expression of 2xBFP, with cell junctions labeled by Arm (red) and Jub labeled by Jub:GFP (green/white). F) Wing disc with clones of RNAi-E2f1-expressing cells grown for 2.5 days, labeled by co-expression of 2xBFP, with cell junctions labeled by Arm (red) and Jub labeled by Jub:GFP (green/white). G) Wing disc with control clones grown for 2.5 days, labeled by expression of 2xBFP, with cell junctions labeled by E-cad (red) and Wts labeled by GFP:Wts (green/white). H) *Minute* heterozygous (*Rps17* ^{Δ}) wing disc with clones of wild-type cells grown for 2.5 days, labeled by presence of BFP marker (blue) using MARCM, with cell junctions labeled by E-cad (red) and Wts labeled by Wts:GFP (green/white); Wts levels at junctions are decreased within clones. I) *Minute* heterozygous (*Rps17* ^{Δ}) wing disc with clones of cells expressing Sqh.EE grown

for 2.5 days, labeled by presence of BFP marker (blue) using MARCM, with cell junctions labeled by E-cad (red) and Wts labeled by Wts:GFP (green/white). J) Tabulation of relative levels of junctional Jub, Wts, Arm or E-cad, based on paired measurements inside of clones of cells of the indicated genotypes, compared to equivalent non-clone regions of the same discs, with variation indicated by the 95% confidence interval (CI); N indicates number of clones measured.



Supplemental Fig. S4 Duration of ban clone growth correlates with loss of Jub

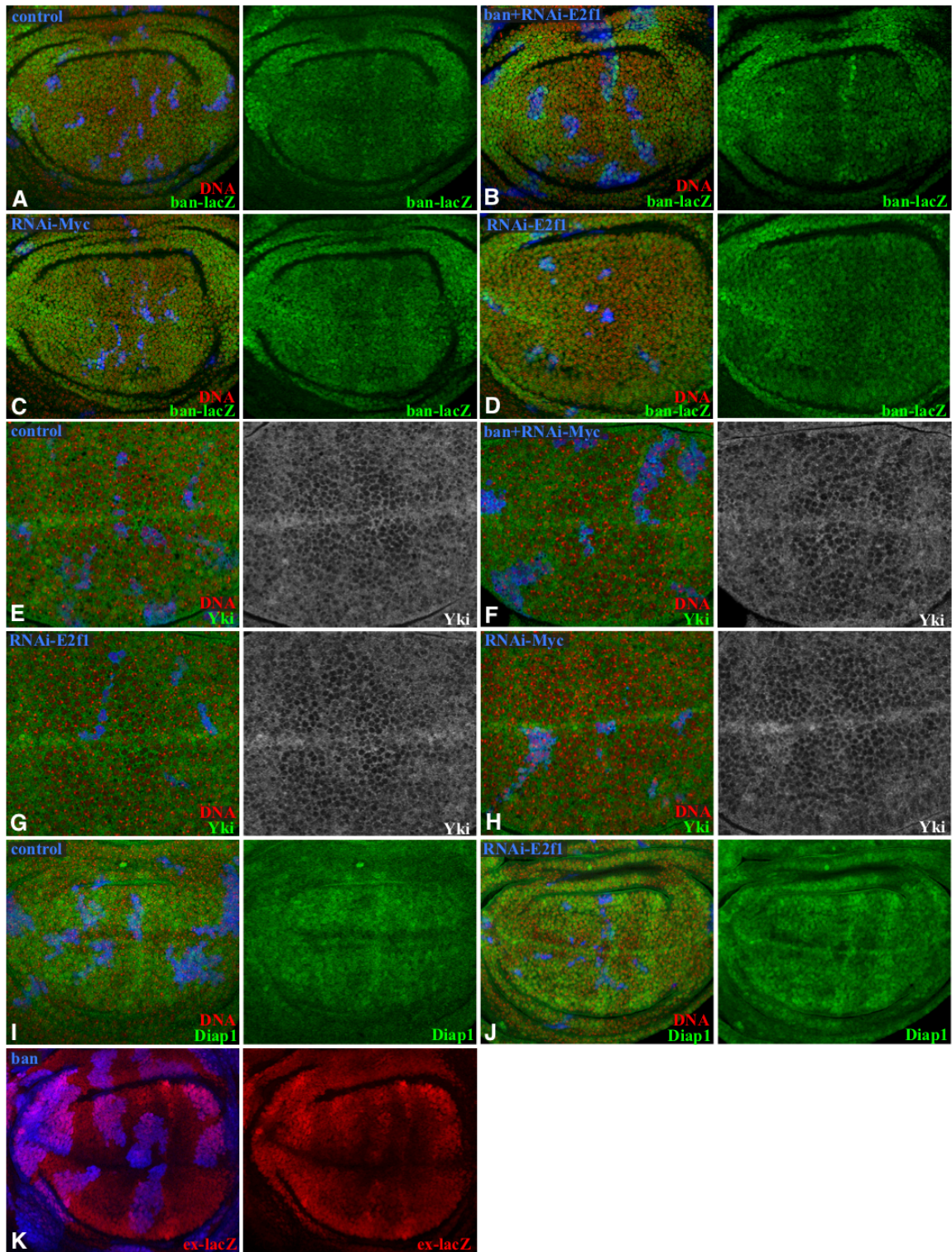
A,C,E Wing discs with clones of ban-expressing cells grown for 1 (A), 2 (B), or 3 (E) days, labeled by co-expression of 2xBFP, with cell junctions labeled by Arm (red) and Jub labeled by Jub:GFP (green/white). Decreased junctional Jub is visible after two or three days. B,D,F) Wing discs with clones of ban-expressing cells grown for 1 (B), 2 (D), or 3 (F) days, labeled by co-expression of 2xBFP, with ban activity revealed by GFP-ban sensor (green). For quantitation see Fig 4G.



Supplemental Fig. S5 Additional analysis of Yki activity related to ban-expressing clones

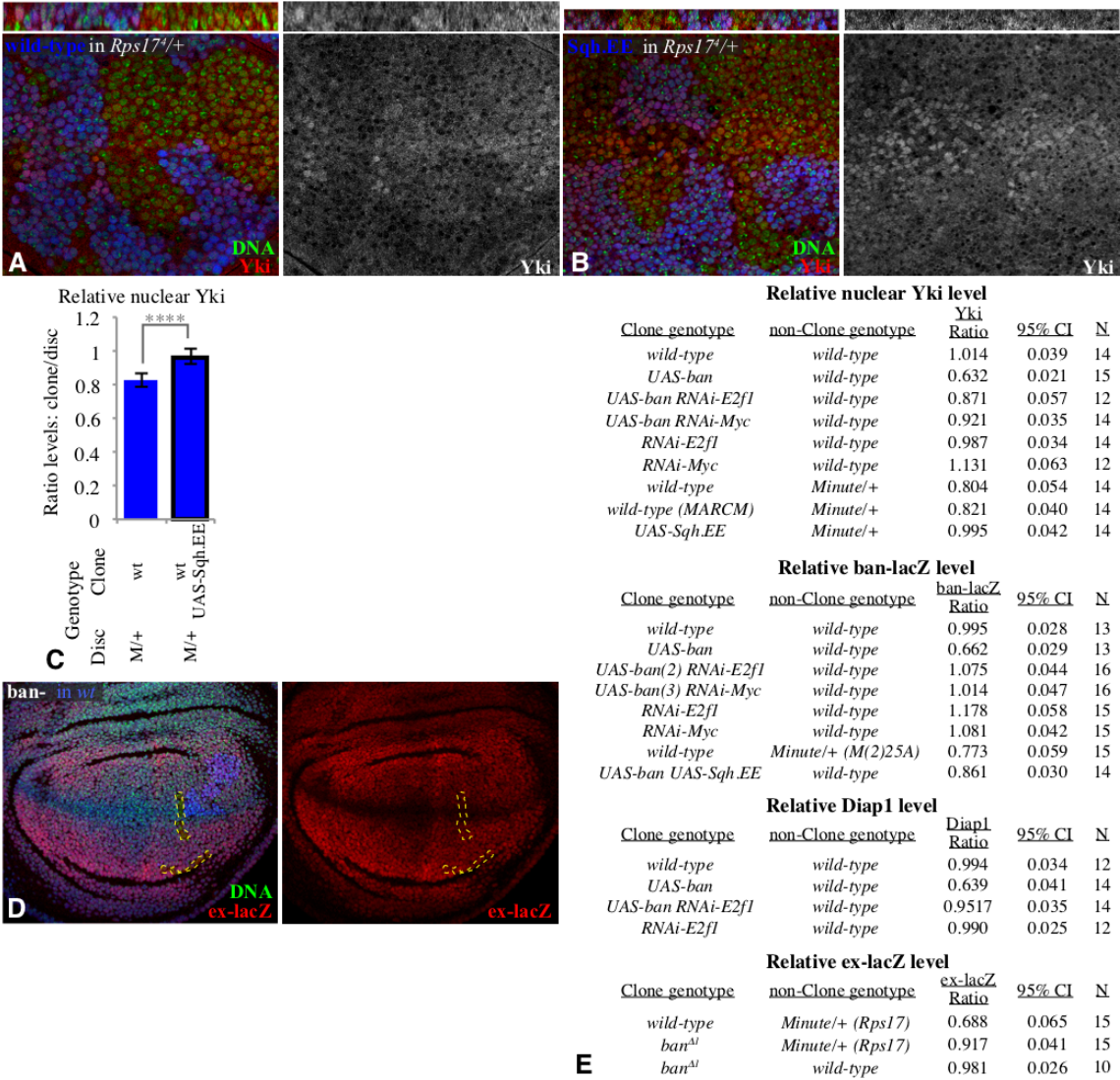
Quantitation of the effects of these clones is provided in Supplemental Fig. S6E. A) Wing disc with clones of BFP-expressing cells (control) grown for 2.5 days, labeled by co-expression of 2xBFP (blue), stained for DNA (red) and ban-lacZ (green). B) Wing disc with clones of cells co-expressing ban and a UAS-RNAi construct targeting E2f1, grown for 2.5 days, labeled by co-expression of 2xBFP (blue), stained for DNA (red) and ban-lacZ (green). C) Wing disc with clones of cells expressing a UAS-RNAi construct targeting Myc, grown for 2.5 days, labeled by co-expression of 2xBFP (blue), stained for DNA (red) and ban-lacZ (green). D) Wing disc with clones of cells expressing a UAS-RNAi construct targeting E2f1, grown for 2.5 days, labeled by co-expression of 2xBFP (blue), stained for DNA (red) and ban-lacZ (green). E) Wing disc with clones of BFP-expressing cells (control) grown for 2.5 days, labeled by co-expression of 2xBFP (blue), stained for DNA (red) and Yki (green/white). F) Wing disc with clones of cells co-expressing ban and a UAS-RNAi construct targeting Myc, grown for 2.5 days, labeled by co-expression of 2xBFP (blue), stained for DNA (red) and Yki (green/white). G) Wing disc with clones of cells expressing a UAS-RNAi construct targeting E2f1, grown for 2.5 days, labeled by co-expression of 2xBFP (blue), stained for DNA (red) and Yki (green/white). H) Wing disc with clones of cells expressing a UAS-RNAi construct targeting Myc, grown for 2.5 days, labeled by co-expression of 2xBFP (blue), stained for DNA (red) and Yki (green/white). I) Wing disc with clones of BFP-expressing cells (control) grown for 2.5 days, labeled by co-expression of 2xBFP (blue), stained for DNA (red) and Diap1 (green). J) Wing disc with clones of cells co-expressing ban and a UAS-

RNAi construct targeting E2f1, grown for 2.5 days, labeled by co-expression of 2xBFP (blue), stained for DNA (red) and Diap1 (green). K) Wing disc with clones of ban-expressing cells grown for 2.5 days, labeled by co-expression of 2xBFP (blue), stained for ex-lacZ (red).



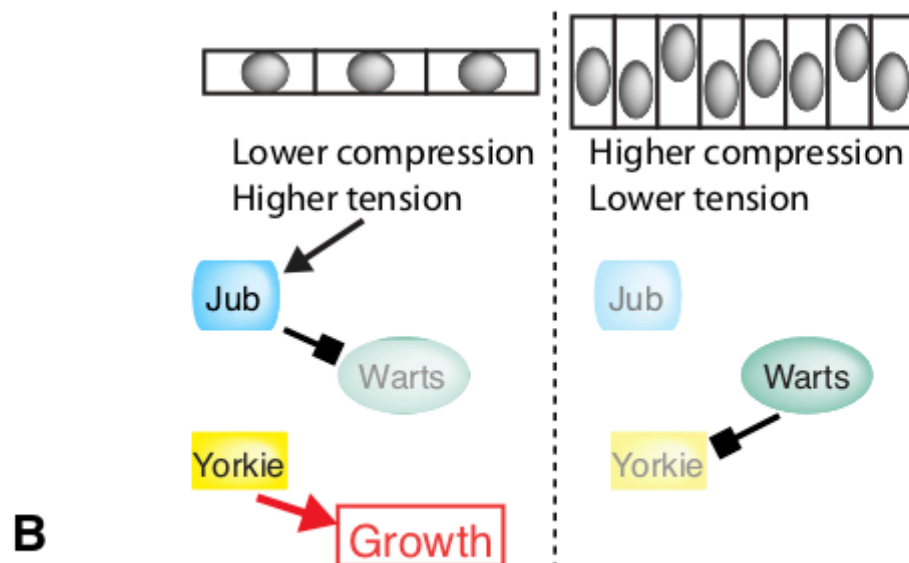
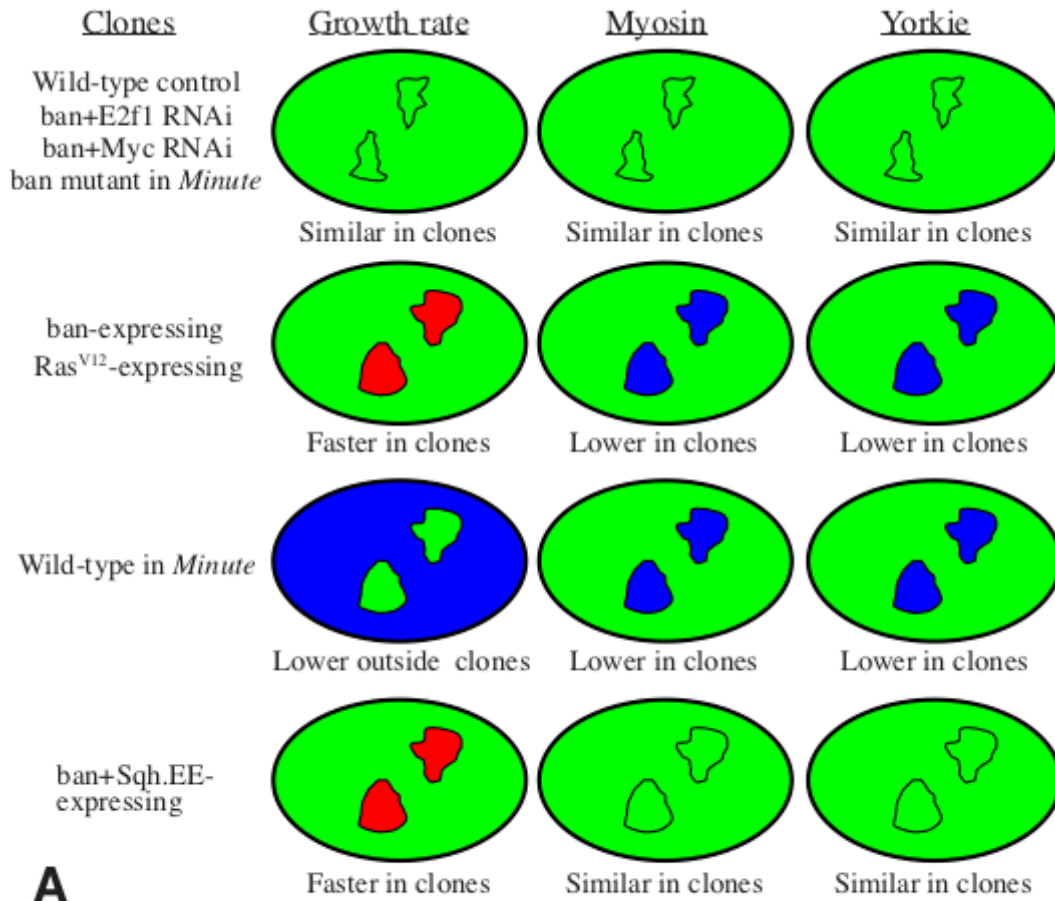
Supplemental Fig. S6 Additional analysis of Yki activity

A) *Minute* heterozygous (*Rps17^d*) wing disc with clones of wild-type cells grown for 2.5 days, labeled by presence of GFP marker (blue) using MARCM, and stained for DNA (green) and Yki (red/white). Thin panels above show vertical sections. Nuclear Yki levels are lower within the clones. B) *Minute* heterozygous (*Rps17^d*) wing disc with clones of cells expressing Sqh.EE grown for 2.5 days, labeled by presence of GFP marker (blue) using MARCM, and stained for DNA (green) and Yki (red/white). Thin panels above show vertical sections. C) Histogram showing relative levels of nuclear Yki in cells within clones of the indicated genotypes, as compared to cells outside of the clones at similar proximal-distal locations within the same wing disc. Values and numbers of clones analyzed are tabulated in E. Comparisons of the significance (by One-way Anova) of differences between some of these mean ratios is indicated by the gray lines, **** indicates $P < 0.0001$. D) Wing disc with clones of *ban^{Δ1}* mutant cells grown for 2.5 days, labeled by absence of GFP marker (blue), and stained for DNA (green) and ex-lacZ (red). Mutant clones are outlined by dashed yellow line. E) Tabulation of relative levels of nuclear Yki, ban-lacZ, Diap1 and ex-lacZ, based on paired measurements inside of clones of cells of the indicated genotypes, compared to equivalent non-clone regions of the same discs, with variation indicated by the 95% confidence interval (CI); N indicates number of clones measured.



Supplemental Fig. S7. Summary and model

A) Summary cartoons illustrating the observed influences of some of the clones examined on growth, myosin, and Yki activity. Green indicates wild-type levels, red faster levels, and blue lower levels. B) Summary model illustrating that lower tension under conditions of higher cellular compression allows higher Wts activity, and thus lower Yki activity and reduced growth.



Chapter 3

The Dynamics of Hippo Signaling during *Drosophila* Wing Disc Development

Results described in Figure 2 of this chapter are part of publication:

Rauskolb C, Sun S, Sun G, Pan Y, Irvine KD. Cytoskeletal tension inhibits Hippo signaling through an Ajuba-Warts complex. *Cell*. 2014 Jul 3;158(1):143-156. doi: 10.1016/j.cell.2014.05.035.

Other results are in preparation for a manuscript:

Yuanwang Pan, Herve Alegot, Cordelia Rauskolb and Kenneth D. Irvine. The Dynamics of Hippo Signaling during *Drosophila* Wing Disc Development.

Author contributions:

Yuanwang Pan and Kenneth Irvine designed the experiment. Cordelia Rauskolb performed some of the *Minute* experiments. All other experiments were done by Yuanwang Pan. Herve Alegot wrote the scripts for intensity map analysis. Yuanwang Pan, Herve Alegot and Kenneth Irvine analyzed the data. Yuanwang Pan and Kenneth Irvine wrote the paper.

Summary

Tissue growth needs to be properly controlled for organs to reach their correct size and shape, but the mechanisms that control growth during normal development are not fully understood. I discovered that the activity of the Hippo signaling transcriptional activator Yorkie gradually decreases in the central region of the developing *Drosophila* wing disc. Spatial and temporal changes in Yorkie activity can be explained by changes in cytoskeletal tension and biomechanical regulators of Hippo signaling. These changes in cellular biomechanics correlate with changes in cell density, and experimental manipulations of cell density are sufficient to alter biomechanical Hippo signaling and Yorkie activity. I also relate the pattern of Yorkie activity in older discs to patterns of cell proliferation. My study shows that spatial differences in Hippo signaling contribute to spatial patterns of growth in vivo, and provides evidence for a contribution of tissue mechanics to regulating patterns of Yorkie activity and growth during wing development.

Introduction

How organs reach a correct size and shape constitutes one of the key questions in developmental biology, but the mechanism is still a mystery (Hafen and Stocker, 2003; Vogel, 2013). Growth of the cells needs to be properly controlled during development for tissues to reach a correct size and proportion. Tissue growth is regulated by extrinsic factors like nutrition, hormones, and intrinsic factors like morphogens and mechanical force (Irvine and Harvey, 2015; Penzo-Mendez and Stanger, 2015). Numerous signaling pathways have been characterized to play important roles in growth control. However, how those factors and pathways are regulated under physiological conditions *in vivo* remains elusive.

Hippo signaling has emerged as an essential growth control pathway from arthropods to vertebrates (Pan, 2010; Yu et al., 2015). It was first discovered in *Drosophila* and later been shown to be conserved in mammals. The central core of this pathway comprises of a kinase cascade including the NDR family kinase Warts (Wts in *Drosophila*, and LATS1 and LATS2 in mammals). And the primary target of this kinase cassette is the transcriptional activator Yorkie (Yki in *Drosophila*, YAP and TAZ in mammals) (Huang et al., 2005). The phosphorylation of Yki by Wts promotes the cytoplasmic localization of Yki, thus reducing transcription and growth (Oh and Irvine, 2008). A notable feature of Hippo signaling is that it serves as an integrator of growth control signals involving both biochemical and biomechanical inputs (Irvine, 2012; Meng et al., 2016). Diverse inputs from positional information, organismal nutrition, developmental stage, cell contacts and mechanical stress regulate or have cross talk with Hippo signaling. Recently,

our lab identified that cytoskeletal tension regulates Hippo Signaling through an Ajuba-Warts complex (Rauskolb et al., 2014). The Wts inhibitor LIM domain protein Ajuba (Jub) can be recruited to the adherens junctions with Wts in a tension dependent manner. When Wts is inhibited at the junctions, Yki enters the nucleus and promotes transcription and growth. Despite this encouraging progress, most previous studies on Hippo signaling regulation were based on genetic manipulations or drug treatment in cell cultures or in vivo. Therefore, how Hippo signaling activity is regulated during normal development is largely unknown.

Mechanical stress has been increasingly appreciated as an important regulator of tissue growth (Eder et al., 2017; Irvine and Shraiman, 2017; LeGoff and Lecuit, 2016). Some molecular mechanisms, including biomechanical Hippo signaling, have been characterized that mediate the influence of mechanical stress on growth. And recent studies began to shed light on the physiological roles of mechanical stress on growth. We recently characterized how cells could experience mechanical forces and coordinate their growth rates by mechanical feedback (Pan et al., 2016). Differences in growth rates trigger a mechanical feedback response that reduces cytoskeletal tension within faster-growing cells, and decreases their Yki activity through the Jub-Wts complex. We also found mechanical feedback plays an important role in achieving homogenous growth in vivo. In addition, mechanical forces have also been suggested to play a role in organ size determination: the accumulated mechanical compression during development causes organs to cease growing on reaching their final size (Aegerter-Wilmsen et al., 2007;

Aegerter-Wilmsen et al., 2012; Hufnagel et al., 2007; Shraiman, 2005). However, whether and how this is working in vivo is not clear.

The *Drosophila* wing imaginal disc has been extensively used to study growth regulation in vivo (Hariharan, 2015; Irvine and Harvey, 2015). During larval stages, the wing disc grows from 30-50 cells to 30,000-50,000 cells (Milan et al., 1996; Worley et al., 2013). Interestingly, the growth rate gradually slows down during larval development (Martin et al., 2009; Wartlick et al., 2011). To understand mechanisms of this change in growth rates and to learn the physiological regulation of Hippo signaling and mechanical stress, I analyzed Yki and the biomechanical Hippo signaling activity at different stages of disc development. I found the dynamic changes of the biomechanical Hippo signaling are consistent with the dynamics of Yki activity. This pattern of Hippo signaling activity could play a role in controlling the pattern of growth during wing disc development.

Results

Dynamics of Yki activity during wing disc development

To investigate patterns of Yki activity during normal wing growth, we examined Yki protein localization within developing wing discs dissected from third instar larvae of different ages (72, 84, 96, 108 and 120 h after egg laying, AEL) (Fig. 1 D-H). Hippo signaling regulates Yki by controlling its localization, and the relative fraction of nuclear Yki is an indicator of Yki activity (Fig. 1C). Our analysis focused on the region of the disc referred to as the wing pouch, which gives rise to the adult wing and is demarcated

by folds that form in the disc (Fig. 1A and B). Visual inspection of wing discs of different ages revealed that in younger wing discs (72 and 84 h AEL) Yki is predominately nuclear within the wing pouch, whereas in older wing discs (108h and 120h AEL) Yki is predominantly cytoplasmic. There is also a spatial pattern of Yki localization, which changes over time. At 72 h AEL Yki is nuclear in most of the wing pouch, but around the periphery of the wing pouch Yki is both cytoplasmic and nuclear. As wing discs age, Yki levels decline throughout the center of the wing pouch, such that by 108 and 120 h AEL, Yki is predominantly cytoplasmic in the center of the wing pouch, except along the dorsal-ventral (D-V) compartment boundary. Around the periphery of the wing pouch, however, relative levels of nuclear Yki decline very little during third instar. Thus in older wing discs (108h and 120h AEL) nuclear Yki is mostly low in the center but relatively higher around the periphery.

We used two approaches to quantify relative nuclear Yki levels. First, we divided the wing pouch into central and peripheral regions, taking half the distance between the center and edges of the pouch as the border between center and periphery (Fig. 1B). The ratio of nuclear (defined by DNA staining) to total Yki was then measured within equally sized cuboids in each central and peripheral quadrant. Cells along the compartment boundaries were excluded from this analysis because of their distinct gene expression profiles and biophysical properties as compared to other wing cells. In a second approach, we divided wing disc images into 5 μm squares and calculated the relative nuclear Yki levels within each square to generate a quantitative intensity map of nuclear Yki. Intensity maps from several discs were averaged, and relative nuclear Yki levels

displayed on a red (high) to blue (low) heat map. These quantitative analyses confirmed the visual impression of declining nuclear Yki levels in the center of the wing pouch throughout third instar larval growth (Fig. 1N), resulting in a spatial profile in older wing discs with Yki lower in the center of the wing pouch than around the periphery, except along the D-V boundary (Fig. 1P and Q).

To confirm that these changes in Yki localization reflect changes in Yki activity, we examined and quantified the expression of two direct targets of Yki, *expanded* (ex) and *thread/Diap1*. Consistent with the dynamics of Yki localization, relative levels of ex transcription, monitored using a nuclear-localized ex-lacZ reporter, gradually decrease in the center of the wing pouch from 72 to 120 h AEL, but remain similar at the peripheral wing pouch (Fig. 1I-M and O). Hence in older wing discs (108h and 120h AEL), ex-lacZ is lower in the center than at the periphery (Fig. 1R and S). Relative Diap1 intensity also declines in the central wing pouch during third instar, resulting in a spatial pattern in older wing discs in which Diap1 levels are lower in the center, except along the compartment boundaries (Fig. S1). Taken together, these observations confirm that Yki activity declines in the center of the wing pouch during larval development, leading to spatial differences in Yki activity between central and peripheral cells.

Dynamics of Jub biomechanical signaling during wing disc development.

The temporal and spatial pattern of Yki activity is reminiscent of changes in cell shape and cytoskeletal tension that occur during wing development (Fig. 2 and Fig. 3. A-E). For example, the recoil velocity of cell junctions after laser ablation can provide an indication of relative tension, and such experiments have revealed higher tension in

younger wing discs as compared to older wing discs (Fig. 2), and higher tension in peripheral versus central regions within older wing discs (LeGoff et al., 2013; Mao et al., 2013; Rauskolb et al., 2014). Changes in tension are thought to stem at least in part from crowding of cells as the disc grows, and examination of apical cell areas implies that cells are more crowded in the center of older wing discs than they are in the periphery of the wing pouch, or in younger discs. (Aegerter-Wilmsen et al., 2012).

To further investigate the relationship between developmental patterns of Yki activity and patterns of cytoskeletal tension, we examined the levels of Non-muscle myosin II (myosin) using a Myosin light chain (Spaghetti squash, Sqh) GFP fusion protein (Fig. 3. F-G). Levels of myosin along cell-cell junctions (defined by staining for E-cadherin, E-cad) were then quantified and compared to E-cad levels. Levels of both Sqh:GFP and E-cad appear to gradually increase from 72 to 120h AEL. However, when junctional Sqh:GFP levels are normalized to E-cad levels, the relative myosin per junction (Sqh:GFP/Ecad ratio) clearly declines over time (Fig. 3O). Moreover, junctional Sqh:GFP declines to a much greater extent in the center of the wing pouch than in the periphery, such that in older wing discs (108 and 120h AEL) junctional myosin is significantly lower in the center than at the periphery (Fig. 3N and O). Notably, this spatial pattern and temporal pattern of declining junctional tension correlate with the pattern of Yki activity described above. We also noted that the cellular distribution of apical myosin differs between younger and older wing discs (Fig. 3K-M). At 72 h AEL, apical myosin is predominantly junctional (Fig. 3K), whereas at 120 h AEL myosin is predominantly junctional in peripheral regions (Fig. 3M), but both junctional and medial in central regions (Fig. 3L).

Tension at adherens junctions promotes Yki activity at least in part by recruiting a Jub-Wts complex that inhibits Wts activity (Rauskolb et al., 2014). To investigate whether the spatial and temporal patterns of Yki and myosin activity might be connected through tension-dependent regulation of Jub and Wts, we analyzed their localization throughout third instar (Fig. 3P-T and Fig. S2C-E). This revealed that junctional Jub and Wts intensities, relative to E-cad, decline in the center of wing pouch, while remaining similar in the periphery of the wing pouch (Fig. 3U-Y). This matches the spatial and temporal dynamics of junctional Sqh:GFP localization, and as for Sqh:GFP, results in a spatial pattern in older wing discs (108 and 120 h AEL) with lower levels of junctional Jub and Wts in the center of the wing pouch, except along the D-V boundary (Fig. 3X and Fig. S2).

Spatial and temporal differences in response to altered tension

The spatial and temporal correlations among patterns of junctional myosin, Jub, Wts and Yki activity imply that cytoskeletal tension contributes to patterns of Yki activity during development, and that this occurs through the Jub biomechanical pathway. To test this, we compared the consequences of a 24h change in cytoskeletal tension within younger (84 h) versus older (120 h) wing discs. Tension was decreased by expressing a UAS-RNAi transgene targeting Rho kinase (Rok), or increased by expressing an activated form of myosin light chain (Sqh.EE) under UAS control. These transgenes were expressed in the posterior half of the developing wing disc by placing them under control of en-Gal4, enabling anterior cells to be used as an internal control.

Expression of UAS transgenes was made conditional by including a temperature-sensitive allele of Gal80.

Increasing tension for 24 h was sufficient to increase recruitment of Jub to adherens junctions, but the increase in Jub was greater in older wing discs than it was in younger wing discs (Fig. 4C, D and M). Conversely, decreasing tension for 24 h was sufficient to decrease recruitment of Jub to adherens junctions, but the decrease in Jub was greater in younger wing discs than it was in older wing discs (Fig. 4E, F and M). These differences between younger and older wing discs are consistent with inferences that cytoskeletal tension decreases in wing disc cells at older stages, resulting in younger wing discs being more sensitive to decreases in tension, and older wing discs being more sensitive to increases in tension.

Similar differential responses to altered tension were observed when we examined the Yki target *ex-lacZ*. Increasing tension significantly augmented *ex-lacZ* expression at 120 h AEL, particularly within the central wing pouch, whereas it only subtly increased *ex-lacZ* at 84 h AEL (Fig. 4I, J and N). Decreasing tension reduced *ex-lacZ* to a significantly greater degree at 84 h AEL, than it did at 120 h AEL (Fig. 4K, L and N). These results further support the conclusion that spatial and temporal differences in tension during wing disc development influence the Jub biomechanical pathway and Yki activity.

Spatial and temporal differences in response to elevated Wts

One implication of our observation of temporal differences in tension-dependent Jub regulation is that the Jub biomechanical pathway contributes more to promoting Yki

activity in younger discs than it does in older discs. Since Jub activates Yki by inhibiting Wts, we hypothesized that younger wing discs might therefore be more sensitive to increases in Wts levels than older wing discs. To test this, we induced Wts over-expression for 24 h in posterior cells using the conditional system described above. Remarkably, this led to a strong reduction in ex-lacZ expression in 84 h AEL discs, but much weaker effects in 120 h AEL discs, particularly in the central region of these older discs (Fig. S2F and G). This observation further supports the conclusion that differences in cytoskeletal tension, acting through the Jub biomechanical pathway, modulate Yki activity during development.

Influence of cell density on cytoskeletal tension and Hippo signaling

The decreased junctional tension in the central wing pouch at late third instar correlates with increased cell density, and there is both theoretical and experimental support for the hypothesis that cytoskeletal tension decreases as cells become more crowded. To directly test the relationship between crowding and junctional tension, and the influence of cellular crowding on the Jub biomechanical pathway, during wing development, we assessed the consequences of experimentally altering cell density.

To decrease cell density, we took advantage of observations that knock-down of Cyclin-dependent kinase 1 (Cdk1) leads to both lower cell density and higher Yki activity (Montes and Morata, 2017). To investigate whether this increase in Yki activity could be due to elevated junctional tension within the lower density cells, we examined Sqh:GFP and Jub:GFP in posterior cells of wing discs 24 h after en-Gal4 driven RNAi knock-down of Cdk1. We first confirmed that this 24 h induction of Cdk1 RNAi reduced cell density,

and increased *ex-lacZ* expression, consistent with the observations of (Montes and Morata, 2017) (Fig. 5A, D, E and H). Examination of *Sqh:GFP* revealed increased levels of junctional myosin (Fig. 5B and G), and examination of *Jub:GFP* confirmed that this increased myosin was sufficient to increase recruitment of junctional *Jub* (Fig. 5C and F). Thus reducing cell density by knockdown of *Cdk1* is sufficient to enhance junctional tension and *Jub* recruitment to junctions, which could account for the increased *Yki* activity observed.

To increase cell density, we used *Minute* mutations, which are mutations that affect ribosome function and cause a dominant slow growth phenotype (Marygold et al., 2007). In heterozygous *Minute/+* animals, making a whole wing compartment wild type through compartment-specific mitotic recombination can lead wing discs with a faster growing wild-type compartment in an otherwise slow-growing *Minute* heterozygous animal (Martin and Morata, 2006). We induced recombination in posterior cells by driving expression of *Flipase* under *en-Gal4* control, which results in posterior compartments with a high cell density due to their faster growth (Fig. 5I and J). These wild-type posterior compartments also exhibit lower *Sqh:GFP* intensity, lower *Jub* recruitment to junctions, and lower *Yki* activity, as compared to the *Minute* heterozygous cells in the anterior compartment (Fig. K-N). These effects appear more pronounced effect in the central wing pouch, where cell density is highest. These observations further support the conclusion that cell density regulates *Yki* activity through influences on junctional tension during wing development.

Degrading basement membrane does not increase cytoskeletal tension

Our observations confirming a key role for tissue mechanics in modulating growth during development contrast with a recent paper claiming to show the opposite (Ma et al., 2017). This study was based on experimental manipulations of basement membrane, which can influence cell density, but did not actually include any experimental assessment of cytoskeletal tension. To resolve the potential discrepancy between this study and ours, we examined wing discs in which basement membrane was degraded by expression of Matrix metalloprotease 2 (Mmp2). Consistent with previous studies (Ma et al., 2017), expression of Mmp2 for 18h to degrade basement membrane altered cell shape, leading to flatter cells with larger apical areas, but did not significantly affect Yki activity (Fig. 6A, C and F). However, examination of Sqh:GFP and Jub:GFP revealed that this degradation of basement membrane also did not significantly affect junctional tension (Fig. 6A, B, D and E). Thus, although disrupting basement membrane alters cell shape and lowers cell density, it does not increase cytoskeletal tension, which explains why Yki activity is not increased despite the change in cell density.

Relationship of Ds-Fat signaling to patterns of Yki activity

Another potential contributor to proximal-distal differences in Yki activity in the wing could be Ds-Fat signaling (Reddy and Irvine, 2008). In this pathway, the activity of the cadherin protein Fat is regulated by another cadherin, Dachsous (Ds), and the Golgi-localized kinase, Four-jointed (Fj), which modulates binding between Ds and Fat (Irvine and Harvey, 2015). Fat is regulated both by the levels of Ds, and the patterns of Ds and Fj expression: steep gradients are associated with strong Yki activation, while uniform

expression is associated with low Yki activity. In wing discs, Ds expression is graded from proximal (high) to distal (low), whereas Fj expression is graded from distal (high) to proximal (low). Ds-Fat signaling is mediated through the atypical myosin Dachs, whose membrane localization is inhibited by Fat through the adapter protein Vamana (Misra and Irvine, 2016). Examination of Dachs localization from 72 to 120 h AEL, using a genomic Dachs:GFP line, revealed membrane localization of Dachs throughout this time (Fig. S3). Younger wing discs exhibit strong anisotropy of Dachs localization throughout the wing pouch of, consistent with studies of Dachs polarization, whereas in 120 h AEL wing discs, Dachs no longer appears polarized in central wing cells, but it nonetheless exhibits a membrane localization (Fig. S3F-H). This change in Dachs localization likely reflects the very low levels of Ds in the center of the wing pouch, but as membrane localized Dachs promotes Yki activity, it cannot explain the reduction in Yki activity in the central wing pouch of older wing discs.

Patterns of cell proliferation during wing disc development

Cell proliferation rates in the wing disc gradually decrease throughout the third larval instar (Martin et al., 2009; Wartlick et al., 2011). To investigate potential contributions of the spatial and temporal patterns of Yki activity that we identified to patterns of cell proliferation, we labeled proliferating cells by EdU incorporation at 72, 84, 96, 108, and 120 h AEL, and quantified the EdU signal, normalized to total DNA labeling, in the same way as we quantified Yki intensity (Fig. 7). EdU staining performed under identical conditions shows much lower rates of incorporation in older discs than in younger discs, consistent with previous studies showing that rates of growth and cell

proliferation gradually decline in older discs (Fig. 7A-E, K and L). Notably, older discs (108h and 120h AEL) exhibit a spatial pattern of EdU labeling that appears largely (except along the D-V boundary) similar to the pattern of Yki activity – higher in the proximal wing pouch, and lower in the central wing pouch (Fig. 7F-I). These observations suggest that the spatial pattern of Yki activity contribute to the spatial pattern of proliferation.

Discussion

During animal development, it is essential that organs stop growing after they reach a certain size. How tissues know they reach a correct size and stop growing is still largely unknown. By analyzing the Hippo signaling activity at different stages of animal development, we provide evidence that this growth control pathway plays a role in the reduction of cell proliferation rates. In addition, I further studied the upstream regulators of Hippo signaling during this process. And I found that mechanical stress could trigger the dynamic changes in Hippo signaling activity during development.

Mechanical stress can regulate tissue growth in vitro and in vivo. It also has been proposed to play a role in organ size determination. However, evidence to support this hypothesis is lacking. Here, by examining the biomechanical Hippo signaling activity during wing disc development at different stages. Our data suggests that the biomechanical input is crucial for the dynamics of Yki activity. Consistent with previous studies using laser ablation (LeGoff et al., 2013; Mao et al., 2013; Rauskolb et al., 2014)

and photoelasticity (Nienhaus et al., 2009), I found that tension is lower in older wing disc than in younger disc, as well as lower in the central region than the peripheral region in older wing discs. The reduction of tension in the central region of older wing disc is correlated with the reduction of junctional Jub and Wts, as well the reduction of Yki activity. Further more, my data showed that Yki activity has different sensitivity to the alteration of tension, and it is affected simply by changing cell density through altering the cell growth rate. Thus mechanical force does play an important role in controlling the Yki activity during normal development. Our study provides experimental support for the mechanical control of organ size determination.

Hippo signaling is essential in diverse organs and organisms. In *Drosophila*, it is required for the growth of imaginal discs and many other tissues. Indeed, many of the Hippo signaling components were identified by the overgrowth phenotype in imaginal discs. However, we are still not clear how Hippo signaling is regulated during normal development. In this study we analyzed the dynamic activity of the transcriptional activator Yki temporally and spatially. Yki activity drops at the central region of wing pouch and thus forms a gradient in later stages. We also studied the mechanisms that regulate the dynamics of Yki activity. One input is the mechanical stress, as indicated above. Another is Fat signaling, which controls Yki activity by modulating the membrane localization of Dachs. However, in older wing disc Dachs localizes on the membrane in both the central and peripheral regions in older wing discs. Thus my data argues against the idea that Fat signaling is essential in controlling the growth pattern in later stages.

Other upstream factors of Hippo signaling may also play a role in controlling the Yki activity during disc development.

The proliferation rate has long been considered uniform during wing disc development. Consistent with this, we found that proliferation is relatively even at 72h, 84h and 96h AEL, but we also found that proliferation rate is lower in the central region at older stages (108h and 120h). This spatial pattern is correlated with the pattern of Yki activity. Considering the fundamental role of Hippo signaling in promoting organ growth, this down-regulation of Yki activity should be sufficient to reduce growth rates during disc development. A previous study also identified a transient period during early wing disc development that cell proliferation rates are higher in the center of the disc (Mao et al., 2013). However, we found that there is no statistically significant difference in proliferation rate between central and peripheral region at 72h, although the EdU intensity appears slightly higher at the central region. We noticed that the stage that exhibits significant higher growth at the central region from the paper was done at very early stages during development (48-72h AEL) (Mao et al., 2013). Therefore at 72h AEL the discs might no longer have the non-uniform proliferation rate. Interestingly, the proliferation rate is decreasing all over the wing disc but the Yki activity remains constant at the periphery region of wing pouch. How to explain this discrepancy? One possibility is that the peripheral region becomes less sensitive to Yki activity at later stages during disc development. Another possibility is that the dynamic changes of other signaling, like the Dpp morphogen activity, regulates this decrease of proliferation at the

peripheral region or in the whole wing disc. Future work is needed to explore these possibilities during wing disc growth control.

Materials and Methods

Drosophila culture

Unless otherwise indicated, crosses were performed at 25°C. To obtain wing discs at different stages, eggs were laid for 2 to 4 h, and larvae were dissected at 72h, 84h, 96h, 108h and 120h AEL. Protein or gene localization and expression was monitored using previously characterized transgenes: *ex-lacZ*, *Jub:GFP* (Sabino et al., 2011), *Wts:GFP* (Rauskolb et al., 2014), *Dachs:GFP* (Bosveld et al., 2012), *Zip:GFP* and *Sqh:GFP* (Royou et al., 2004).

To manipulate gene expression in the posterior compartment, *en-gal4 tub-Gal80ts*; *UAS-dcr2* flies were crossed with *UAS-RhoK-RNAi* (vdrc104675), *UAS-Sqh.EE* (Winter et al., 2001), *UAS-CdkI-RNAi* (Bloomington 36117), *UAS-wts:myc* (from Tian Xu), or *UAS-Mmp2* (Bloomington 58706) flies. Crosses were first maintained at 18°C and then shifted to 29°C for the indicated times (18, 24 or 36 h). For collecting wing discs at young (equivalent to 84h AEL at 25°C) or old (equivalent to 120h AEL at 25°C) stages, eggs were laid for 6 h, and larvae were first kept at 18°C for 120 h (young) or 192 h (old), and then shifted to 29°C for 24 h before dissection. This protocol yielded discs similar in size to wild-type wing discs maintained at 25°C for 84 or 120 h AEL.

For increasing cell density in the Minute/+ animals, *y w; en-Gal4 UAS-Flp; FRT80B* flies were crossed with *w; Rps17⁴ arm-lacZ FRT80B/TM6B* (Bloomington 6358), or *w; Rps17⁴ His:RFP FRT80B/TM6B* flies. Genotypes are *y w; en-Gal4 UAS-Flp/Zip:GFP; Rps17⁴ arm-lacZ FRT80B/ FRT80B* (Fig. 5K), *y w; en-Gal4 UAS-Flp/Jub:GFP; Rps17⁴ arm-lacZ FRT80B/ FRT80B* (Fig. 5L), *y w; en-Gal4 UAS-Flp/+; Rps17⁴ arm-lacZ FRT80B/ FRT80B* (Fig. 5M) and *y w; en-Gal4 UAS-Flp/ex-lacZ; Rps17⁴ His:RFP FRT80B/ FRT80B* (Fig. 5N).

Histology and Imaging

For most experiments wing discs were fixed in 4% paraformaldehyde for 15 min. at room temperature. Wts:GFP discs were fixed for 8 min., and Sqh:GFP or Zip:GFP discs were fixed for 12 min. Primary antibodies used were rabbit anti-Yki (1:400) (Oh and Irvine, 2008), mouse anti- β -galactosidase (1:200, DSHB), mouse anti-Wg (DSHB), mouse anti-Diap1 (1: 200, B. Hay) and rat anti-E-cad (1:400 DCAD2; DSHB). Secondary antibodies were purchased from Jackson ImmunoResearch Laboratories and Invitrogen. DNA was stained using Hoechst (Invitrogen). Confocal images were captured on a Leica SP8.

For EdU labeling, larvae were dissected in Ringers and anterior halves were immediately placed in 250uL room temperature WM1 (Zartman et al., 2013). An equal volume of 20 μ M EdU (Click-iT EdU Alexa Fluor 555 Imaging Kit, Invitrogen) in WM1 was added for a final concentration of 10 μ M EdU and samples incubated for 10 minutes at room temperature. Tissue was then fixed for 15 minutes with 4% paraformaldehyde in PBS. Subsequent standard antibody staining protocol using mouse anti-WG (DSHB) was then

followed by 30 minutes EdU detection using 1.2 μ L Alexa Fluor azide 555 per 500uL Click-iT reaction cocktail. Afterwards tissues were treated with Hoechst and then washed by PBT. Wing discs were removed and mounted on a slide in Vectashield.

Image Processing and Quantitative Image Analysis

To compensate for aberrations due to the curvature of wing disc and signals from the peripodial epithelium, we used the Matlab toolbox ImSAnE (Heemskerk and Streichan, 2015) to detect and isolate a slice of the disc epithelium surrounding the adherens junctions, using E-cadherin as a reference, as described previously (Pan et al., 2016). The Sqh:GFP, Zip:GFP, Jub:GFP and Wts:GFP images were created using ImSAnE.

Quantification of Sqh:GFP, Zip:GFP, Jub:GFP and Wts:GFP was performed as previously described (Rauskolb et al., 2014), using Volocity (Perkin Elmer) software. In brief, E-cadherin was used as a junctional reference to define the volumes to be quantified, the relative Sqh:GFP, Zip:GFP, Jub:GFP to Wts:GFP to E-cadherin intensities were compared. Quantification of Yki, ex-lacZ and EdU was performed similarly, except we quantified and compared their relative nuclear intensities (Yki, ex-lacZ or EdU to DNA ratio), using DNA staining to define nuclei. To compare relative nuclear Yki at different developmental stages, nuclear Yki versus total Yki ratio was calculated for the comparison. To quantify the signals at central and peripheral regions of wing pouch, we took half the distance between the center and edges of the pouch as the border between center and periphery (Fig. 1A, B). Equally sized cuboids in each central and peripheral quadrant were measured. To compare signals at anterior and posterior compartment of

wing discs, equally sized cuboids in the anterior and posterior compartment at similar regions were measured.

To make the cell area color map, confocal stacks were first processed by ImSAnE to make 2D surface images. The processed images were then segmented using ilastik software, and the segmented pictures were used to perform cell area analysis with a custom Matlab script. The fluorescence intensity heat maps were generated using a custom Matlab script. In brief, the channel used to normalize (E-cadherin or DNA) serves as a 3D mask to keep only the relevant pixels in the channel for the analysis. The center of the wing disc (AP-DV boundaries intersections) is manually picked for each image. We then split the picture into blocks of a given xy size ($4 \times 4 \mu\text{m}$), starting from the center. We measured the average intensity per pixel of each channel. And the intensity of both the reference channel and the channel of interest is normalized over their respective average intensity. The ratio of the channel of interest over the reference channel is then determined. The ratio of each position is stored in a matrix for each image. To average several discs, only matrices of the same xy size blocks were used. The center of the disc serves as a reference point; smaller matrices were expanded to correspond to the size of the biggest matrix and filled with NaN (Not-a-Number). We determined the minimum number of value (usually 2) required to average the ratio for a given position. This means that the edges of the average disk are composed of the same minimum number of value, this correspond to the n given for each experiment. Finally, signals from several wing discs were averaged and represented by the heat map picture.

Variability in mean ratios is presented using 95% confidence intervals, determined using GraphPad Prism7 software. Statistical comparisons between these mean ratios was performed by student T-test or One-way Anova with Tukey's correction, on the log of the ratios, using GraphPad Prism7 software.

Figure 1: Dynamics of Yki activity during wing disc development

(A) Schematic of *Drosophila* wing disc. The yellow ellipse shows the wing pouch region. The horizontal magenta line indicates the dorsal-ventral (D-V) compartment boundary; the vertical blue line indicates the anterior-posterior (A-P) compartment boundary. (B) Schematic of wing pouch of the disc. The dashed ellipse is drawn approximately in the middle between the A-P/D-V intersection and the edge of pouch to separate the center and periphery part of wing pouch. Same sized regions (dashed box) were quantified in the center and periphery region. (D-H and D'-H') Wing discs at 72h, 84h, 96h, 108h and 120h AEL (After egg laying) stained with DNA (Blue, A-E) and Yki (green, A'-E'). Pictures were taken under the same conditions. Scale bar, 20 μ m. (I-M) Wing discs at 72h, 84h, 96h, 108h and 120h AEL stained for the expression of ex-lacZ (Red). Pictures were taken under the same conditions. (M') is a less zoomed in picture of ex-lacZ at 120h AEL, same wing disc of as in (M). Scale bar, 20 μ m. (N) Histogram showing relative Yki levels (nucleus/total) in the central and peripheral region at different stages. (O) Histogram showing relative ex-lacZ intensity to DNA in the central and peripheral region wing disc at different stages. (P, Q) Heat map of relative nuclear Yki intensities of 108h (P) and 120h (Q) AEL (red, high; blue, low). (R, S) Heat map of relative ex-lacZ intensities of 108h (R) and 120h (s) AEL wing disc (red, high; blue, low).

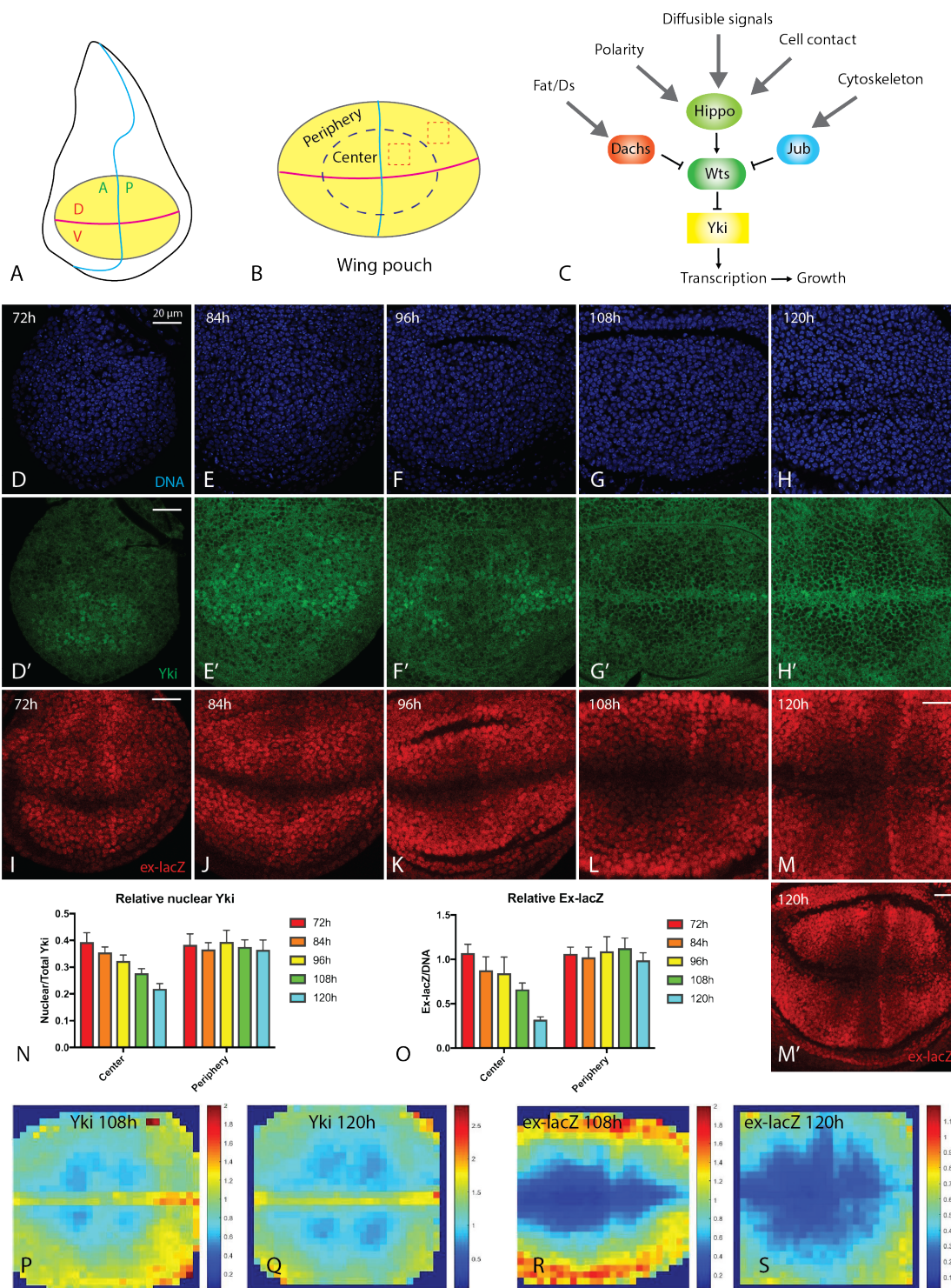


Figure 2. Cytoskeletal tension declines during wing development

(A and B) Horizontal (upper) and vertical (lower, marked by prime symbols) confocal sections through younger (A) or older (B) third-instar wing discs, stained for E-cad (green), DNA (blue), and Discs large (Dlg, red). Insets show lower magnification views of DNA staining (white) with the entire wing pouch visible. (C and D) Confocal sections through live younger (C) or older (D) third-instar wing discs, expressing for E-cad:GFP (green) and UAS-BFP (blue) marking dorsal and A-P boundary cells. (E and F) High-magnification views of the discs in (C) and (D), 1 s before and 8 s after laser cutting of cell junctions between the white arrows. (G) Quantitation of mean displacement velocities of vertices adjacent to cut junctions within the first 300 ms after cutting. Averages are based on 36 (older) or 37 (younger) cuts, and error bars show SEM.

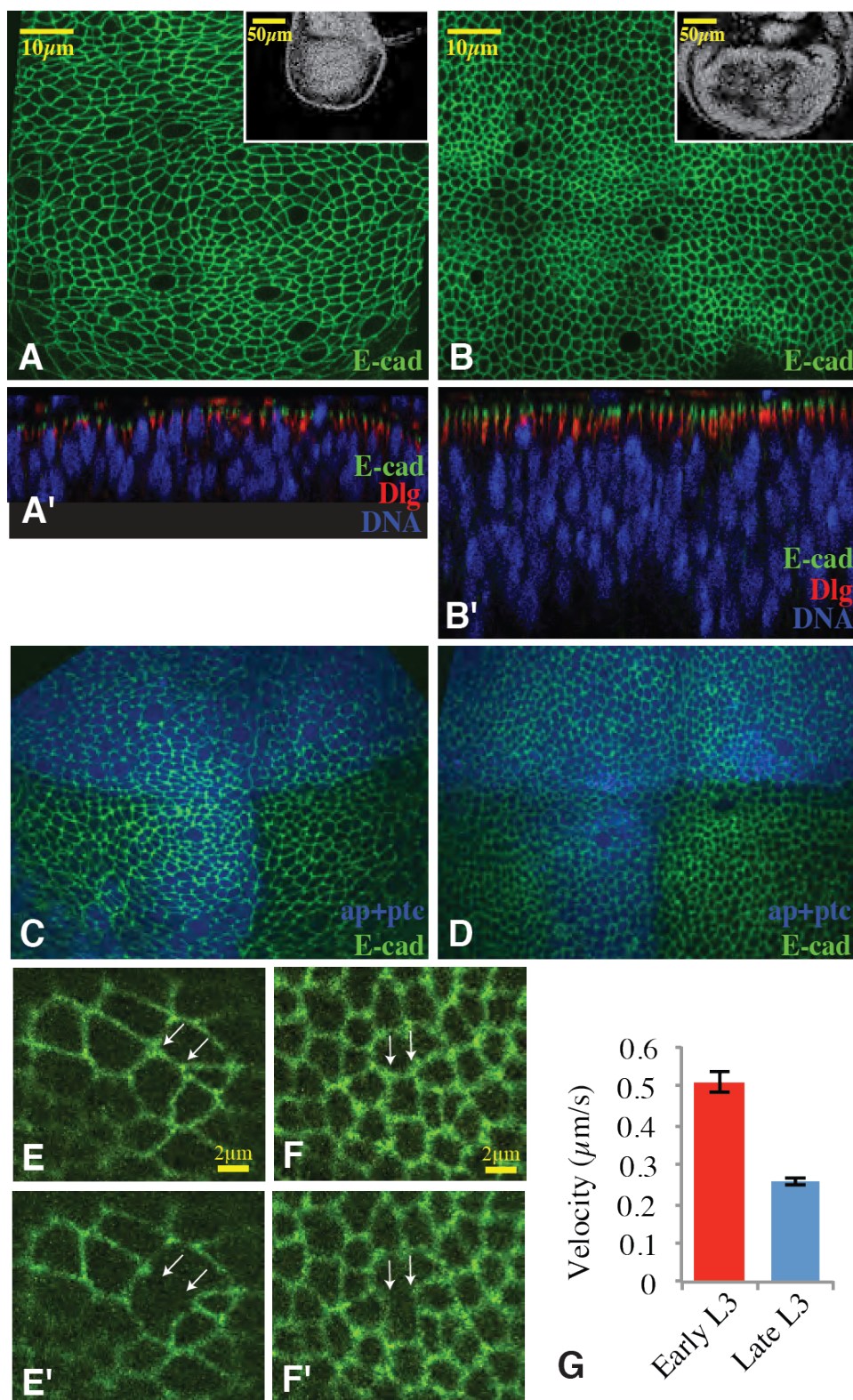


Figure 3: Dynamics of biomechanical Hippo signaling during wing disc development

(A-E) Cell area color map of wing disc at 72h, 84h, 96h, 108h and 120h AEL (red, large; blue, small). (F-J, F'-J') Wing discs stained with Ecad (Red, F-J) and expressing Sqh:GFP (Green, F'-J') at 72h, 84h, 96h, 108h and 120h AEL. Pictures were taken under the same conditions. Scale bar, 20 μ m. (K-M) Zoomed in pictures of wing discs expressing Sqh:GFP (white) at 72h (K), 120h center (L) and periphery (M) region. Junctional Sqh:GFP is weaker in 120h central region. Scale bar, 5 μ m. (N, X) Heat map of relative Sqh:GFP (N) and Jub:GFP (X) intensity of 120hL AEL wing disc (red, high; blue, low). (O, Y) Histograms showing relative Sqh:GFP (O) and Jub:GFP (Y) intensity to Ecad in the central and peripheral region wing disc at different stages. (P-T) Wing discs expressing Sqh:GFP (Green) at 72h, 84h, 96h, 108h and 120h AEL. Pictures are taken under the same conditions. (U-W) Zoomed in pictures of wing discs expressing Jub:GFP (white) at 72h (U), 120h center (V) and periphery (W) region. Junctional Jub:GFP is weaker in 120h central region. Scale bar, 5 μ m.

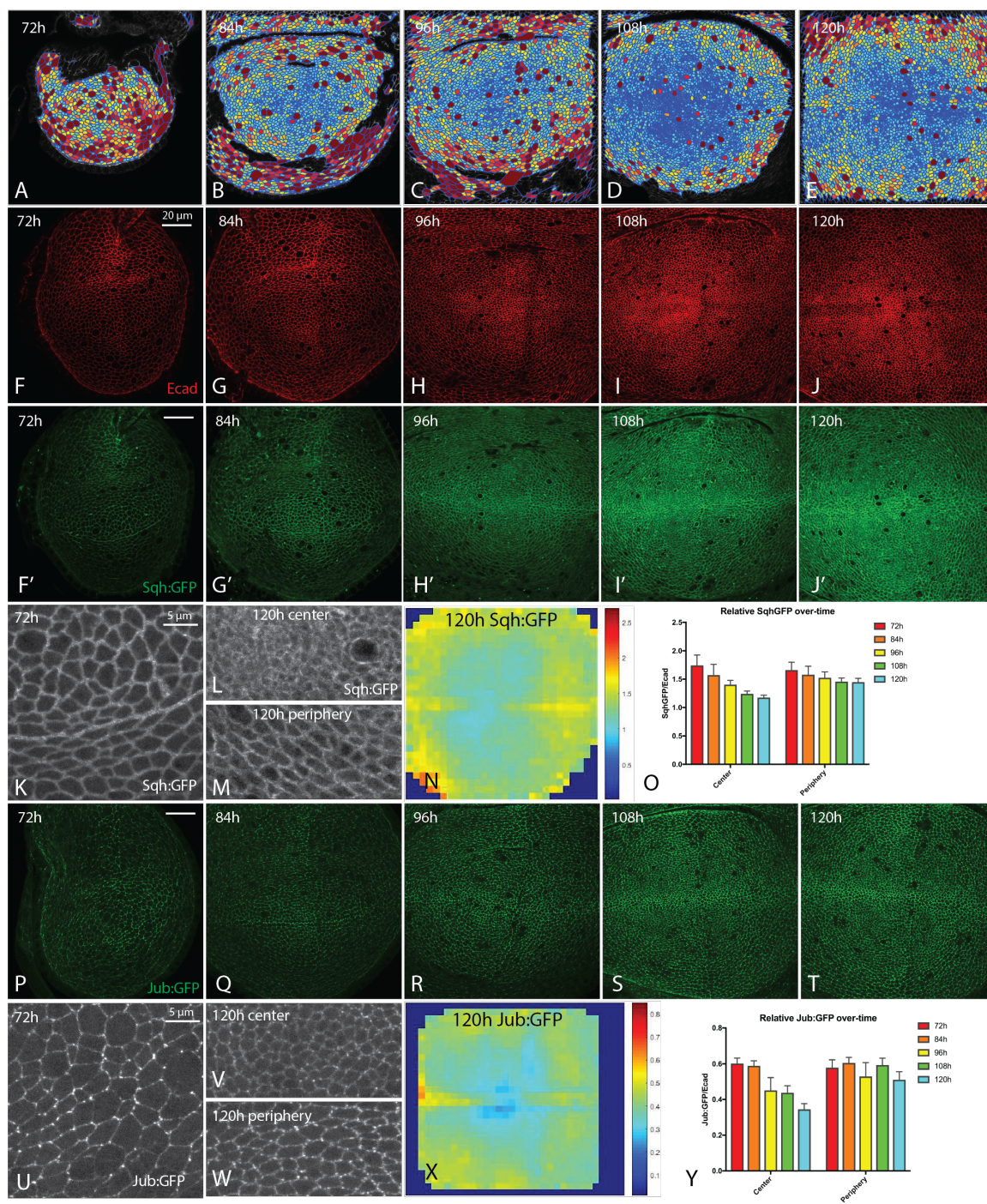


Figure 4: Spatial and temporal differences in response to altered tension

(A-F) Wing discs expressing en-Gal4 UAS-dcr2 tub-Gal80ts Jub:GFP (green) and (A, B) control, (C, D) UAS-SqhEE and (E, F) UAS-Rhok-RNAi stained with Ecad (Red) and Dcr2 (blue). Wing discs were shifted to the restrictive temperature (29 °C) for 24h and fixed at 84h (A, C, E) 120h (B, D, F) AEL. (G-L) Wing discs expressing en-Gal4 UAS-GFP UAS-dcr2 tub-Gal80ts ex-lacZ and (G, H) control, (I, J) UAS-SqhEE and (K, L) UAS-Rhok-RNAi stained for expression of ex-lacZ (red/white) and DNA (Blue). Wing discs were shifted to the restrictive temperature (29 °C) for 24h and fixed at 84h (G, I, K) 120h (H, J, L) AEL. (M, N) Histogram showing relative P to A Jub:GFP (M) and ex-lacZ (N) for the indicated genotypes at 84h and 120h AEL. ****P < 0.0001.

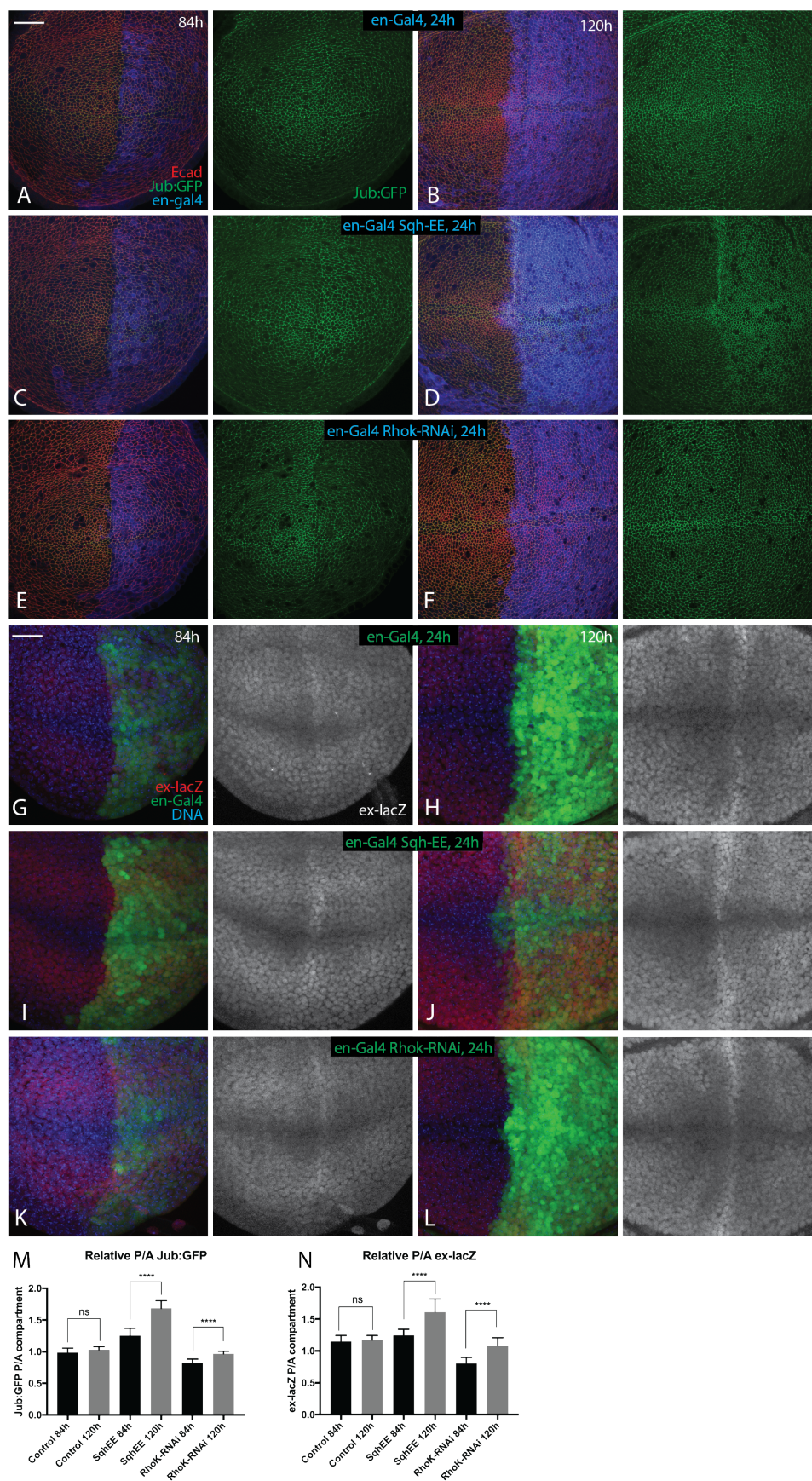


Figure 5. Influence of cell density on cytoskeletal tension and Hippo signaling

(A, B) Wing disc expressing en-Gal4 UAS-dcr2 tub-Gal80ts UAS-Cdk1-RNAi Sqh:GFP was stained with dcr2 (Blue) and Ecad (Red). Discs were shifted to the restrictive temperature (29 °C) for 24h before dissection. (A') Cell area color map (red, large; blue, small) of disc in (A). Cells in the posterior compartment are larger. (B') shows the zoomed in picture from the yellow box. (C) Wing disc expressing en-Gal4 UAS-dcr2 tub-Gal80ts UAS-Cdk1-RNAi Jub:GFP was stained with dcr2 (Blue) and Ecad (Red). Discs were shifted to the restrictive temperature (29 °C) for 24h. (C') shows the zoomed in picture from the yellow box. (D, E) Wing disc expressing en-Gal4 UAS-GFP UAS-dcr2 tub-Gal80ts UAS-Cdk1-RNAi ex-lacZ was stained with for expression of ex-lacZ (red) and DNA (Blue). Discs were shifted to the restrictive temperature (29 °C) for 24h (D) or 36h (E) before dissection. (F-H) Histogram showing relative P to A Jub:GFP (F), Sqh:GFP (G) and ex-lacZ for the control and Cdk-RNAi wing discs. (I) Cartoon illustrating the experimental strategy: the posterior compartment of wing disc is composed of faster-growing wild-type (WT) cells, while the anterior compartment has the slower-growing *Minute/+* (*Rps17*) cells. (J) The anterior compartment is marked by the staining of β -gal (blue), while the posterior compartment lacks the blue color. Wing disc was also stained with Ecad (Red/white), the right panel is the cell area color map (red, large; blue, small). The posterior cells have smaller apical size. (K-N) The anterior compartment is marked by the staining of β -gal (blue) or His:RFP (Blue), while the posterior compartment lacks the blue color. Wing disc was also stained with Ecad (Red) or DNA (Red). Zip:GFP (K), Jub:GFP (L), Yki (M) and ex-lacZ (N) are labeled in green.

Junctional Zip:GFP, Jub:GFP and nuclear Yki, and ex-lacZ are decreased in the posterior compartment.

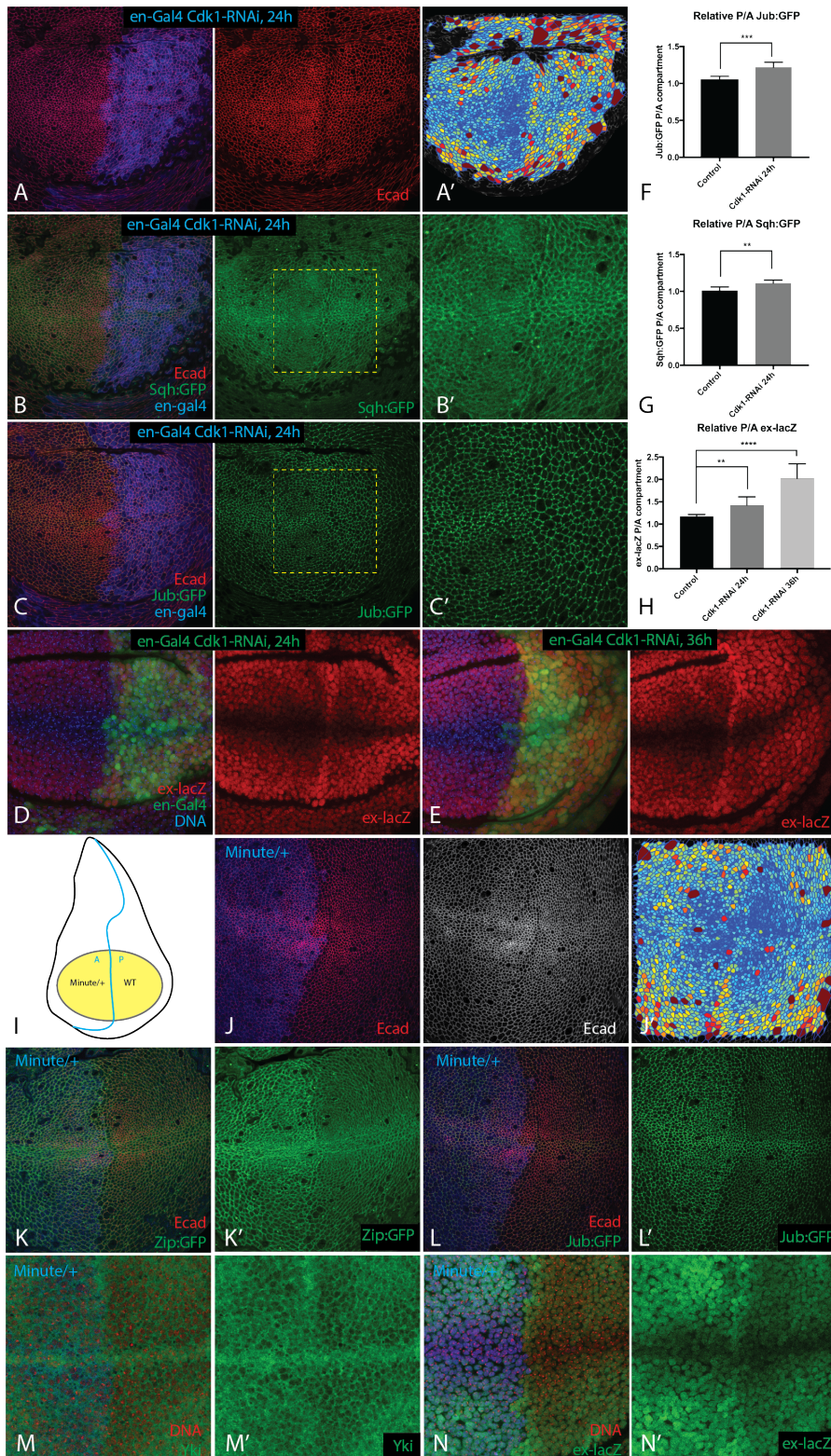


Figure 6. Degrading basement membrane does not increase cytoskeletal tension

(A, B) Wing discs expressing en-Gal4 UAS-dcr2 tub-Gal80ts UAS- Mmp2 Sqh:GFP (A) or Jub:GFP (B) were stained with dcr2 (Blue) and Ecad (Red). Discs were shifted to the restrictive temperature (29 °C) for 18h before dissection. (C) Wing disc expressing en-Gal4 UAS-GFP UAS-dcr2 tub-Gal80ts UAS- Mmp2 ex-lacZ was stained with for expression of ex-lacZ (red) and DNA (Blue). Discs were shifted to the restrictive temperature (29 °C) for 18h before dissection. (D-F) Histogram showing relative P to A Sqh:GFP (D), Jub:GFP (E) and ex-lacZ (F) for the control and Mmp2 overexpression wing discs.

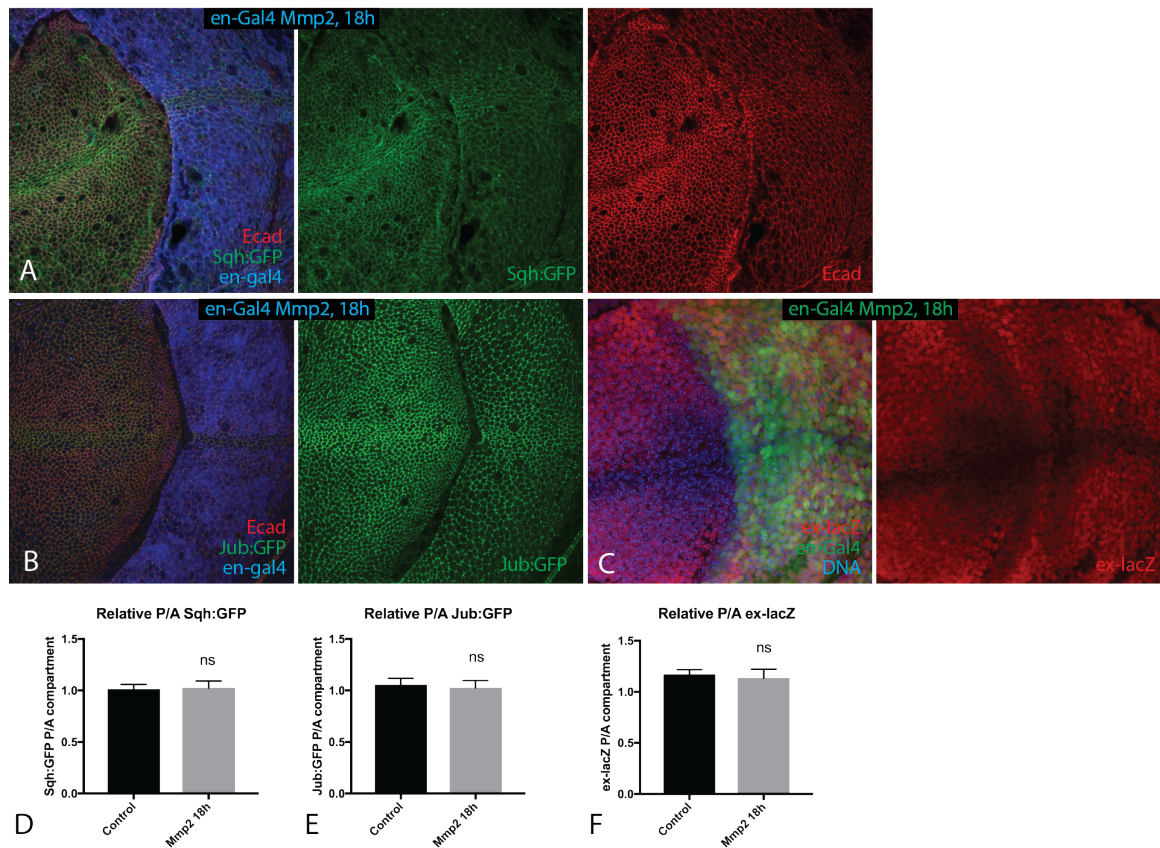
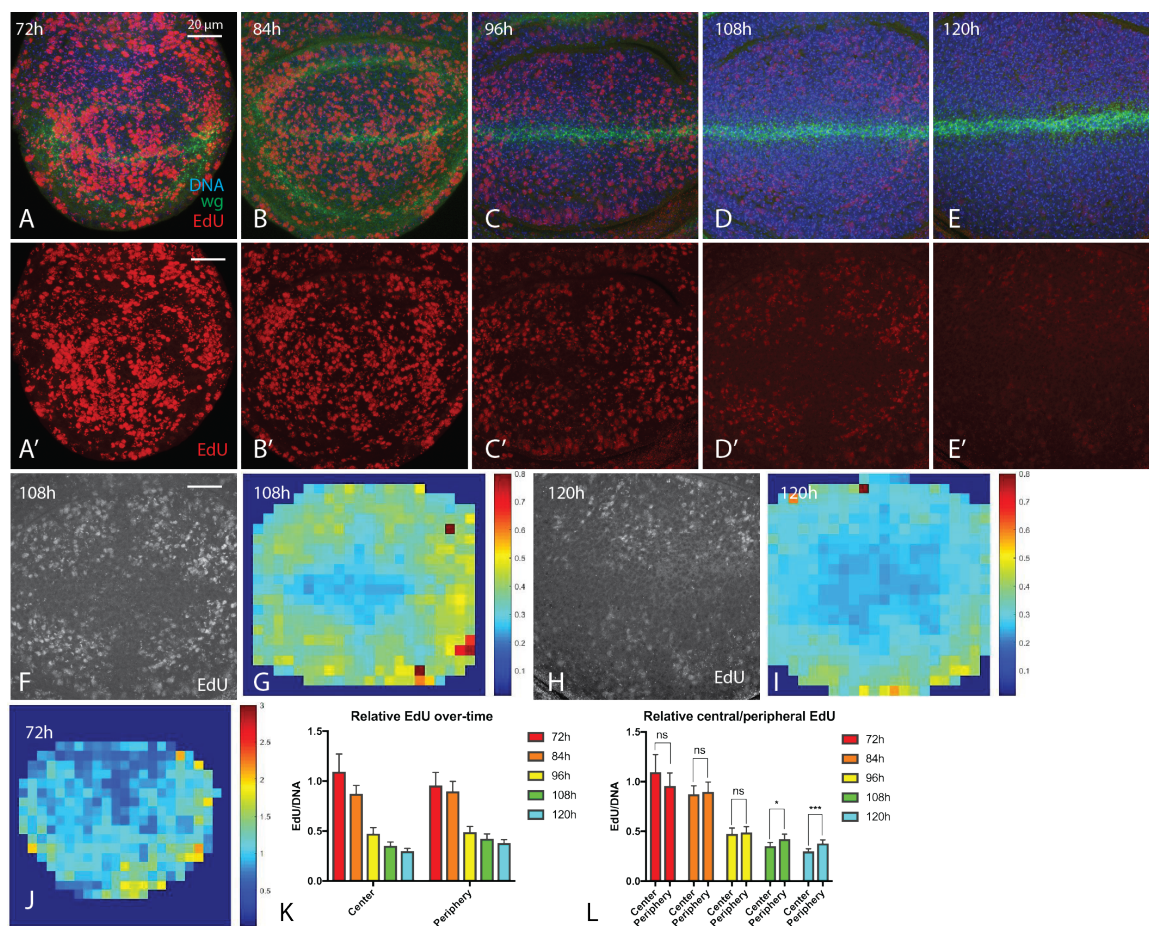


Figure 7: Patterns of cell proliferation during wing disc development

(A-E) Wing discs at 72h, 84h, 96h, 108h and 120h AEL stained with DNA (Blue), wg (green) and EdU (Red). Pictures were taken under the same conditions. Scale bar, 20 μ m. (F and H) Images with enhanced brightness and contrast to illustrate the spatial pattern of EdU (white) at 108h (F) and 120h (H) AEL. (G, I and J) Heat map of relative EdU intensity to DNA of 108h (G), 120h (I) and 72h (J) AEL (red, high; blue, low). (K) Histogram showing relative EdU intensity normalized to DNA at different developmental stages. The relative EdU intensities decrease in both the central and peripheral region of wing pouch. (L) Histogram showing relative EdU intensity in the central and peripheral region. Central region has lower relative EdU intensity at 108h and 120h AEL (After egg laying). * $P < 0.05$, *** $P < 0.001$.

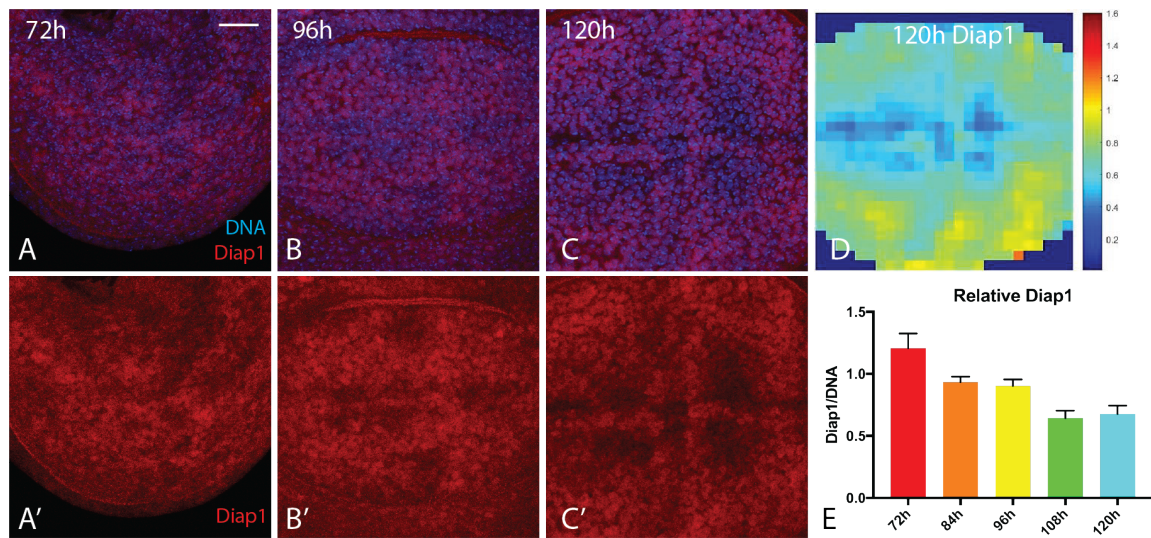


Supplement 1: Additional analysis of Yki activity during wing disc development

(A-C) Wing discs at 72h, 96h, and 120h AEL stained with DNA (Blue) and Diap1 (Red).

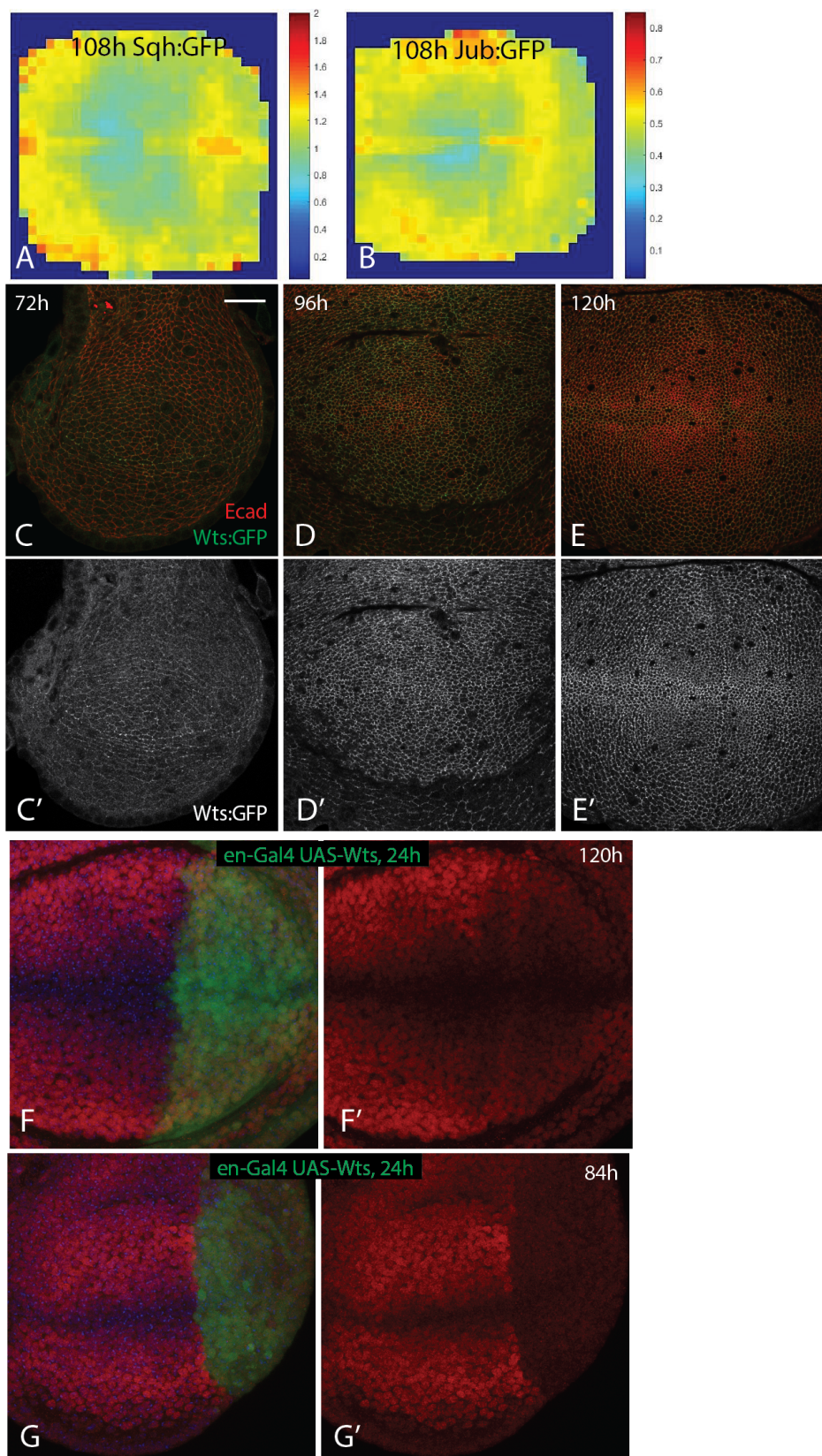
(D) Heat map of relative Diap1 intensities to DNA at 120h AEL (red, high; blue, low).

(E) Histogram showing relative Diap1 intensities in the central region of wing disc at different stages.



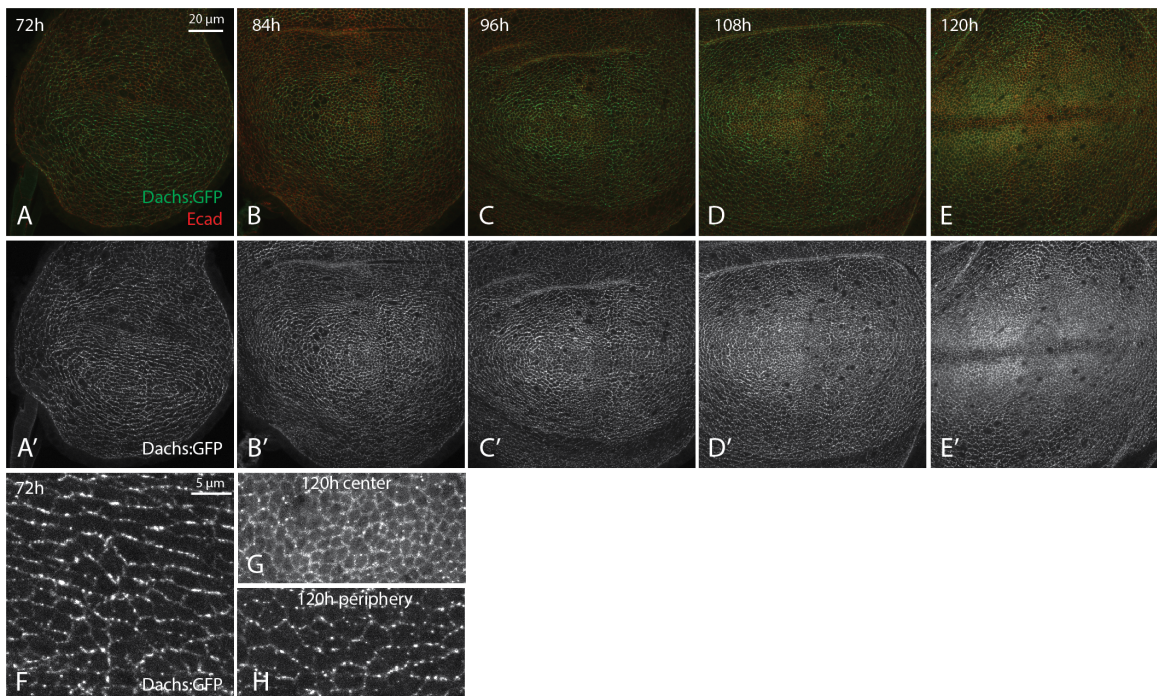
Supplement 2: Additional analysis of the biomechanical Hippo signaling during wing disc development

(A and B) Heat map of relative Sqh:GFP (A) and Jub:GFP (B) intensities to DNA at 108h AEL (red, high; blue, low). (C-E) Wing discs at 72h, 96h, and 120h AEL express Wts:GFP (Green/White) and stained with Ecad (Red). (F and G) Wing discs expressing en-Gal4 UAS-GFP UAS-dcr2 tub-Gal80ts ex-lacZ and UAS-Wts stained for expression of ex-lacZ (red) and DNA (Blue). Wing discs were shifted to the restrictive temperature (29 °C) for 24h and fixed at 84h (G) and 120h (F) AEL.



Supplement 3: Relationship of Ds-Fat signaling to patterns of Yki activity

(A-E) Wing discs expressing Dachs:GFP (Green/White) and stained with Ecad (Red) at 72h, 84h, 96h, 108h and 120h AEL. Pictures were taken under the same conditions. Scale bar, 20 μ m. (F-H) Zoomed in pictures of wing discs expressing Dachs:GFP (white) at 72h (F), 120h center (G) and periphery (H) region. 72h AEL wing discs exhibit strong anisotropy of Dachs localization throughout the wing pouch of; whereas in 120 h AEL wing discs, Dachs no longer appears polarized in central wing cells, but it nonetheless exhibits a membrane localization. Scale bar, 5 μ m.



Chapter 4

The potential roles of peripodial membrane and hinge on tissue mechanics and wing growth

The results described in this chapter are preliminary and exploratory. More work needs to be done to reach a conclusion. All experiments and analysis described in this chapter were done by Yuanwang Pan.

Summary

Studies of growth control have generally treated wing discs as single flat epithelial sheets. Anatomically, however, the disc comprises a columnar cell monolayer covered by a squamous epithelium known as the peripodial membrane. In addition, the wing pouch, which would give rise to adult wing, is surrounded by the hinge tissue in the disc during larval development. The roles of the peripodial membrane and the hinge on wing development are not fully understood. I hypothesized that the peripodial membrane or hinge might mechanically constrain the wing pouch growth during development. To test this idea, I checked some tools to modulate gene expression in the peripodia and hinge. I also altered some gene expression in the peripodia and hinge to modulate their growth or shape. Consistent with previous studies, my preliminary data suggests that the peripodia might contribute to wing growth. Future work is needed to clarify the roles of peripodial membrane and hinge on disc proper growth and mechanics.

Introduction

The *Drosophila* wing disc is an invaluable model to study growth control and pattern formation. It grows into flattened sacs comprising two different cell layers: the columnar epithelium called disc proper and a peripodial membrane (Aldaz and Escudero, 2010) (Fig. 1A and B). Most previous studies, however, consider wing disc as a two dimensional monolayer and focus on the columnar epithelia, which gives rise to the most of adult structures. But there is growing evidence that the peripodial membrane is required for the growth, pattern formation and morphogenesis of the disc proper epithelia (Aldaz et al., 2013; Gibson et al., 2002; Gibson and Schubiger, 2000; Pallavi and Shashidhara, 2003). The mechanisms that coordinate the growth between the two layers of epithelia are not fully understood.

In the third larval instar, wing pouch epithelial cells in the disc proper become increasingly crowded during development (LeGoff et al., 2013; Mao et al., 2013) (Also see Chapter 3 Fig. 3). On the contrary, the peripodial membrane appears stretched (Hariharan, 2015) (Fig. 1C). Interestingly, the cells in peripodial membrane divide at a slower rate than the cells in the disc proper during 3rd instar larvae (McClure and Schubiger, 2005) . Therefore the stretched peripodial might physically restrict the disc proper cells; thus lead to the crowding in wing pouch region (Fig. 1C).

In wing discs, cells are grouped into several distinct regions by folds during the third instar larval stage; the wing pouch region is surrounded by hinge (Klein, 2001) (Fig. 1A). The epithelium of the disc proper becomes buckled in a characteristic way (Fig. 1 B and

C). Several signaling networks have been shown to be involved in the patterning and fold formation in the folds (Ayala-Camargo et al., 2013; Sui et al., 2012; Wang et al., 2016a). However, the mechanical role of hinge on wing pouch growth is not clear. As the hinge region physically surrounds the wing pouch region, the hinge might also play a role in the increased crowding of wing pouch cells.

I tested some Gal4 lines that are specifically expressed in the peripodia or hinge region. I performed some preliminary studies to modulate growth or cell fate in peripodia and hinge. In the future more work need to be done to clarify the roles of peripodia and hinge on wing pouch mechanics.

Results and Discussion

I first tested some Gal4 fly strains that might be expressed in the peripodial membrane. I crossed these tissue specific Gal4 flies with UAS-mCD8:RFP reporter flies to check the Gal4 expression pattern. Gal4 line 45402, 46744 and 49683 are specifically expressed in the third instar wing disc peripodial membrane; and no signal was detected in the disc proper cells (Fig. 2A-C). These three lines exhibited slightly different expressing patterns in the peripodia. Line 49683 appears to have more expression domain in peripodial cells than the 45402 and 46744 lines (Fig. 2A-C). Line 45402 exhibits a gap in the peripodial expression (Fig. 2A).

I then checked if reducing or promoting growth in peripodia affects the adult wing size. Knocking down Yki in the peripodia (no UAS-dcr2 was present in the crosses) leads to smaller adult wing (Fig. 2D-F), suggesting peripodial growth is required for the wing growth. I also promoted growth in peripodia by a couple of approaches. Some genotypes lead to bigger adult wings but not others. When line 45402 was crossed with UAS-E2f UAS-DP (Fig. 2H), UAS-CycD UAS-cdk4 (Fig. 2I) and UAS-TSC1-RNAi (J), the adult wings become larger (Fig. 2N). However, when line 45402 was crossed with UAS-Bantam (Fig. 2K) or UAS-Myc (Fig. 2L), the adult wing size is similar to the control (Fig. 2N). When 46744 fly was crossed with UAS-Bantam (Fig. 2M), the adult fly wings also become larger (Fig. 2N). The reasons why some genotypes have bigger wings but not others are not clear. In the future, an important question is: could increase growth or decrease growth in the peripodia change the disc proper's mechanical properties, like cell shape and cytoskeletal tension?

Next, I tested some lines that might be expressed in the hinge. Ds-Gal4, Zfh2-Gal4 and Gal4 line 49928 are all specifically expressed in the hinge (Fig. 3A-C). As the folds in the hinge region might mechanically constrain the wing pouch region, I tested if getting rid of the folds in hinge could alter mechanical properties of wing pouch cells. One way to remove the fold is to convert the cell fate of hinge cells to wing pouch cells by overexpressing pouch fate specification gene *vg* (vestigial) (Halder et al., 1998; Williams et al., 1991). When I crossed the Ds-Gal4 flies with the UAS-*vg* flies, the folds at the hinge region are reduced (Fig. 3F and G). The Ds-Gal4 UAS-*vg* flies seem to have more nuclear Yki than control (Fig. 3H and I). However, *vg* overexpression in the hinge region

does not lead to more proliferation revealed by PH3 staining (Fig 3D and E); it also does not significantly alter the cell apical shape shown by Ecad staining (Fig. 3J-K).

In summary, my study on whether how peripodial membrane and hinge affect the mechanics and growth was preliminary. The peripodia is required for the growth of disc proper in my analysis. But roles of peripodia and hinge on wing pouch mechanics are not known. Future work could make use of the tools I tested to further explore the idea.

Materials and Methods

***Drosophila* culture**

To check the expression of peripodia or hinge specific Gal4 lines. 45402 (Bloomington 45402), 46744 (Bloomington 46744), 49683 (Bloomington 49683), Ds-Gal4, Zhf2-Gal4 or 48829 (Bloomington 48829) flies were crossed with UAS-mCD8:RFP (Bloomington 27398). The crosses were performed at 25 °C.

For analysis of wing growth, crosses were done at 29 °C. 45402, 46744 or 49683 flies were crossed with UAS-E2f UAS-Dp, UAS-CycD UAS-Cdk4, UAS-TSC1-RNAi, UAS-Yki-RNAi, UAS-Bantam or control flies. Female wings were mounted in Methyl salicylate:Canada Balsam and wings were photographed at the same magnification on a Zeiss Axioplan2. Wing sizes (adult wings and wing discs) were measured using ImageJ.

To convert the cell fate in the hinge to wing cells, Ds-Gal4 flies were crossed with UAS-Vg flies. The crosses were performed at 25 °C.

Histology and Imaging

Wing discs were fixed in 4% paraformaldehyde for 15 min. at room temperature. Primary antibodies used were rabbit anti-Yki (1:400) (Oh and Irvine, 2008), mouse anti-Wg (DSHB), mouse anti-Phospho-Histone H3 (Cell signaling) and rat anti-E-cad (1:400 DCAD2; DSHB). Secondary antibodies were purchased from Jackson ImmunoResearch Laboratories and Invitrogen. DNA was stained using Hoechst (Invitrogen). Confocal images were captured on a Leica SP8.

Figure 1. *Drosophila* wing disc structure

(A) Different regions in wing disc. The green marks the wing pouch region. The yellow marks the hinge and the blue marks the body wall (notum). (B) Side view of wing disc. It comprises a columnar cell epithelia and the squamous epithelium known as the peripodial membrane. (A and B) from (Butler et al., 2003). (C) Comparison between the morphology of the epithelia of the disc proper and the peripodial epithelium. The peripodial membrane appears stretched (top). The disc proper is buckled (top) and the wing pouch region appears compressed (bottom). Pictures are modified from (Hariharan, 2015).

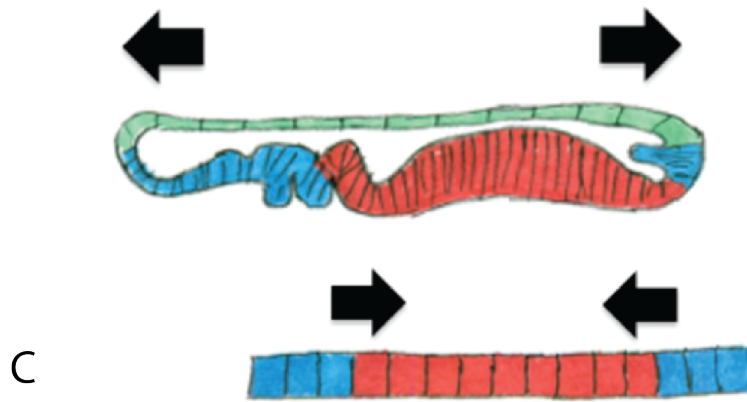
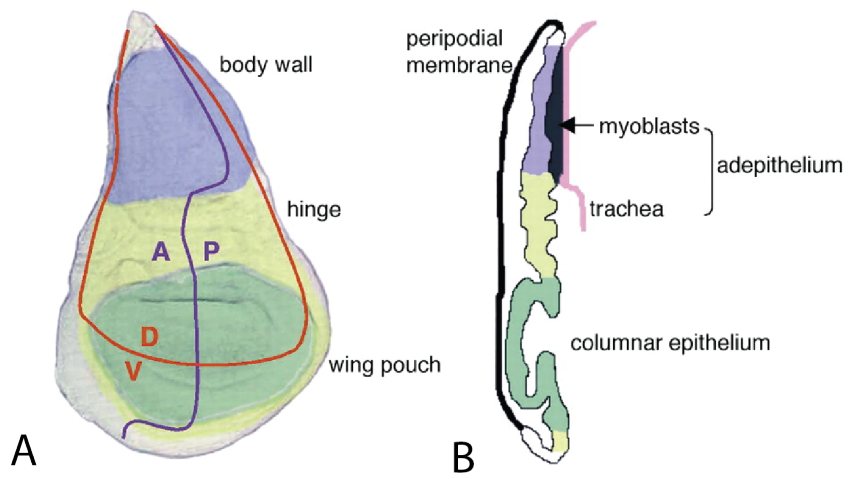


Figure 2. The role of peripodial membrane on wing size control

(A-C) Gal4 lines that specifically expressed in the peripodial membrane. 45402 (A), 46744 (B) and (C) 49683 UAS-mCD8:RFP (Red) wing discs stained with DNA (Blue). The bottom panels also show a XYZ slice of wing disc for the indicated genotype. (D-F) Adult wings from flies expressing control (D), 45402 UAS-Yki-RNAi (E) and 46744 UAS-Yki-RNAi (F). No UAS-dcr2 was present in those flies. (G-M) Adult wings from flies expressing control (G), 45402 UAS-E2f UAS-DP (H), 45402 UAS-CycD UAS-cdk4 (I), 45402 UAS-TSC1-RNAi (J), 45402 UAS-Bantam (K), 45402 UAS-Myc (L) and 46744 UAS-Bantam (M). (N) Histogram showing the quantifications of adult wing size of the indicated genotypes.

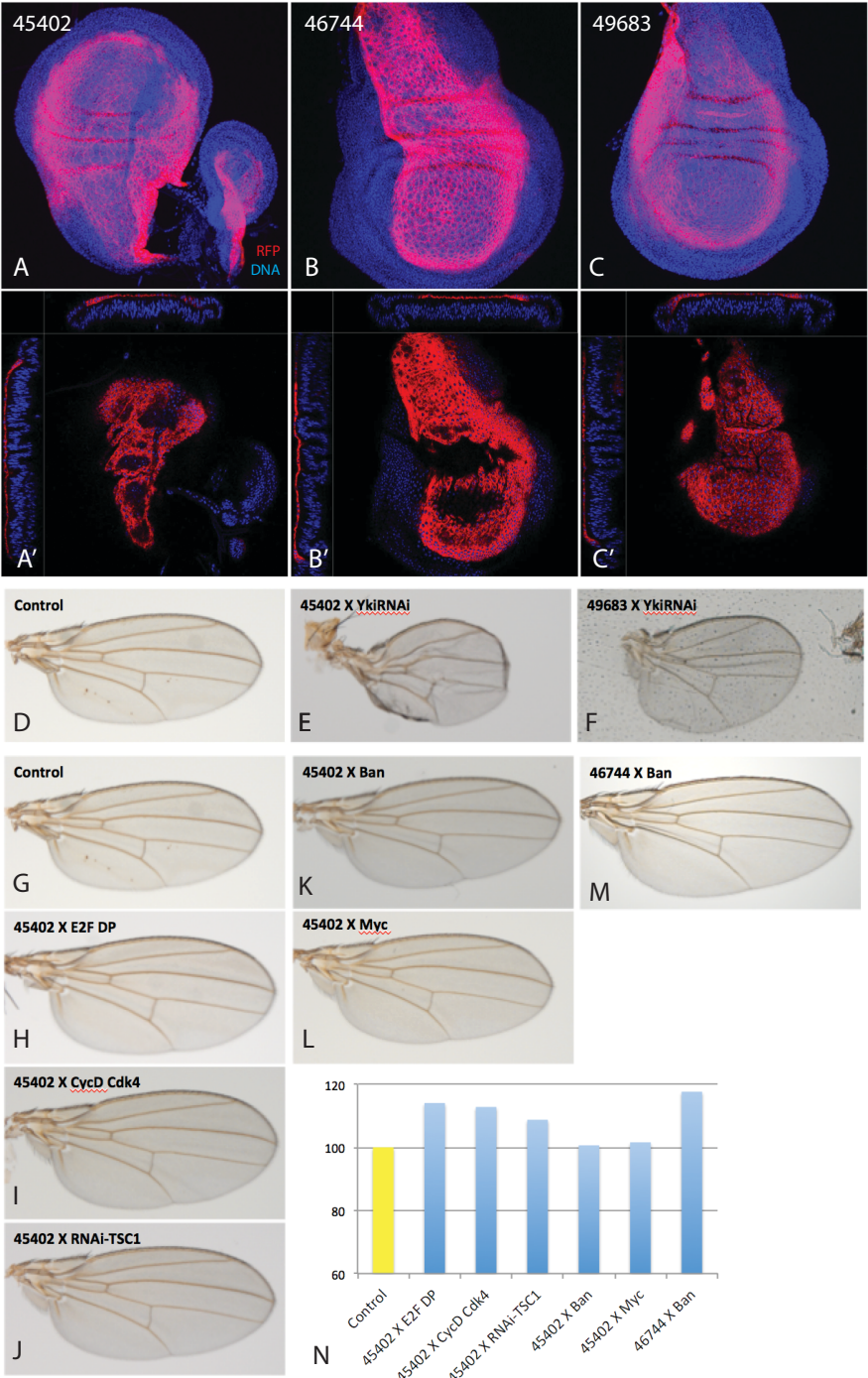
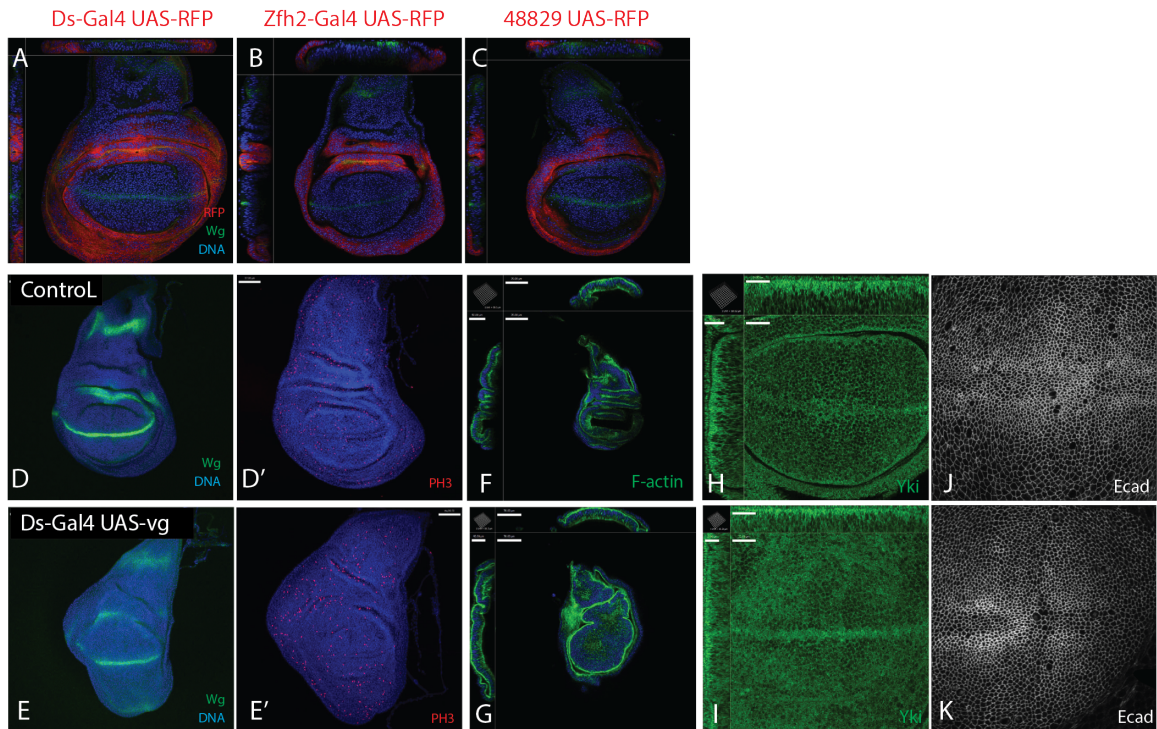


Figure 3. The roles of hinge on wing pouch growth

(A-C) Gal4 lines that specifically expressed in the hinge of wing disc. Ds-Gal4 (A), Zfh2-Gal4 (B) and 49928 (C) with UAS-mCD8:RFP (red) stained with wg (green) and DNA (blue). (D and E) 112h after egg laying (AEL) wing discs of control (D) and Ds-Gal4 UAS-vg (E) stained with wg (green), DNA (blue) and PH3 (red). (F and G) 112h after egg laying (AEL) wing discs of control (F) and Ds-Gal4 UAS-vg (G) stained with F-actin (green) and DNA (blue). (H and I) 112h after egg laying (AEL) wing discs of control (H) and Ds-Gal4 UAS-vg (I) stained with Yki (green) and DNA (blue). (J and K) 112h after egg laying (AEL) wing discs of control (J) and Ds-Gal4 UAS-vg (K) stained with Ecad (white).



Chapter 5

General discussion

To form organs of correct size and proportion, growth must be tightly controlled. Previous studies have focused on the biochemical signals that influence organ growth. However, in addition to the biochemical environment, cells in a developing organ are also in a mechanical environment: they constantly experience forces from their neighbors and the extracellular matrix. Indeed, mechanical stress has been appreciated as an important regulator of tissue growth

A breakthrough for the understanding of mechanical stress on growth is the elucidation of signaling networks that transduce tissue mechanics to biochemical signals (Fernandez-Sanchez et al., 2015; Irvine and Shraiman, 2017). Among the different pathways, Hippo signaling is essential for linking the mechanical signals to gene expression that regulate growth (Meng et al., 2016; Sun and Irvine, 2016). Most of our understanding of the molecular underpinnings, however, was performed in vitro by tissue culture systems. Due to limited tools to modulate and measure mechanical forces in vivo, our understanding on how mechanical forces regulate tissue growth is limited.

Recent research began to shed light on how Hippo signaling or Yki/Yap interplays with tissue mechanics in vivo. For example, Yap is involved in atheroprotective effect of unidirectional shear flow (Wang et al., 2016b). Interaction between Yap and mechanical stress has also been shown during fish embryo development (Porazinski et al., 2015) and mammalian lung branching (Lin et al., 2017). In *Drosophila*, My lab previously identified a biomechanical Hippo signaling through which tension regulates tissue growth in vivo (Rauskolb et al., 2014). It depends upon tension-dependent formation of a

complex between Wts and a Wts inhibitor called Jub, which is recruited to the adherens junction component α -catenin under tension. Importantly, the physiological roles of this biomechanical Hippo signaling were not clear. Moreover, how mechanical stress contributes to in vivo growth regulation also remains unclear. My study on mechanical feedback and the dynamics of the biomechanical Hippo signaling during animal development provide insights for how mechanical force control tissue growth in vivo through Hippo signaling.

Mechanical feedback. Using the mechanical feedback model described by Dr. Shraiman as a framework, I discovered that local differences in growth within a growing tissue could lead to mechanical strain. The mechanical strain is particularly pronounced under conditions where mechanical feedback is blocked, as, for example, when bantam is overexpressed. I further established that the mechanical strain results in a decrease in cytoskeletal tension within the faster-growing cells. Collaborating with Dr. Shraiman's group, we proposed a theoretical model to explain the observed reduction of tension, which is supported by computer simulations based on a generalized vertex model. Further more, taking advantage of the recently discovered biomechanical Hippo signaling in vivo, I showed that the decreased tension within faster-growing cells is sufficient to elevate Hippo signaling. As Hippo signaling is one of the major growth regulatory pathways in animals, this defines a process by which forces experienced by cells in living tissues can modulate their growth rates.

I proposed that mechanical feedback regulation of growth is a homeostatic mechanism that suppresses local overgrowth to prevent tissue distortion. Several distinct approaches to generate local differences in growth rates all trigger the mechanical effects that decrease cytoskeletal tension and modulate the biomechanical Hippo signaling. I further identified that reducing growth rates or increasing tension within the faster growing clones is sufficient to reverse their effects on Hippo signaling. Therefore these effects on tension and Hippo signaling should not stem from the various genotypes analyzed. Mechanical feedback is thus a general mechanism to maintain homeostatic growth in the developing wing disc. Remarkably, mechanical strain and tissue distortion are particularly evident when mechanical feedback is blocked in the faster-growing tissues, for example when *bantam* is overexpressed or when *Yki* is over activated in the clones (LeGoff et al., 2013; Mao et al., 2013). Therefore, one role of mechanical feedback during normal development should be to ensure cells proliferate at similar rates to minimize tissue distortion.

What is the contribution of mechanical feedback during normal wing disc growth control?

It has been a puzzle for decades that how the non-uniform distributed growth factors (like Dpp) generate an even growth pattern in wing disc. Theoretical models suggest that mechanical feedback could play a role here (Aegerter-Wilmsen et al., 2012; Shraiman, 2005). Remarkably, when I blocked mechanical feedback in the wing disc, the growth pattern is altered: the elevated cell proliferation rate observed in the center of the wing disc, near the anterior–posterior compartment boundary, is consistent with the hypothesis that higher mitogenic signaling in the center of the disc is normally balanced by higher

mechanical compression, which triggers mechanical feedback. Thus, my observations also implicate mechanical feedback in the normal growth pattern within developing organs (Fig. 1).

In addition to the discovery of physiological roles of mechanical feedback in tissue shape and growth control, I also delineated the molecular mechanism through which mechanical feedback functions in vivo. Several approaches of making faster-growing clones all lead to the reduction in junctional Jub and Wts, as well as the Yki activity. The biomechanical Hippo signaling is hence a sensor for cells in a growing organ to experience the mechanical status and coordinate their growth rates.

Dynamics of tissue mechanics and Hippo signaling during disc development. How do mechanical forces or mechanical feedback work at different stages during wing disc development? To answer this question, I analyzed the cell mechanical properties over-time in wing discs during third instar larval development. Disc proper epithelia become thicker from early to late third instar larvae, and their apical areas become increasingly smaller, especially in the central regions. This observation suggests that cells could become increasingly compressed during disc development. Laser ablation experiment showed that tension is indeed decreased from younger to older discs. Junctional Myosin is also decreased over-time, especially in the central region. My observations indicated that tissue mechanics are changing during wing disc development: cytoskeletal tension of the cells decreases over-time, and at later stages the tension exhibits a spatial pattern (lower at center, higher at periphery).

As cytoskeletal tension can regulate tissue growth through a biomechanical Hippo signaling, I also analyzed the biomechanical Hippo signaling and Yki activity at different stages of wing disc development. Yki activity gradually decreases in the central region of wing disc; and the temporal and spatial changes in Yki activity is related to the changes in junctional Jub and Wts. Noticeably, altering tension in younger and older wing discs does have different effects on Yki activity. Therefore, tissue mechanics contribute to the dynamics of Yki activity (Fig. 2).

Cell culture studies suggested that cells tend to proliferate more in low density than in high density (McClatchey and Yap, 2012; Streichan et al., 2014). The Hippo signaling network has been shown to be essential for density mediated growth control (Zhao et al., 2007). But the mechanisms are not fully understood. Moreover, how cell density coordinates with growth control during animal development is not clear. During *Drosophila* wing disc development, cell density is gradually increasing. My research also found cytoskeletal tension is also declining over-time. Importantly, changing cell density is sufficient to alter cytoskeletal tension and Yki activity during disc development. Thus my study established the connection the between cell density with tissue mechanics, as well as the growth control Hippo signaling pathway. Because Hippo signaling is an essential conserved pathway, similar processes could occur in other animal development to control proper growth pattern.

Growth needs to be tightly controlled during development for tissues to reach a correct size and proportion. During *Drosophila* wing disc development, the proliferation rate gradually slows down (Mao et al., 2013; Martin et al., 2009; Wartlick et al., 2011); the underlying mechanisms are not fully understood. Dpp signaling dynamics have been proposed to contribute to the growth reduction; but models based on Dpp dynamics are in debate (Irvine and Harvey, 2015). My observation that cytoskeletal tension is decreasing from younger to older stages suggests mechanical stress could play a role in this growth rate reduction. Supporting this idea, I found that proliferation rate is lower in the central region of wing pouch than the peripheral region in older wing discs; this proliferation pattern is consistent with the pattern of cytoskeletal tension and Yki activity. Thus the spatial differences in Hippo signaling activity could contribute to spatial patterns of growth in vivo. However, Yki activity remains relatively constant at the peripheral region during disc development; how proliferation rates decrease in this region requires more studies. Above all, my study provided evidence that mechanical stress contributes to growth during animal development.

Future directions. My research provides evidence of how mechanical strain regulate growth in vivo; it also motivates some interesting future directions. For example, how general mechanical feedback is? So far my research has been focus on the *Drosophila* wing imaginal disc. So does it also happen in other fly tissues? Is mechanical feedback a conserved mechanism to maintain homogenous growth during animal development? As the Jub biomechanical Hippo signaling has recently been shown to conserve in mammals

(Ibar et al., 2018), could the mammalian Hippo signaling play a role in mammalian mechanical feedback?

My research suggests that mechanical feedback could suppress tissue from overgrowing. As tumor cells have the feature of uncontrolled growth (Hanahan and Weinberg, 2011), mechanical feedback could thus serve as a tumor suppressor mechanism. On the contrary, altered tissue mechanics or/and constitutively active Yap could enable cells to bypass mechanical feedback to maintain tumor growth. Indeed, many tumors do have altered mechanical properties (Northey et al., 2017) and active Yap activity (Yu et al., 2015). It would be interesting to explore the roles of mechanical feedback during tumorigenesis.

Difference in growth rates can trigger mechanical feedback to reduce tissue distortion. But what would happen if the tissues need particular folds to form three-dimensional structures? The differential growth mechanisms have been used to explain the formation of the gyri in the brain (Tallinen et al., 2014) and the villi in the gut lumen (Shyer et al., 2013). Actually, the wing disc proper epithelia also become buckled in a characteristic way in later third instar. Could the difference in growth rates cause those folds? How does mechanical feedback function in those regions?

Why do cells in the *Drosophila* wing disc become increasingly crowded during development? Considering the sac-like three-dimensional structure of the disc, one model could be the peripodial membrane or the hinge region restricts the growth of wing pouch epithelia. Therefore the wing pouch epithelial cells become increasingly compressed

because of the physical restriction from peripodia and hinge. I generated some tools to manipulate gene expression in peripodia and hinge. Unfortunately, I do not have a conclusion yet. One simple idea to test in the future is that does the growth or mechanics of peripodia or hinge affect the physical properties and hence growth of disc proper cells?

Consistent with previous findings, I observed the proliferation rate declines from younger to older wing disc. This decline in proliferation rate is evident in both the central and peripheral regions of wing pouch. However, Yki activity is only significantly decreased in the central part of wing disc. How to explain this discrepancy? One possibility is that the periphery region becomes less sensitive to Yki activity. Another possibility is that the dynamic changes of other signals, like the Dpp morphogen and ecdysone, regulate the decrease of proliferation at the peripheral region or the whole wing disc. Future work is needed to explore these possibilities during wing disc growth control. Above all, it would be interesting to study the cross talk and coordination between other growth factors (like Dpp) with mechanical signals during disc development.

My study discovered that Yki activity gradually declined in the central region of wing disc, and this decline could control of the slow down of growth rates in wing disc. How general is this? Does other fly tissues have also decreased Yki activity during development? What happens in mammalian organs? Future research needs to address these questions.

Figure 1. Patterns of Dpp activity and cell proliferation in the wing disc

Schematics of part of the *Drosophila* wing imaginal disc. (A) The morphogen growth factor Dpp is produced from cells at a localized source along the center of the disc, and spreads out forming a concentration gradient. (B) Cell proliferation (shown by the dots) is essentially evenly distributed throughout the wing disc. Lines mark the compartment boundaries. (C) When Jub-mediated mechanical feedback is blocked proliferation becomes unevenly distributed, with higher levels where Dpp signaling is higher. Picture from (Irvine and Shraiman, 2017).

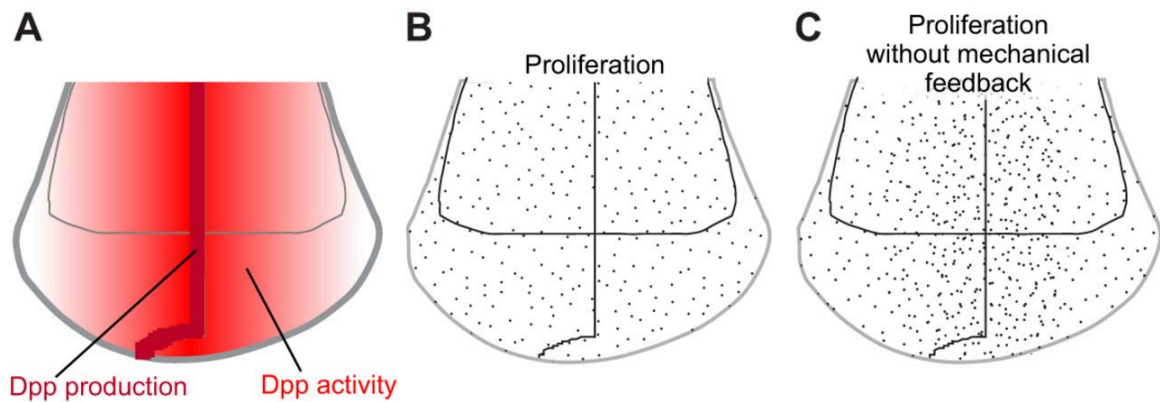
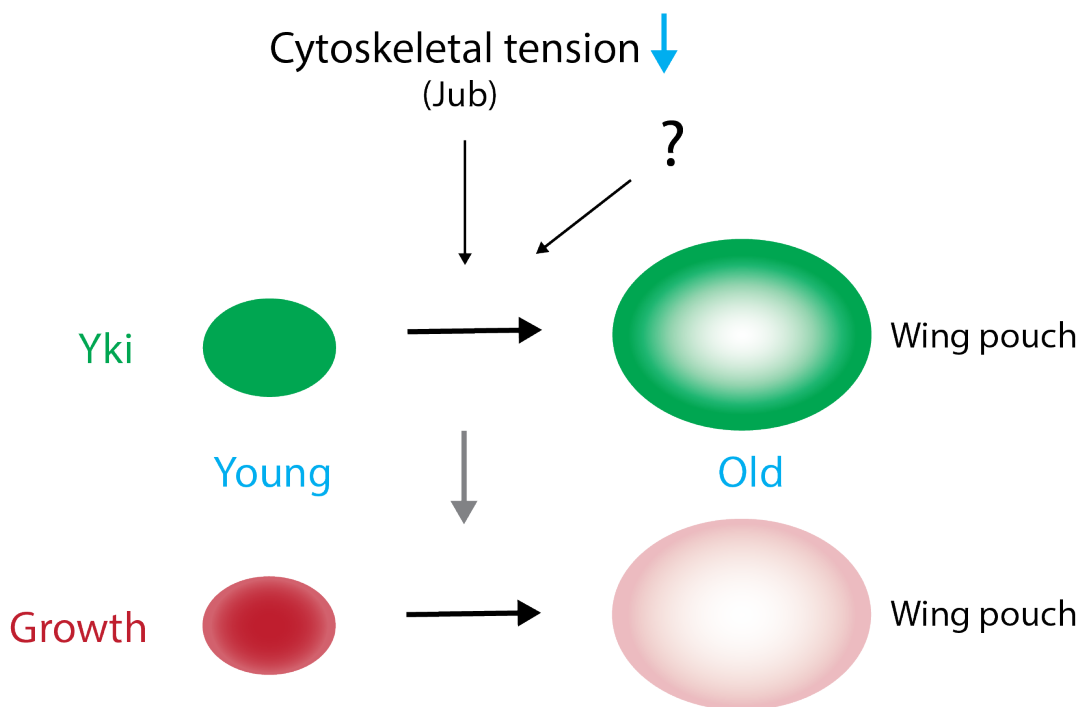


Figure 2. The dynamics of Hippo signaling activity and growth in vivo

Yki activity gradually decreases in the central region of the developing *Drosophila* wing disc. Spatial and temporal changes in Yki activity can be explained by changes in cytoskeletal tension and biomechanical regulators of Hippo signaling. Other upstream factors might also contribute to the dynamics of Yki activity. The proliferation rate in wing disc is also declining over-time, and forms a spatial pattern (center low, periphery high) in older wing disc. The spatial differences in Hippo signaling contribute to spatial patterns of growth in vivo.



Reference

- Aegerter-Wilmsen, T., Aegerter, C.M., Hafen, E., and Basler, K. (2007). Model for the regulation of size in the wing imaginal disc of *Drosophila*. *Mech Develop* *124*, 318-326.
- Aegerter-Wilmsen, T., Heimlicher, M.B., Smith, A.C., de Reuille, P.B., Smith, R.S., Aegerter, C.M., and Basler, K. (2012). Integrating force-sensing and signaling pathways in a model for the regulation of wing imaginal disc size. *Development* *139*, 3221-3231.
- Affolter, M., and Basler, K. (2007). The Decapentaplegic morphogen gradient: from pattern formation to growth regulation. *Nat Rev Genet* *8*, 663-674.
- Aldaz, S., and Escudero, L.M. (2010). Imaginal discs. *Curr Biol* *20*, R429-431.
- Aldaz, S., Escudero, L.M., and Freeman, M. (2013). Dual role of myosin II during *Drosophila* imaginal disc metamorphosis. *Nat Commun* *4*, 1761.
- Aragona, M., Panciera, T., Manfrin, A., Giulitti, S., Michielin, F., Elvassore, N., Dupont, S., and Piccolo, S. (2013). A mechanical checkpoint controls multicellular growth through YAP/TAZ regulation by actin-processing factors. *Cell* *154*, 1047-1059.
- Ayala-Camargo, A., Anderson, A.M., Amoyel, M., Rodrigues, A.B., Flaherty, M.S., and Bach, E.A. (2013). JAK/STAT signaling is required for hinge growth and patterning in the *Drosophila* wing disc. *Dev Biol* *382*, 413-426.
- Benham-Pyle, B.W., Pruitt, B.L., and Nelson, W.J. (2015). Cell adhesion. Mechanical strain induces E-cadherin-dependent Yap1 and beta-catenin activation to drive cell cycle entry. *Science* *348*, 1024-1027.
- Bosveld, F., Bonnet, I., Guirao, B., Tlili, S., Wang, Z., Petitalot, A., Marchand, R., Bardet, P.L., Marcq, P., Graner, F., *et al.* (2012). Mechanical control of morphogenesis by Fat/Dachsous/Four-jointed planar cell polarity pathway. *Science* *336*, 724-727.
- Bosveld, F., Guirao, B., Wang, Z., Riviere, M., Bonnet, I., Graner, F., and Bellaiche, Y. (2016). Modulation of junction tension by tumor suppressors and proto-oncogenes regulates cell-cell contacts. *Development* *143*, 623-634.
- Boulan, L., Milan, M., and Leopold, P. (2015). The Systemic Control of Growth. *Csh Perspect Biol* *7*.
- Brennecke, J., Hipfner, D.R., Stark, A., Russell, R.B., and Cohen, S.M. (2003). *bantam* encodes a developmentally regulated microRNA that controls cell proliferation and regulates the proapoptotic gene *hid* in *Drosophila*. *Cell* *113*, 25-36.
- Brunette, D.M. (1984). Mechanical stretching increases the number of epithelial cells synthesizing DNA in culture. *J Cell Sci* *69*, 35-45.

- Bryant, P.J., and Levinson, P. (1985). Intrinsic Growth-Control in the Imaginal Primordia of *Drosophila*, and the Autonomous Action of a Lethal Mutation Causing Overgrowth. *Dev Biol* 107, 355-363.
- Buchmann, A., Alber, M., and Zartman, J.J. (2014). Sizing it up: The mechanical feedback hypothesis of organ growth regulation. *Semin Cell Dev Biol* 35, 73-81.
- Butler, M.J., Jacobsen, T.L., Cain, D.M., Jarman, M.G., Hubank, M., Whittle, J.R., Phillips, R., and Simcox, A. (2003). Discovery of genes with highly restricted expression patterns in the *Drosophila* wing disc using DNA oligonucleotide microarrays. *Development* 130, 659-670.
- Cho, E., Feng, Y., Rauskolb, C., Maitra, S., Fehon, R., and Irvine, K.D. (2006). Delineation of a Fat tumor suppressor pathway. *Nat Genet* 38, 1142-1150.
- Codelia, V.A., Sun, G.P., and Irvine, K.D. (2014). Regulation of YAP by Mechanical Strain through Jnk and Hippo Signaling. *Curr Biol* 24, 2012-2017.
- Curtis, A.S., and Seehar, G.M. (1978). The control of cell division by tension or diffusion. *Nature* 274, 52-53.
- Das Thakur, M., Feng, Y., Jagannathan, R., Seppa, M.J., Skeath, J.B., and Longmore, G.D. (2010). Ajuba LIM proteins are negative regulators of the Hippo signaling pathway. *Curr Biol* 20, 657-662.
- Deng, H., Wang, W., Yu, J., Zheng, Y., Qing, Y., and Pan, D. (2015). Spectrin regulates Hippo signaling by modulating cortical actomyosin activity. *Elife* 4, e06567.
- Dupont, S. (2016). Role of YAP/TAZ in cell-matrix adhesion-mediated signalling and mechanotransduction. *Exp Cell Res* 343, 42-53.
- Dupont, S., Morsut, L., Aragona, M., Enzo, E., Giulitti, S., Cordenonsi, M., Zanconato, F., Le Digabel, J., Forcato, M., Bicciato, S., *et al.* (2011). Role of YAP/TAZ in mechanotransduction. *Nature* 474, 179-183.
- Eder, D., Aegerter, C., and Basler, K. (2017). Forces controlling organ growth and size. *Mech Develop* 144, 53-61.
- Fan, R., Kim, N.G., and Gumbiner, B.M. (2013). Regulation of Hippo pathway by mitogenic growth factors via phosphoinositide 3-kinase and phosphoinositide-dependent kinase-1. *Proc Natl Acad Sci U S A* 110, 2569-2574.
- Farhadifar, R., Roper, J.C., Aigouy, B., Eaton, S., and Julicher, F. (2007). The influence of cell mechanics, cell-cell interactions, and proliferation on epithelial packing. *Curr Biol* 17, 2095-2104.

- Fernandez, B.G., Gaspar, P., Bras-Pereira, C., Jezowska, B., Rebelo, S.R., and Janody, F. (2011). Actin-Capping Protein and the Hippo pathway regulate F-actin and tissue growth in *Drosophila*. *Development* *138*, 2337-2346.
- Fernandez-Sanchez, M.E., Brunet, T., Roper, J.C., and Farge, E. (2015). Mechanotransduction's impact on animal development, evolution, and tumorigenesis. *Annu Rev Cell Dev Biol* *31*, 373-397.
- Fletcher, G.C., Elbediwy, A., Khanal, I., Ribeiro, P.S., Tapon, N., and Thompson, B.J. (2015). The Spectrin cytoskeleton regulates the Hippo signalling pathway. *Embo J* *34*, 940-954.
- Gibson, M.C., Lehman, D.A., and Schubiger, G. (2002). Luminal transmission of decapentaplegic in *Drosophila* imaginal discs. *Dev Cell* *3*, 451-460.
- Gibson, M.C., and Schubiger, G. (2000). Peripodial cells regulate proliferation and patterning of *Drosophila* imaginal discs. *Cell* *103*, 343-350.
- Gokhale, R.H., and Shingleton, A.W. (2015). Size control: the developmental physiology of body and organ size regulation. *Wires Dev Biol* *4*, 335-356.
- Hafen, E., and Stocker, H. (2003). How are the sizes of cells, organs, and bodies controlled? *Plos Biol* *1*, 319-323.
- Halder, G., Polaczyk, P., Kraus, M.E., Hudson, A., Kim, J., Laughon, A., and Carroll, S. (1998). The Vestigial and Scalloped proteins act together to directly regulate wing-specific gene expression in *Drosophila*. *Genes Dev* *12*, 3900-3909.
- Hanahan, D., and Weinberg, R.A. (2011). Hallmarks of cancer: the next generation. *Cell* *144*, 646-674.
- Hariharan, I.K. (2015). Organ Size Control: Lessons from *Drosophila*. *Dev Cell* *34*, 255-265.
- Heemskerk, I., Lecuit, T., and LeGoff, L. (2014). Dynamic clonal analysis based on chronic in vivo imaging allows multiscale quantification of growth in the *Drosophila* wing disc. *Development* *141*, 2339-2348.
- Heemskerk, I., and Streichan, S.J. (2015). Tissue cartography: compressing bio-image data by dimensional reduction. *Nat Methods* *12*, 1139-1142.
- Helmlinger, G., Netti, P.A., Lichtenbeld, H.C., Melder, R.J., and Jain, R.K. (1997). Solid stress inhibits the growth of multicellular tumor spheroids. *Nat Biotechnol* *15*, 778-783.
- Hipfner, D.R., Weigmann, K., and Cohen, S.M. (2002). The bantam gene regulates *Drosophila* growth. *Genetics* *161*, 1527-1537.

- Holley, R.W., and Kiernan, J.A. (1968). "Contact inhibition" of cell division in 3T3 cells. *Proc Natl Acad Sci U S A* *60*, 300-304.
- Hong, X., Nguyen, H.T., Chen, Q., Zhang, R., Hagman, Z., Voorhoeve, P.M., and Cohen, S.M. (2014). Opposing activities of the Ras and Hippo pathways converge on regulation of YAP protein turnover. *Embo J* *33*, 2447-2457.
- Huang, J.B., Wu, S., Barrera, J., Matthews, K., and Pan, D.J. (2005). The Hippo signaling pathway coordinately regulates cell proliferation and apoptosis by inactivating Yorkie, the *Drosophila* homolog of YAP. *Cell* *122*, 421-434.
- Huang, S., and Ingber, D.E. (1999). The structural and mechanical complexity of cell-growth control. *Nat Cell Biol* *1*, E131-138.
- Hufnagel, L., Teleman, A.A., Rouault, H., Cohen, S.M., and Shraiman, B.I. (2007). On the mechanism of wing size determination in fly development. *P Natl Acad Sci USA* *104*, 3835-3840.
- Ibar, C., Kirichenko, E., Keepers, B., Enners, E., Fleisch, K., and Irvine, K.D. (2018). Tension-dependent regulation of mammalian Hippo signaling through LIMD1. *J Cell Sci* *131*.
- Irvine, K.D. (2012). Integration of intercellular signaling through the Hippo pathway. *Semin Cell Dev Biol* *23*, 812-817.
- Irvine, K.D., and Harvey, K.F. (2015). Control of Organ Growth by Patterning and Hippo Signaling in *Drosophila*. *Csh Perspect Biol* *7*.
- Irvine, K.D., and Shraiman, B.I. (2017). Mechanical control of growth: ideas, facts and challenges. *Development* *144*, 4238-4248.
- Johnston, L.A., Prober, D.A., Edgar, B.A., Eisenman, R.N., and Gallant, P. (1999). *Drosophila* myc regulates cellular growth during development. *Cell* *98*, 779-790.
- Karim, F.D., and Rubin, G.M. (1998). Ectopic expression of activated Ras1 induces hyperplastic growth and increased cell death in *Drosophila* imaginal tissues. *Development* *125*, 1-9.
- Kasza, K.E., and Zallen, J.A. (2011). Dynamics and regulation of contractile actin-myosin networks in morphogenesis. *Curr Opin Cell Biol* *23*, 30-38.
- Kim, N.G., and Gumbiner, B.M. (2015). Adhesion to fibronectin regulates Hippo signaling via the FAK-Src-PI3K pathway. *J Cell Biol* *210*, 503-515.
- Kim, N.G., Koh, E., Chen, X., and Gumbiner, B.M. (2011). E-cadherin mediates contact inhibition of proliferation through Hippo signaling-pathway components. *Proc Natl Acad Sci U S A* *108*, 11930-11935.

- Klein, T. (2001). Wing disc development in the fly: the early stages. *Curr Opin Genet Dev* 11, 470-475.
- Lai, Z.C., Wei, X., Shimizu, T., Ramos, E., Rohrbaugh, M., Nikolaidis, N., Ho, L.L., and Li, Y. (2005). Control of cell proliferation and apoptosis by mob as tumor suppressor, *mat*. *Cell* 120, 675-685.
- Lawrence, P.A., and Struhl, G. (1996). Morphogens, compartments, and pattern: lessons from *Drosophila*? *Cell* 85, 951-961.
- Lecuit, T., and Yap, A.S. (2015). E-cadherin junctions as active mechanical integrators in tissue dynamics. *Nat Cell Biol* 17, 533-539.
- LeGoff, L., and Lecuit, T. (2016). Mechanical Forces and Growth in Animal Tissues. *Csh Perspect Biol* 8.
- LeGoff, L., Rouault, H., and Lecuit, T. (2013). A global pattern of mechanical stress polarizes cell divisions and cell shape in the growing *Drosophila* wing disc. *Development* 140, 4051-4059.
- Lin, C., Yao, E., Zhang, K., Jiang, X., Croll, S., Thompson-Peer, K., and Chuang, P.T. (2017). YAP is essential for mechanical force production and epithelial cell proliferation during lung branching morphogenesis. *Elife* 6.
- Low, B.C., Pan, C.Q., Shivashankar, G.V., Bershadsky, A., Sudol, M., and Sheetz, M. (2014). YAP/TAZ as mechanosensors and mechanotransducers in regulating organ size and tumor growth. *FEBS Lett* 588, 2663-2670.
- Mao, Y.L., Tournier, A.L., Hoppe, A., Kester, L., Thompson, B.J., and Tapon, N. (2013). Differential proliferation rates generate patterns of mechanical tension that orient tissue growth. *Embo J* 32, 2790-2803.
- Martin, F.A., Herrera, S.C., and Morata, G. (2009). Cell competition, growth and size control in the *Drosophila* wing imaginal disc. *Development* 136, 3747-3756.
- Marygold, S.J., Roote, J., Reuter, G., Lambertsson, A., Ashburner, M., Millburn, G.H., Harrison, P.M., Yu, Z., Kenmochi, N., Kaufman, T.C., *et al.* (2007). The ribosomal protein genes and Minute loci of *Drosophila melanogaster*. *Genome Biol* 8.
- McClatchey, A.I., and Yap, A.S. (2012). Contact inhibition (of proliferation) redux. *Curr Opin Cell Biol* 24, 685-694.
- McClure, K.D., and Schubiger, G. (2005). Developmental analysis and squamous morphogenesis of the peripodial epithelium in *Drosophila* imaginal discs. *Development* 132, 5033-5042.
- Meng, Z.P., Moroishi, T., and Guan, K.L. (2016). Mechanisms of Hippo pathway regulation. *Gene Dev* 30, 1-17.

- Milan, M., Campuzano, S., and GarciaBellido, A. (1996). Cell cycling and patterned cell proliferation in the wing primordium of *Drosophila*. *P Natl Acad Sci USA* *93*, 640-645.
- Misra, J.R., and Irvine, K.D. (2016). Vamana Couples Fat Signaling to the Hippo Pathway. *Dev Cell* *39*, 254-266.
- Neufeld, T.P., de la Cruz, A.F., Johnston, L.A., and Edgar, B.A. (1998). Coordination of growth and cell division in the *Drosophila* wing. *Cell* *93*, 1183-1193.
- Nienhaus, U., Aegerter-Wilmsen, T., and Aegerter, C.M. (2009). Determination of mechanical stress distribution in *Drosophila* wing discs using photoelasticity. *Mech Develop* *126*, 942-949.
- Noll, N., Mani, M., Heemskerk, I., Streichan, S.J., and Shraiman, B.I. (2017). Active tension network model suggests an exotic mechanical state realized in epithelial tissues. *Nat Phys* *13*, 1221-+.
- Nolo, R., Morrison, C.M., Tao, C., Zhang, X., and Halder, G. (2006). The bantam microRNA is a target of the hippo tumor-suppressor pathway. *Curr Biol* *16*, 1895-1904.
- Northey, J.J., Przybyla, L., and Weaver, V.M. (2017). Tissue Force Programs Cell Fate and Tumor Aggression. *Cancer Discov* *7*, 1224-1237.
- Oda, H., and Tsukita, S. (2001). Real-time imaging of cell-cell adherens junctions reveals that *Drosophila* mesoderm invagination begins with two phases of apical constriction of cells. *J Cell Sci* *114*, 493-501.
- Oh, H., and Irvine, K.D. (2008). In vivo regulation of Yorkie phosphorylation and localization. *Development* *135*, 1081-1088.
- Oh, H., and Irvine, K.D. (2009). In vivo analysis of Yorkie phosphorylation sites. *Oncogene* *28*, 1916-1927.
- Oh, H., and Irvine, K.D. (2010). Yorkie: the final destination of Hippo signaling. *Trends in Cell Biology* *20*, 410-417.
- Pallavi, S.K., and Shashidhara, L.S. (2003). Egfr/Ras pathway mediates interactions between peripodial and disc proper cells in *Drosophila* wing discs. *Development* *130*, 4931-4941.
- Pan, D.J. (2010). The Hippo Signaling Pathway in Development and Cancer. *Dev Cell* *19*, 491-505.
- Pan, Y.W., Heemskerk, I., Ibar, C., Shraiman, B.I., and Irvine, K.D. (2016). Differential growth triggers mechanical feedback that elevates Hippo signaling. *P Natl Acad Sci USA* *113*, E6974-E6983.

- Penzo-Mendez, A.I., and Stanger, B.Z. (2015). Organ-Size Regulation in Mammals. *Csh Perspect Biol* 7.
- Porazinski, S., Wang, H., Asaoka, Y., Behrndt, M., Miyamoto, T., Morita, H., Hata, S., Sasaki, T., Krens, S.F.G., Osada, Y., *et al.* (2015). YAP is essential for tissue tension to ensure vertebrate 3D body shape. *Nature* 521, 217-221.
- Rauskolb, C., Pan, G., Reddy, B.V., Oh, H., and Irvine, K.D. (2011). Zyxin links fat signaling to the hippo pathway. *Plos Biol* 9, e1000624.
- Rauskolb, C., Sun, S.G., Sun, G.P., Pan, Y.W., and Irvine, K.D. (2014). Cytoskeletal Tension Inhibits Hippo Signaling through an Ajuba-Warts Complex. *Cell* 158, 143-156.
- Reddy, B.V., and Irvine, K.D. (2011). Regulation of Drosophila glial cell proliferation by Merlin-Hippo signaling. *Development* 138, 5201-5212.
- Reddy, B.V., and Irvine, K.D. (2013). Regulation of Hippo signaling by EGFR-MAPK signaling through Ajuba family proteins. *Dev Cell* 24, 459-471.
- Reddy, B.V.V.G., and Irvine, K.D. (2008). The Fat and Warts signaling pathways: new insights into their regulation, mechanism and conservation. *Development* 135, 2827-2838.
- Restrepo, S., Zartman, J.J., and Basler, K. (2014). Coordination of Patterning and Growth by the Morphogen DPP. *Curr Biol* 24, R245-R255.
- Rogulja, D., and Irvine, K.D. (2005). Regulation of cell proliferation by a morphogen gradient. *Cell* 123, 449-461.
- Royou, A., Field, C., Sisson, J.C., Sullivan, W., and Karess, R. (2004). Reassessing the role and dynamics of nonmuscle myosin II during furrow formation in early Drosophila embryos. *Mol Biol Cell* 15, 838-850.
- Sabino, D., Brown, N.H., and Basto, R. (2011). Drosophila Ajuba is not an Aurora-A activator but is required to maintain Aurora-A at the centrosome. *J Cell Sci* 124, 1156-1166.
- Sansores-Garcia, L., Bossuyt, W., Wada, K., Yonemura, S., Tao, C., Sasaki, H., and Halder, G. (2011). Modulating F-actin organization induces organ growth by affecting the Hippo pathway. *Embo J* 30, 2325-2335.
- Santinon, G., Pocaterra, A., and Dupont, S. (2016). Control of YAP/TAZ Activity by Metabolic and Nutrient-Sensing Pathways. *Trends Cell Biol* 26, 289-299.
- Schlegelmilch, K., Mohseni, M., Kirak, O., Pruszk, J., Rodriguez, J.R., Zhou, D., Kreger, B.T., Vasioukhin, V., Avruch, J., Brummelkamp, T.R., *et al.* (2011). Yap1 acts downstream of alpha-catenin to control epidermal proliferation. *Cell* 144, 782-795.

- Schroeder, M.C., and Halder, G. (2012). Regulation of the Hippo pathway by cell architecture and mechanical signals. *Semin Cell Dev Biol* 23, 803-811.
- Shraiman, B.I. (2005). Mechanical feedback as a possible regulator of tissue growth. *P Natl Acad Sci USA* 102, 3318-3323.
- Shyer, A.E., Tallinen, T., Nerurkar, N.L., Wei, Z., Gil, E.S., Kaplan, D.L., Tabin, C.J., and Mahadevan, L. (2013). Villification: how the gut gets its villi. *Science* 342, 212-218.
- Spencer, F.A., Hoffmann, F.M., and Gelbart, W.M. (1982). Decapentaplegic: a gene complex affecting morphogenesis in *Drosophila melanogaster*. *Cell* 28, 451-461.
- Stocker, H., and Hafen, E. (2000). Genetic control of cell size. *Curr Opin Genet Dev* 10, 529-535.
- Streichan, S.J., Hoerner, C.R., Schneidt, T., Holzer, D., and Hufnagel, L. (2014). Spatial constraints control cell proliferation in tissues. *P Natl Acad Sci USA* 111, 5586-5591.
- Sui, L., Pflugfelder, G.O., and Shen, J. (2012). The Dorsocross T-box transcription factors promote tissue morphogenesis in the *Drosophila* wing imaginal disc. *Development* 139, 2773-2782.
- Sun, S., and Irvine, K.D. (2016). Cellular Organization and Cytoskeletal Regulation of the Hippo Signaling Network. *Trends Cell Biol* 26, 694-704.
- Sun, S., Reddy, B.V., and Irvine, K.D. (2015). Localization of Hippo signalling complexes and Warts activation in vivo. *Nat Commun* 6, 8402.
- Tabata, T. (2001). Genetics of morphogen gradients. *Nat Rev Genet* 2, 620-630.
- Tallinen, T., Chung, J.Y., Biggins, J.S., and Mahadevan, L. (2014). Gyrification from constrained cortical expansion. *Proc Natl Acad Sci U S A* 111, 12667-12672.
- Thompson, B.J., and Cohen, S.M. (2006). The Hippo pathway regulates the bantam microRNA to control cell proliferation and apoptosis in *Drosophila*. *Cell* 126, 767-774.
- Twitty, V.C., and Schwind, J.L. (1931). The growth of eyes and limbs transplanted heteroplastically between two species of *Amblystoma*. *J Exp Zool* 59.
- Vogel, G. (2013). How Do Organs Know When They Have Reached the Right Size? *Science* 340, 1156-1157.
- Vollmer, J., Casares, F., and Iber, D. (2017). Growth and size control during development. *Open Biol* 7.
- Vrabioiu, A.M., and Struhl, G. (2015). Fat/Dachsous Signaling Promotes *Drosophila* Wing Growth by Regulating the Conformational State of the NDR Kinase Warts. *Dev Cell* 35, 737-749.

- Wang, D., Li, L., Lu, J., Liu, S., and Shen, J. (2016a). Complementary expression of optomotor-blind and the Iroquois complex promotes fold formation to separate wing notum and hinge territories. *Dev Biol* *416*, 225-234.
- Wang, L., Luo, J.Y., Li, B., Tian, X.Y., Chen, L.J., Huang, Y., Liu, J., Deng, D., Lau, C.W., Wan, S., *et al.* (2016b). Integrin-YAP/TAZ-JNK cascade mediates atheroprotective effect of unidirectional shear flow. *Nature*.
- Wartlick, O., Mumcu, P., Kicheva, A., Bittig, T., Seum, C., Julicher, F., and Gonzalez-Gaitan, M. (2011). Dynamics of Dpp Signaling and Proliferation Control. *Science* *331*, 1154-1159.
- Williams, J.A., Bell, J.B., and Carroll, S.B. (1991). Control of Drosophila wing and haltere development by the nuclear vestigial gene product. *Genes Dev* *5*, 2481-2495.
- Winter, C.G., Wang, B., Ballew, A., Royou, A., Karess, R., Axelrod, J.D., and Luo, L. (2001). Drosophila Rho-associated kinase (Drok) links Frizzled-mediated planar cell polarity signaling to the actin cytoskeleton. *Cell* *105*, 81-91.
- Wong, K.K., Li, W., An, Y., Duan, Y., Li, Z., Kang, Y., and Yan, Y. (2015). beta-Spectrin regulates the hippo signaling pathway and modulates the basal actin network. *J Biol Chem* *290*, 6397-6407.
- Worley, M.I., Setiawan, L., and Hariharan, I.K. (2013). TIE-DYE: a combinatorial marking system to visualize and genetically manipulate clones during development in Drosophila melanogaster. *Development* *140*, 3275-3284.
- Wu, S., Huang, J., Dong, J., and Pan, D. (2003). hippo encodes a Ste-20 family protein kinase that restricts cell proliferation and promotes apoptosis in conjunction with salvador and warts. *Cell* *114*, 445-456.
- Yang, C.C., Graves, H.K., Moya, I.M., Tao, C., Hamaratoglu, F., Gladden, A.B., and Halder, G. (2015). Differential regulation of the Hippo pathway by adherens junctions and apical-basal cell polarity modules. *Proc Natl Acad Sci U S A* *112*, 1785-1790.
- Yin, F., Yu, J., Zheng, Y., Chen, Q., Zhang, N., and Pan, D. (2013). Spatial organization of Hippo signaling at the plasma membrane mediated by the tumor suppressor Merlin/NF2. *Cell* *154*, 1342-1355.
- Yonemura, S., Wada, Y., Watanabe, T., Nagafuchi, A., and Shibata, M. (2010). alpha-Catenin as a tension transducer that induces adherens junction development. *Nat Cell Biol* *12*, 533-542.
- Yu, F.X., and Guan, K.L. (2013). The Hippo pathway: regulators and regulations. *Genes Dev* *27*, 355-371.
- Yu, F.X., Zhao, B., and Guan, K.L. (2015). Hippo Pathway in Organ Size Control, Tissue Homeostasis, and Cancer. *Cell* *163*, 811-828.

Yu, F.X., Zhao, B., Panupinthu, N., Jewell, J.L., Lian, I., Wang, L.H., Zhao, J., Yuan, H., Tumaneng, K., Li, H., *et al.* (2012). Regulation of the Hippo-YAP pathway by G-protein-coupled receptor signaling. *Cell* *150*, 780-791.

Zartman, J., Restrepo, S., and Basler, K. (2013). A high-throughput template for optimizing *Drosophila* organ culture with response-surface methods. *Development* *140*, 667-674.

Zecca, M., Basler, K., and Struhl, G. (1995). Sequential organizing activities of engrailed, hedgehog and decapentaplegic in the *Drosophila* wing. *Development* *121*, 2265-2278.

Zhao, B., Li, L., Wang, L., Wang, C.Y., Yu, J., and Guan, K.L. (2012). Cell detachment activates the Hippo pathway via cytoskeleton reorganization to induce anoikis. *Genes Dev* *26*, 54-68.

Zhao, B., Wei, X., Li, W., Udan, R.S., Yang, Q., Kim, J., Xie, J., Ikenoue, T., Yu, J., Li, L., *et al.* (2007). Inactivation of YAP oncoprotein by the Hippo pathway is involved in cell contact inhibition and tissue growth control. *Genes Dev* *21*, 2747-2761.